NAA-SR-8617, VOL III
REACTOR TECHNOLOGY
TID-4500 (36th Ed.)
SNAP REACTORS,
SNAP PROGRAM
M-3679 (38th Ed.)
148 PAGES

SNAP TECHNOLOGY HANDBOOK

VOLUME III

REFRACTORY FUELS AND CLADDINGS

Compiled & Edited
By
G.F. BURDI

Contributors:
G.G. BENTLE
R.E. JOHNSON
A.K. SMALLEY
D.H. STONE

ATOMICS INTERNATIONAL

A DIVISION OF NORTH AMERICAN AVIATION, INC.
P.O. BOX 309 CANOGA PARK, CALIFORNIA

CONTRACT: AT(11-1)-GEN-8
ISSUED:APR 30 1965

LEGAL NOTICE

This report was prepared as an account of Government sponsored work. Neither the United States, nor the Commission, nor any person acting on behalf of the Commission:

A. Makes any warranty or representation, express or implied, with respect to the accuracy, completeness, or usefulness of the information contained in this report, or that the use of any information, apparatus, method, or process disclosed in this report may not infringe privately owned rights; or

B. Assumes any liabilities with respect to the use of, or for damages resulting from the use of information, apparatus, method, or process disclosed in this report.

As used in the above, "person acting on behalf of the Commission" includes any employee or contractor of the Commission, or employee of such contractor, to the extent that such employee or contractor of the Commission, or employee of such contractor prepares, disseminates, or provides access to, any information pursuant to his employment or contract with the Commission, or his employment with such contractor.

Price $5.00
Available from the Office of Technical Services
Department of Commerce
Washington 25, D. C.

DISTRIBUTION

This report has been distributed according to the category REACTOR TECHNOLOGY, UC-80, as given in "Standard Distribution for Unclassified Scientific and Technical Reports," TID-4500 (37th Edition), December 1, 1964, with nonduplicating distribution from the category SNAP REACTORS, SNAP PROGRAM, C-92b, given in "Standard Distribution for Classified Scientific and Technical Reports," M-3679 (38th Edition), September 15, 1964. A total of 850 copies was printed.

CONTENTS

CONTENTS

TABLES

TABLES

TABLES

FIGURES

FIGURES

FIGURES

FIGURES

FIGURES

ABSTRACT

This report contains currently available property data on high temperature nuclear reactor compounds (UC, UN, and UO_2), ceramic dispersions (Al_2O_3-UO_2 and BeO-UO_2), and cermet (Mo-UC, -UN, and -UO_2) fuels and potential claddings (Cb, Ir, Mo, Re, Ta, Ti, V, and W). This handbook is one of three volumes that have been compiled under the direction of the Atomics International SNAP General Supporting Technology Program. Volume I contains information on the current status of liquid metal technology, while volume II contains information on the current status of hydride fuels and associated coatings and claddings as well as a brief description of SNAP 2, 8, and 10A fuel elements.

INTRODUCTION

A thorough knowledge of relevant fuel and cladding properties is a basic requirement of effective high temperature reactor design. The purpose of this handbook is to collect most of the available property data and present this information in a consistent and systematic form as an aid to engineers designing compact high temperature nuclear reactors. The present work is not intended to be all inclusive. The materials considered in this handbook as potential high temperature nuclear reactor fuels are UC, UN, and UO_2 compounds; Al_2O_3-UO_2 and BeO-UO_2 ceramic dispersions; and Mo-UC, -Un and -UO_2 cermets. Potential elemental claddings included in this report are columbium (niobium), iridium, molybdenum, rhenium, tantalum, titanium, vanadium, and tungsten.

To facilitate the addition of information, a loose-leaf format has been adopted. Periodic revisions will be performed to incorporate current property data in this and other SNAP TECHNOLOGY HANDBOOKS.

1.0 COMPOUNDS

1.1 COMPOSITIONS

1.1.1 Uranium Carbides[1.1]

Uranium monocarbide (UC) contains 4.8 wt % carbon, while uranium sesquicarbide (U_2C_3) contains 7.0 wt % carbon, and uranium dicarbide (UC_2) contains 9.2 wt % carbon. U_2C_3 decomposes to UC + UC_2 above 1800°C (3272°F).

1.1.2 Uranium Nitrides[1.1,1.2]

Uranium mononitride (UN) is the stable compound containing 5.56 wt % nitrogen while the uranium sesquinitride (U_2N_3) is stable only to 1300°C (2372°F) and the uranium dinitride (UN_2) is stable only to around 700°C (1292°F). Both U_2N_3 and UN_2 decompose to UN plus nitrogen at temperatures above those mentioned above.

1.1.3 Uranium Oxides[1.1]

Stoichiometric uranium dioxide (UO_2) contains 11.85 wt % oxygen. With the addition of excess oxygen U_4O_9 is formed containing 13.14 wt % oxygen. As more oxygen is added U_3O_7 is formed containing 13.56 wt % oxygen, but is unstable above 200°C (392°F). U_3O_8 is then formed containing 15.20 wt % oxygen. With still more excess oxygen UO_3 is formed containing 16.78 wt % oxygen.

1.2 PHYSIOCHEMICAL PROPERTIES

1.2.1 Physical

1.2.1.1 Phase Diagrams and Crystal Structures

Figure 1.2.1 best represents the phase relationships of the uranium-carbon system. Uranium carbides have strong metal-carbon bonding and weak metal-metal bonding within the crystal structure itself.[1.6] The crystalline structure of UC is face centered cubic (f.c.c.) with a lattice constant (a_o) in the range of 4.96 ± 0.01 Å at room temperature.[1.5-1.13] U_2C_3 has a body centered cubic (b.c.c.) crystalline structure with a lattice constant (a_o) of 8.088 ± 0.001 Å at temperatures less than 1700°C (3092°F).[1.5,1.6,1.8,1.14,1.15] UC_2 has a face centered tetragonal (f.c.t.) crystalline structure with a side lattice constant (a_o) of 3.52 ± 0.01 Å at room temperature[1.8,1.10,1.15] and also at temperatures below 1700°C (3092°F).[1.6] Hallse[1.5] reports a value for a_o of 4.96 Å at room temperature which is in disagreement with other investigators and is probably wrong. The other lattice parameter (c_o) for UC_2 is in the range of 5.95 ± 0.05 Å at room temperature.[1.5,1.6,1.8,1.10,1.15] It should be noted that UC_2 undergoes a phase transformation at 1800°C (3272°F) from f.c.t. to f.c.c. with a lattice constant (a_o) of 5.47 Å.[1.16] Ferguson, et al[1.17] presented an experimental equation for finding the lattice parameters of UC and UC_2 as a function of temperature which is given below.

For UC:

$$a_o = 4.9592\left[1 + (10.98 \pm 0.08)\ 10^{-6}T\right] \pm 0.0015\ \text{Å}\ , \qquad \ldots(1.2.1)$$

$$a_o = 4.9601\ \text{Å at } 20°C\ , \qquad \ldots(1.2.2)$$

For UC_2:

$$a_o = 3.5256\left[1 + (16.56 \pm 0.23)\ 10^{-6}T\right] \pm 0.0005\ \text{Å}\ , \qquad \ldots(1.2.3)$$

$$a_o \cong 3.5266\ \text{Å}\ , \qquad \ldots(1.2.4)$$

$$c_o = 6.0014\left[1 + (10.43)\ 10^{-6}T\right]\ , \qquad \ldots(1.2.5)$$

$$c_o \cong 6.0023\ \text{Å at } 20°C\ , \qquad \ldots(1.2.6)$$

where a_o and c_o are in units of angstroms and T is in °C.

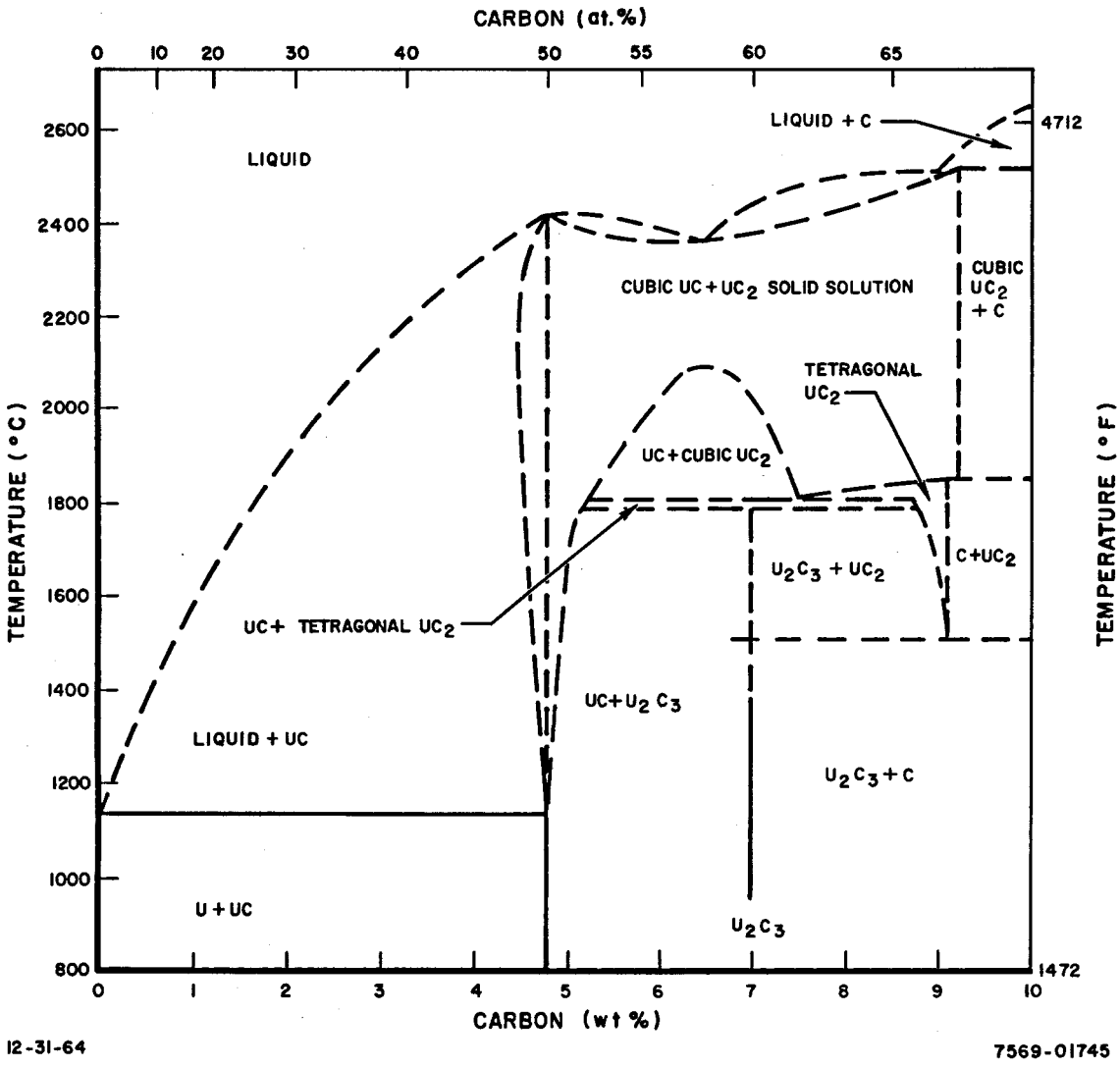

Figure 1.2.1. Phase Diagram of Uranium-Carbon System

Apparently three phase diagrams have been constructed for the uranium-nitrogen system, using high purity uranium-nitrogen materials. The U-N phases are directly affected by temperatures, as well as the environmental nitrogen pressure, as illustrated in Figures 1.2.2 - 1.2.4. At nitrogen pressures above 2.5 atm, UN melts congruently at 2850°C as shown in Figure 1.2.4. The 10 ppm shown in Figure 1.2.3 is the estimated nitrogen solubility in uranium at the uranium melting point. Since a uranium-UN eutectic is believed to form, the solubility of nitrogen in solid uranium is believed to be lower, perhaps ~1ppm. Of the three compounds that are known to exist, UN is the stable one. At 5,1, and 10^{-4} atm of nitrogen, U_2N_3 is stable to 1520, 1345, and 780°C, respectively. Higher pressure and lower temperature favor the formation of higher nitrogen compositions, such as UN_2.[1.141] UN has a face centered cubic (f.c.c.) crystalline structure with a_o = 4.880 Å.[1.2] The crystalline structure for U_2N_3 is body centered cubic (b.c.c.) with a_o = 10.678 Å, while for UN_2 it is body centered cubic (ideal fluorite structure type) with $a_o = 5.31 \pm 0.01$Å.[1.77]

The phase diagram of the uranium-oxygen system is presented in Figure 1.2.5. The crystal structure of uranium-oxygen systems is difficult to determine. Most investigators do agree that UO_2 is f.c.c. (fluorite type) with $a_o = 5.470 \pm 0.001$Å.[1.20, 1.24]

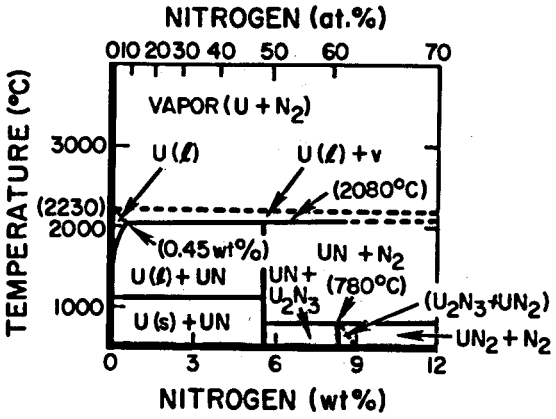

12-30-64 7569-01746

Figure 1.2.2. Phase Diagram of Uranium-Nitrogen Compound System Under 10^{-4} atm of Nitrogen (Reference 1.141)

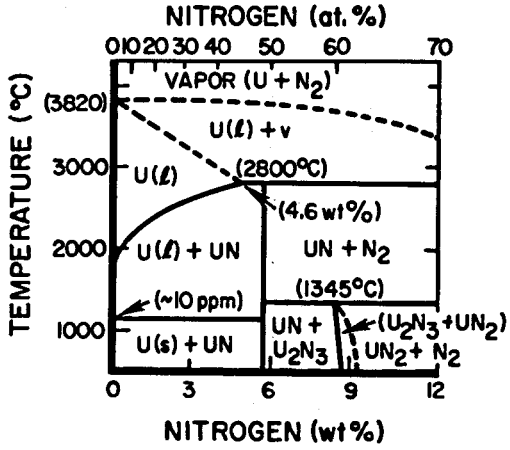

12-30-64 7569-01747

Figure 1.2.3. Phase Diagram of Uranium-Nitrogen Compound System Under 1 atm of Nitrogen (Reference 1.141)

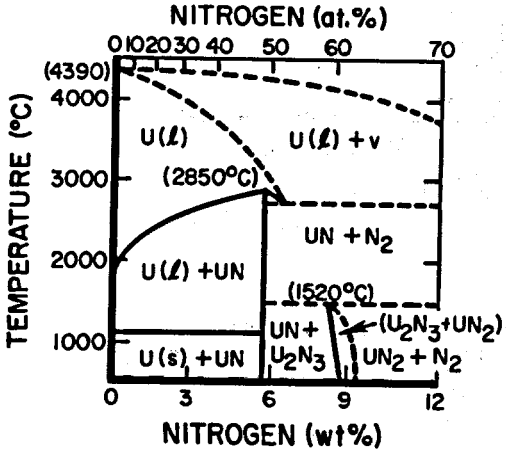

12-30-64 7569-01748

Figure 1.2.4. Phase Diagram of Uranium-Nitrogen Compound System Under 5 atm of Nitrogen (Reference 1.141)

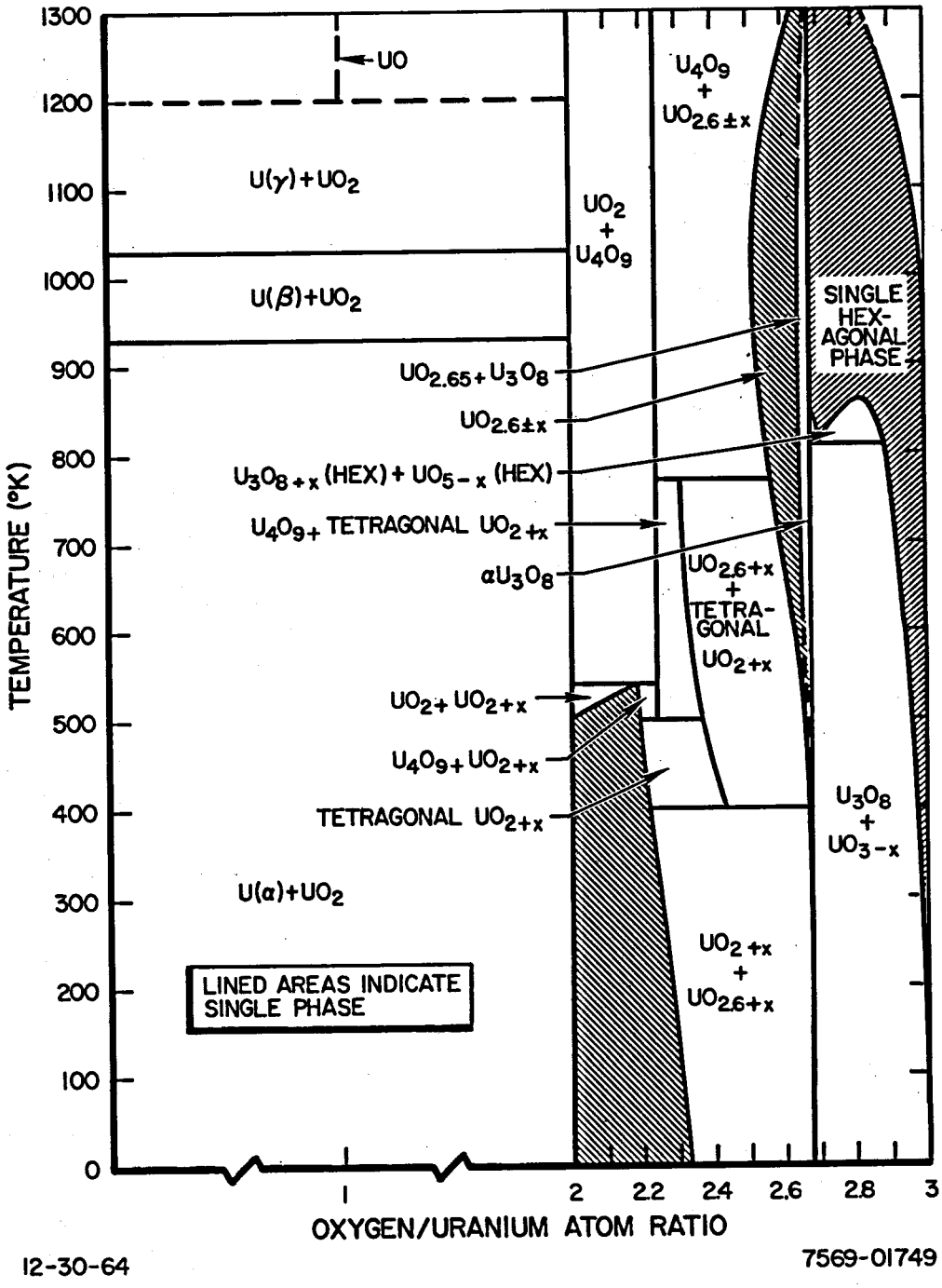

Figure 1.2.5. Phase Diagram of Uranium-Oxygen System (References 1.18 and 1.19)

1.2.1.2 Density

Table 1.2.1 lists the theoretical densities of uranium-carbon, uranium-nitrogen, and uranium-oxygen compounds. Also included in this table are theoretical densities obtained from x-ray data.[1.9, 1.10, 1.14, 1.20, 1.27, 1.28] No density data as a function of temperature are available. Figure 1.2.6 illustrates graphically the effect of carbon on the room temperature density of the uranium-carbon system; similarly, Figure 1.2.7 shows the effect of oxygen on the uranium-oxygen system.

TABLE 1.2.1

DENSITY OF FUELED COMPOUNDS AT ROOM TEMPERATURE

Compound	Theoretical Density (gm/cc)	Reference
UC	13.56 13.63	1.5 1.9, 1.10, 1.27
U_2C_3	12.88	1.5, 1.14
UC_2	11.52	1.5
UN	14.32	1.10
U_2N_3	11.24	1.77
UN_2	11.73	1.77
UO_2	10.96	1.20, 1.28

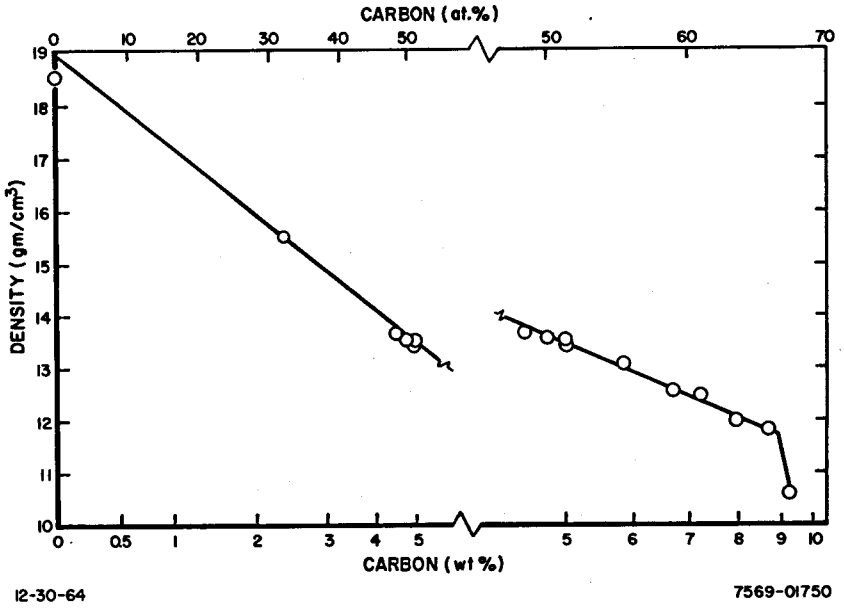

Figure 1.2.6. Effect of Carbon on the Room Temperature Density of Uranium-Carbon Compounds (Reference 1.11, 1.37)

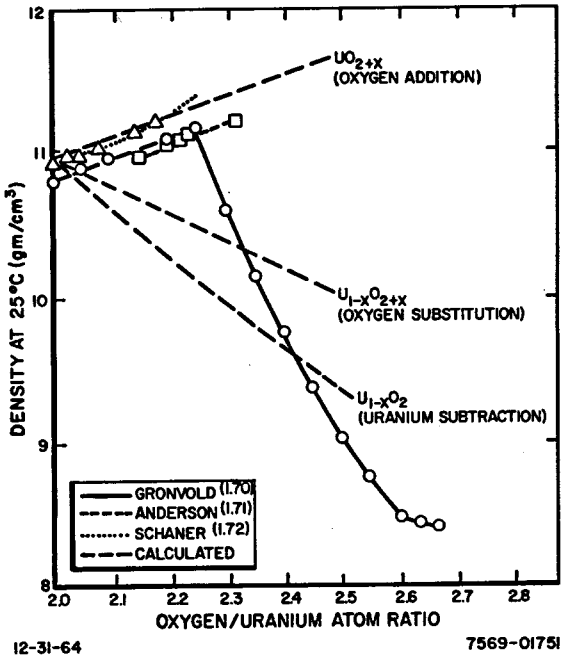

Figure 1.2.7. Room Temperature Uranium Oxide Density as a Function of Composition (Reference 1.73)

1.2.1.3 Melting Point

Table 1.2.2 presents the melting points of the uranium compounds considered in this handbook. U_2C_3 decomposes above 1800°C into UC and UC_2.[1.5, 1.14] U_2N_3 and UN_2 also decompose but at 1300°C (2372°F) and 700°C (1292°F), respectively.[1.2]

Some of the UO_2 melting point data were obtained in vacuum,[1.18, 1.33] while some were in hydrogen, helium, and argon[1.34] atmospheres.

TABLE 1.2.2
MELTING POINTS OF URANIUM COMPOUNDS

Compound	Melting Point (°C)	Melting Point (°F)	Reference
UC	2375 ± 25	4307 ± 77	1.5, 1.29
	2280 ± 50	4136 ± 122	1.21
	2550	4622	1.30
	2590 ± 50	4694 ± 122	1.31
UC_2	2475 ± 25	4487 ± 77	1.5, 1.29
UN	2480 ± 50	4496 ± 122	1.21
	2900	5252	1.30
	2650 ± 100	4802 ± 212	1.31, 1.32
UO_2	2405 ± 16	4361 ± 60.8	1.18
	2860 ± 45	5180 ± 113	1.33
	2760 ± 30	5000 ± 86	1.34
	3000	5432	1.30
	2800	5072	1.20
	2880 ± 20	5216 ± 68	1.35, 1.36
	2700 ± 50	4892 ± 122	1.21

1.2.1.4 Vapor Pressure

Uranium carbide undergoes congruent vaporization at a composition of $UC_{1.07}$.[1.1,1.38,1.39] This vaporization occurs between temperatures of 2010°C (3650°F) and 2230°C (4046°F); the rate in high vacuum varies between 2.0×10^{-6} gm/cm^2-sec and 38.3×10^{-6} gm/cm^2-sec, respectively, at these temperatures.[1.39] The vapor pressure of uranium over a UC sample varies linearly from 1.3×10^{-7} atm at 2010°C to 26×10^{-7} atm at 2230°C, while the vapor pressure of carbon varies linearly from 0.3×10^{-7} atm at 2010°C to 6.4×10^{-7} atm at 2230°C.[1.39] At high carbon contents carbon is preferentially lost by vaporization. For a UC_2 sample exposed to a carbon saturated atmosphere, the vapor pressure of uranium is given by the following expressions.[1.1,1.8]

From 1660°C (3020°F) to 2092°C (3797.6°F):[1.8]

$$\ln p_u = -\frac{67,164}{T} - 0.111\left(\ln T + \frac{2000}{T}\right) + 12.140 \qquad \ldots(1.2.7)$$

From 2175°C (3947°F) to 2458°C (4456.4°F):[1.38]

$$\log p_u = -\frac{30,600}{T} + 6.36 \quad , \qquad \ldots(1.2.8)$$

where p_u and T are in units of atm and °K, respectively.

No vapor pressure data are available on uranium-nitrogen systems.

Some vapor pressure data are available on stoichiometric UO_2 and on UO_3. Ackerman et al.[1.40] presents equations for finding the vapor pressure of stoichiometric UO_2 over two temperature ranges.

From 1600°K (2420.6°F) to 2000°K (3140.6°F):

$$\log p = -\frac{33,115}{T} - 4.026 \log T + 25.686 \quad . \qquad \ldots(1.2.9)$$

Above 2000°K:

$$\log p = 13.298 - \frac{3.7195 \times 10^4}{T} + \frac{3.5612 \times 10^6}{T^2} + \frac{2.6178 \times 10^9}{T^3} \quad . \qquad \ldots(1.2.10)$$

Additionally, Ackerman[1.18] presents a different form of equation to approximate the vapor pressure relationship with temperature of UO_2.

From 1600°K to 2200°K (3500.6°F):

$$\log p = 13.340 - \frac{3.7337 \times 10^4}{T} + \frac{3.67 \times 10^6}{T^2} + \frac{2.4638 \times 10^9}{T^3} \quad , \qquad \ldots(1.2.11)$$

where p and T in the above equations are in units of mm of Hg and °K, respectively. Typical values from Equation 1.2.11 are listed in Table 1.2.3.

TABLE 1.2.3
VAPOR PRESSURE OF UO_2
(Reference 1.18)

Temperature (°C)	Temperature (°F)	Pressure (mm Hg)
1351	2463.8	1.65×10^{-8}
1504	2739.2	7.06×10^{-7}
1727	3140.6	1.67×10^{-5}
1955	3551	0.0036
2151	3903.8	0.0421
2388	4330.4	0.966

Ackerman et al.[1.41] also determined the vapor pressure of UO_3 from thermodynamic data on crystalline UO_2 and gaseous UO_3 below 2000°K.

$$\log p = -\frac{13,100}{T} + 4.73 + 1/2 \log (p_{O_2}) \quad , \qquad \ldots(1.2.12)$$

where p_{O_2} is the partial pressure of oxygen over UO_3, and p and T are in units of atm and °K, respectively.

1.2.2 Electrical

1.2.2.1 Electrical Resistivity

The electrical resistivity of as-cast uranium carbon compounds at room temperature[1.1, 1.47] is presented in Figure 1.2.8. Figure 1.2.9 illustrates the effect of temperature on the electrical resistivity of UC.[1.1, 1.37, 1.42, 1.43, 1.44, 1.45] Grossman et al.[1.46] obtained the following equation which best represents their UC electrical resistivity data in the temperature range of $500 < T < 2050°K$.

$$\rho = \left(24.9 \times 10^{-6}\right) + \left(107.4 \times 10^{-9}\right)T \quad , \qquad \ldots(1.2.13)$$

where ρ and T are in units of ohm-cm and °K, respectively.

Figure 1.2.10 shows the electrical resistivity of a 97% dense UN specimen as a function of temperature.[1.48] No other data are available on the uranium-nitrogen compounds.

Illustrated in Figure 1.2.11 is the electrical conductivity of sintered UO_2 as a function of temperature.[1.49, 1.50] Figure 1.2.12 gives some additional data[1.73] on the electrical resistivity versus temperature for sintered UO_2 specimens where the data were separated according to the "type" of electrical conduction (n-type structure is where there exists an excess of electrons for flow as apposed to the p-type where there exists excess positive "holes" for electrical conduction). Figure 1.2.13 illustrates the effect of oxygen on the electrical conductivity of pressed uranium-oxygen compounds with the data separated again according to "type".[1.1]

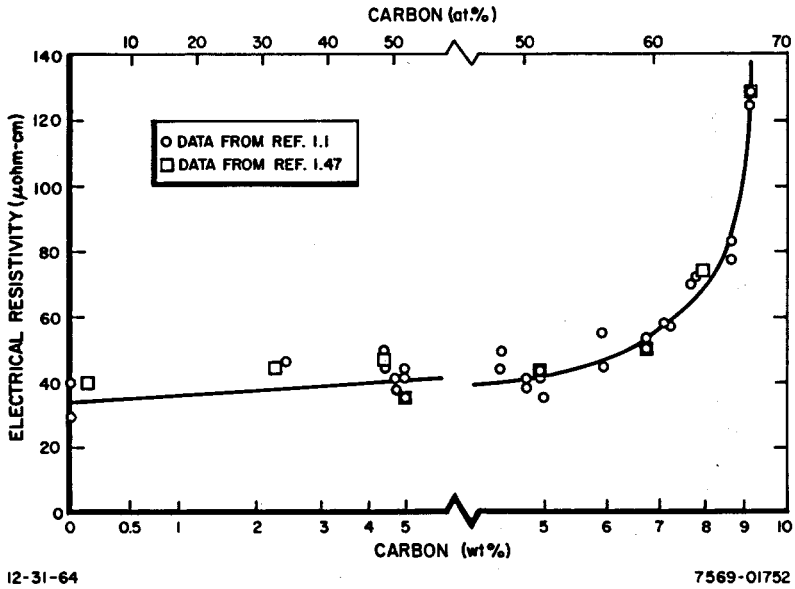

Figure 1.2.8. Room Temperature Electrical Resistivity of As-Cast Uranium-Carbon Compounds

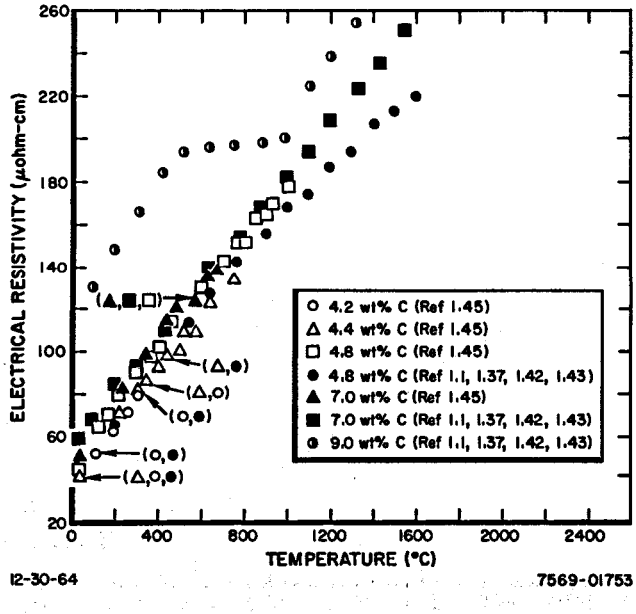

Figure 1.2.9. Effect of Temperature on Electrical Resistivity of As-Cast Uranium-Carbon Compounds

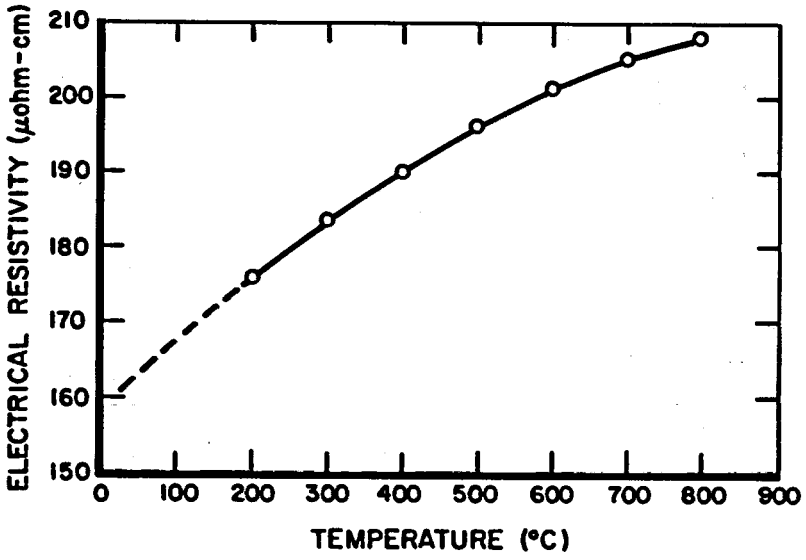

7569-01754

Figure 1.2.10. Electrical Resistivity of UN
(Reference 1.1, 1.48)

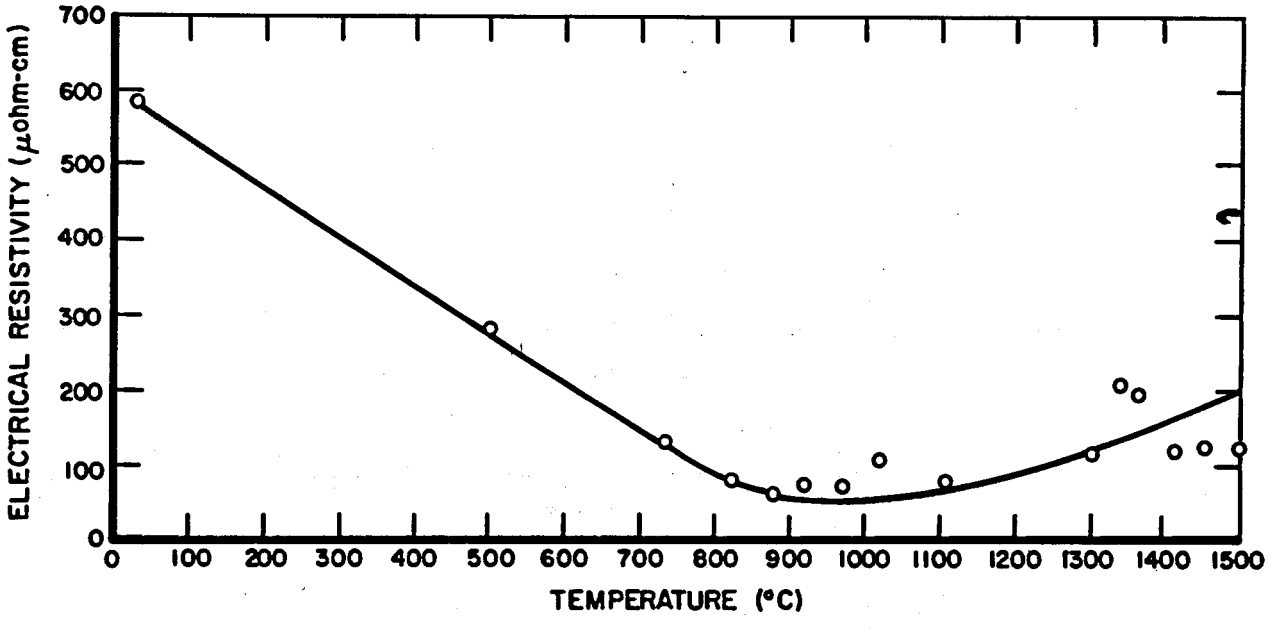

7569-01755

Figure 1.2.11. Electrical Resistivity of Sintered UO_2
(Reference 1.50)

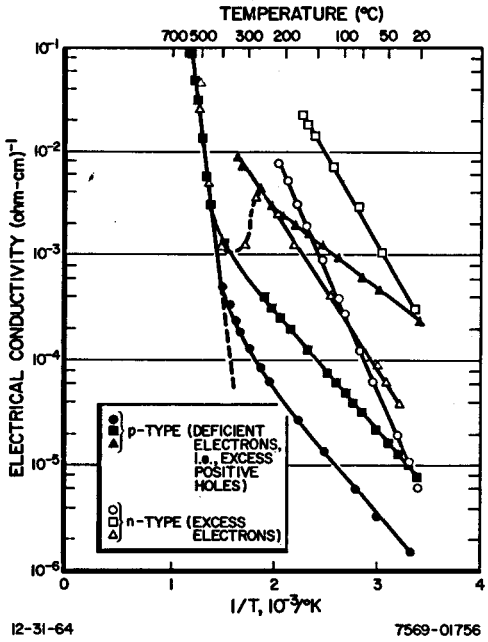

Figure 1.2.12 Electrical Conductivity of Sintered Specimens of n- and p-type UO_2 (Reference 1.73)

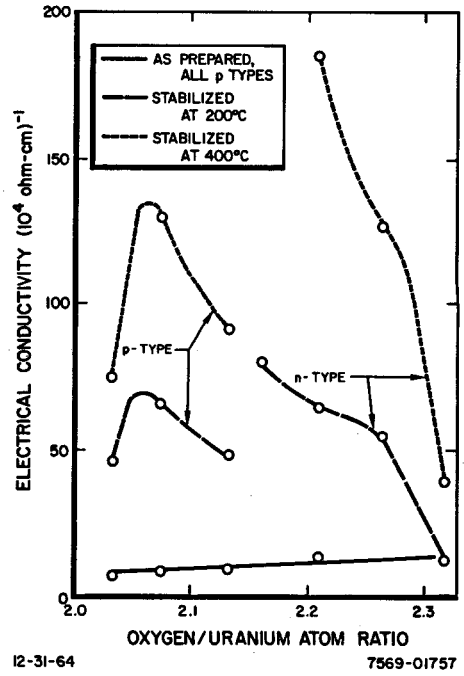

Figure 1.2.13. Room-Temperature Electrical Conductivity as a Function of Oxygen/Uranium Ratio of Pressed Specimens of UO_2 (Reference 1.73)

1.2.2.2 Magnetic Susceptibility

No data are available for the uranium-carbon compounds. Trzebiatowski, et al.[1.53] states that the magnetic susceptibility of the uranium nitrides is greater than that for metallic uranium.

Willardson, Moody, and Goering[1.52] determined that the magnetic susceptibility of uranium-oxygen compounds decreases with increases in the temperature. Oxygen was shown to decrease the magnetic susceptibility from 8×10^6 e.m.u. to 2×10^6 e.m.u. at 300°K when the oxygen/uranium atom ratio was varied from 2.0 to 2.7. Dawson and Lister[1.54] presented some data on UO_2 which is presented in Figure 1.2.14.

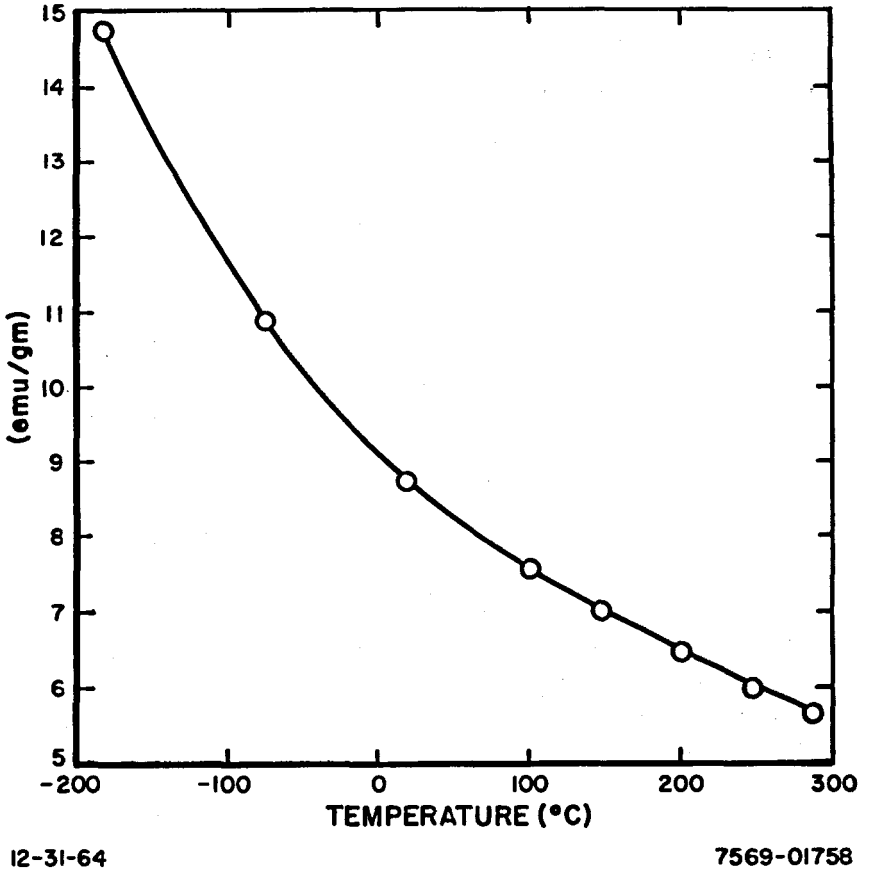

Figure 1.2.14. Magnetic Susceptibility of UO_2 (Reference 1.54)

1.2.3 Thermal

1.2.3.1 Thermal Conductivity

Figure 1.2.15 illustrates the effect of temperature and carbon on the thermal conductivity of uranium-carbon compounds. The data presented are approximately within +0.003 kcal/cm-sec-°C of other investigators.[1.55-1.58, 1.60, 1.61] For a uranium-carbon compound containing 5.1 wt % carbon, Grossman[1.46] presents the following equation for the temperature range of $500 \leq T \leq 2050$°K ($433.4 \leq T \leq 3230.6$°F):

$$k = 0.054 + \left(0.006 \times 10^{-3}\right) T, \pm 0.004 \quad , \qquad \ldots (1.2.14)$$

where k and T are in kcal/cm-sec-°C and °K, respectively.

The thermal conductivity of a 97% dense UN specimen as a function of temperature is presented in Figure 1.2.16.[1.1, 1.48, 1.62]

Figure 1.2.17 illustrates the effect of temperature on the thermal conducitivity of UO_2. A band is used to represent the range of data from various investigators.[1.63-1.65] The data presented in this figure have been adjusted linearly with density to 100% theoretical.[1.1] Runnak[1.66] studied the effect of oxygen on a UO_2 specimen having a density of 10.3 gm/cc. Runnak's results are shown in Figure 1.2.18. It has been found that by adding 0.1% TiO_2 the curve is lowered and flattened out but still retains the same average slope.[1.66]

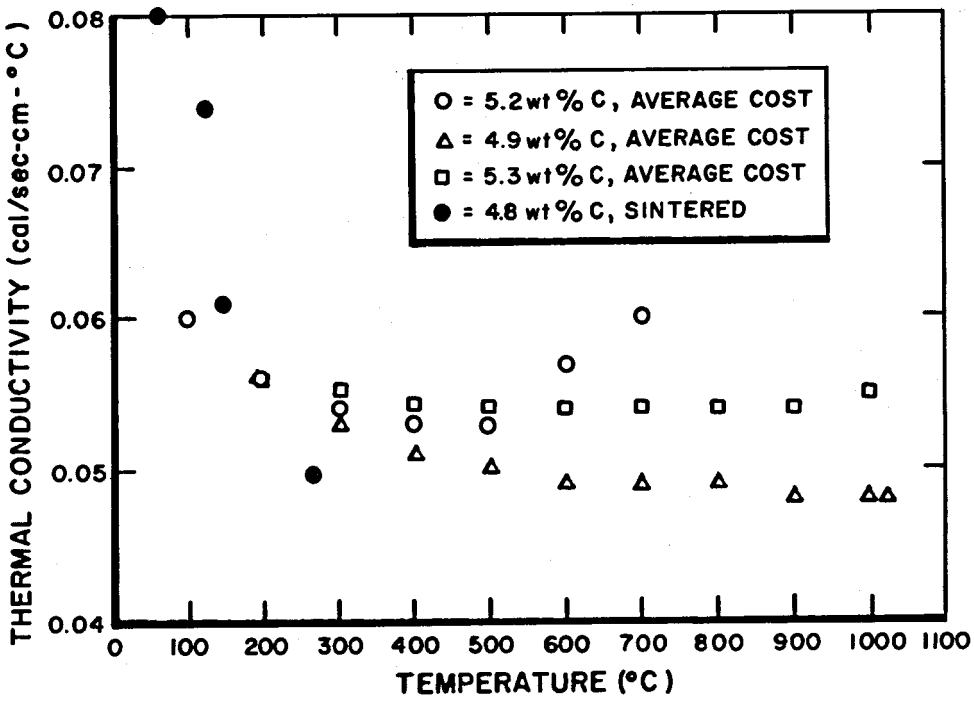

Figure 1.2.15. Effect of Temperature and Carbon on the Thermal Conductivity of Uranium-Carbon Compound (Reference 1.59)

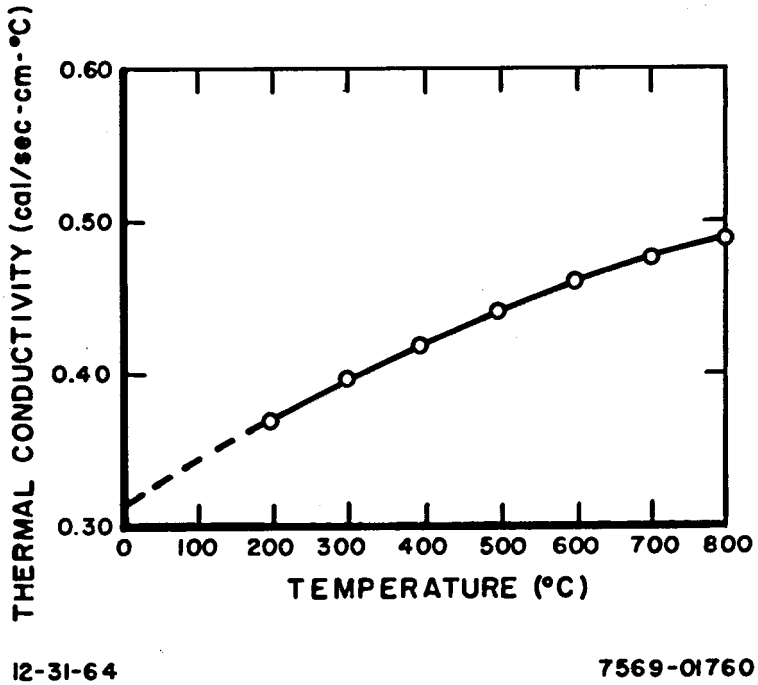

Figure 1.2.16 Thermal Conductivity of UN (Reference 1.1, 1.48, 1.62)

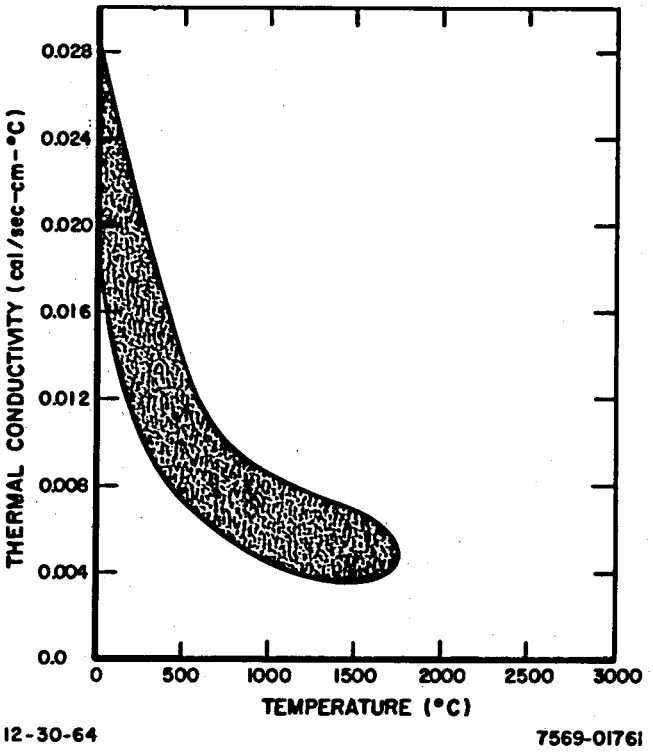

Figure 1.2.17. Thermal Conductivity vs Temperature of UO_2 (Reference 1.1, 1.63, 1.64, 1.65)

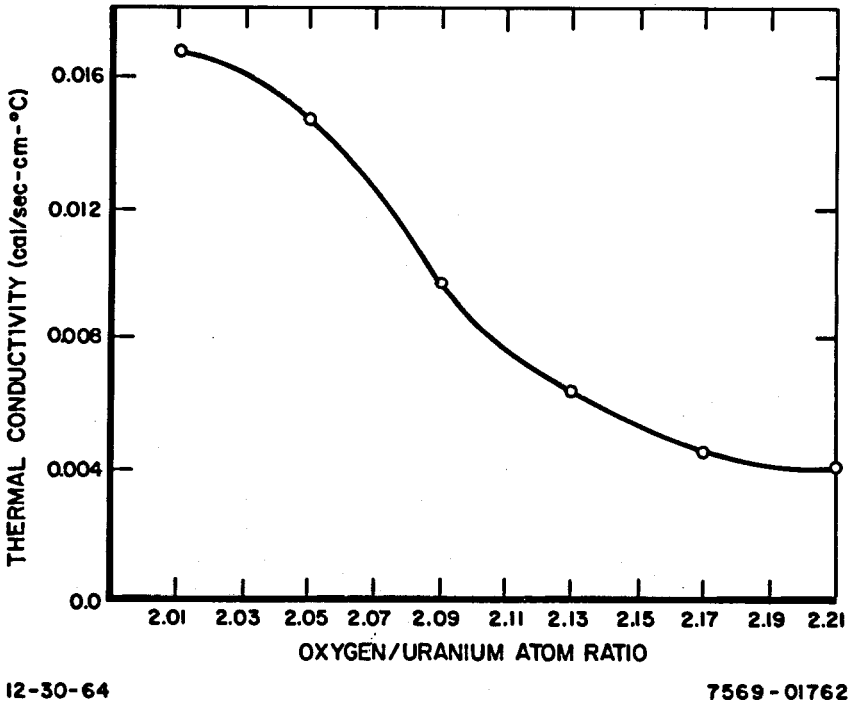

Figure 1.2.18. Effect of Oxygen on the Thermal Conductivity of Uranium-Oxygen Compounds (Reference 1.66)

1.2.3.2 Specific Heat

Table 1.2.4 lists typical specific heat values as a function of temperature for uranium carbon compounds experimentally determined by Mukaibo, et al.[1.67]

TABLE 1.2.4
SPECIFIC HEATS FOR URANIUM-CARBON COMPOUNDS
(Reference 1.67)

Temperature		Specific Heat (cal/gm-°C)	
(°C)	(°F)	UC	UC_2
100	212	0.0478	0.0565
140	284	0.0507	0.0591
180	356	0.0522	0.0611
220	428	0.0541	0.0631
260	500	0.0550	0.0650
300	572	0.0549	0.0661
340	644	0.0553	0.0672
380	716	0.0556	0.0674
400	752	0.0599	0.0674

Krikorian[1.68] covered a wider range and presented his results on terms of three equations, which are presented below.

For UC and $300 \leq T \leq 2000°K$ ($80.6 \leq T \leq 3140.6°F$):

$$c_p = 13.73 + \left(1.82 \times 10^{-3}\right) T - \left(2.42 \times 10^{5}\right) T^{-2} \qquad \ldots (1.2.15)$$

For U_2C_3 and $300 \leq T \leq 2000°K$:

$$c_p = 34.35 + \left(4.68 \times 10^{-3}\right) T - \left(6.20 \times 10^{5}\right) T^{-2} \qquad \ldots (1.2.16)$$

For UC_2 and $300 \leq T \leq 2000°K$:

$$c_p = 20.37 + \left(2.70 \times 10^{-3}\right) T - \left(3.68 \times 10^{5}\right) T^{-2} \qquad \ldots (1.2.17)$$

where c_p and T are in units of cal/gm mole-°K and °K, respectively.

Figure 1.2.19 illustrates graphically, with the units of c_p converted to cal/gm-°K, the above equations, in addition to an equation presented by Tripler[1.69] which is given below.

For UC and $298 \leq T \leq 2400°K$:

$$c_p = 7.6 + \left(2.85 \times 10^{-3}\right) T \qquad \ldots (1.2.18)$$

where c_p and T are in units of cal/gm-mole-°K and °K, respectively.

No data are available on the specific heats of uranium-nitrogen compounds.

Stavrotakis and Barr[1.74] obtained an equation from experimental data for the specific heat of UO_2, and their equation is presented below with c_p and T given in units of cal/gm-mole-°K and °K, respectively.

For UO_2 and $300 \leq T \leq 1500°K$ ($80.6 \leq T \leq 2732°F$):

$$c_p = 18.45 + \left(2.431 \times 10^{-3}\right) T - \left(2.272 \times 10^{5}\right) T^{-2} \qquad \ldots (1.2.19)$$

Nichols[1.27] also presents an equation for the specific heat of UO_2 over the same temperature range which is presented below with c_p and T given in units of cal/gm-°K and °K, respectively.

$$c_p = 0.071 + \left(6.0 \times 10^{-6}\right) T - 1466\, T^{-2} \qquad \ldots (1.2.20)$$

Figure 1.2.20 illustrates graphically the above equations for UO_2 with the units of c_p converted to cal/gm-°K.

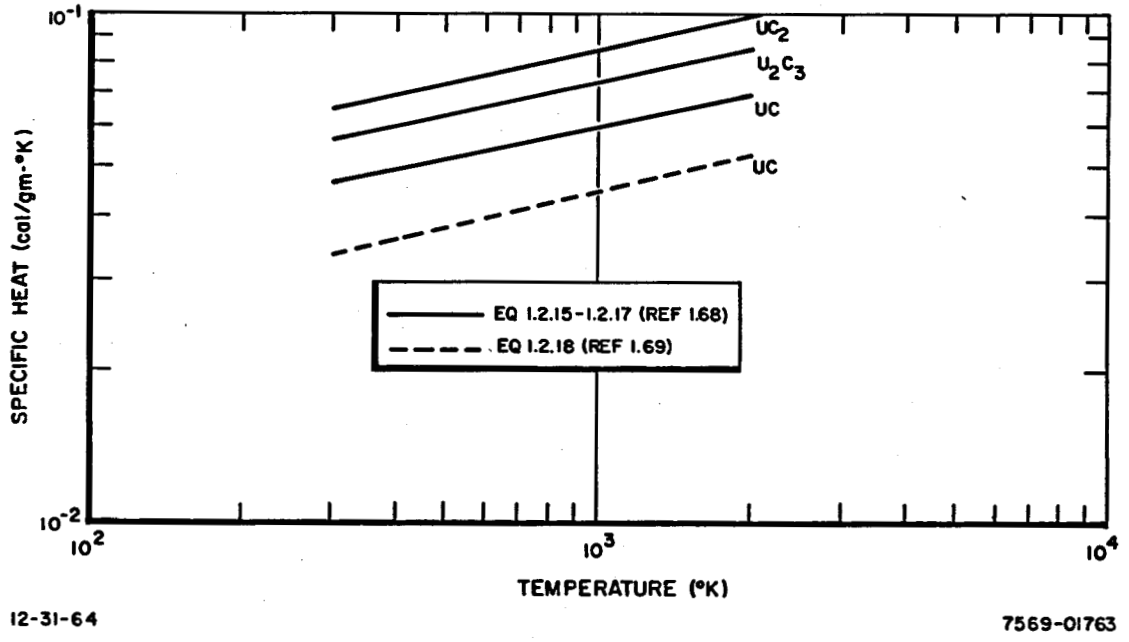

Figure 1.2.19. Specific Heat of Uranium-Carbide Compounds vs Temperature

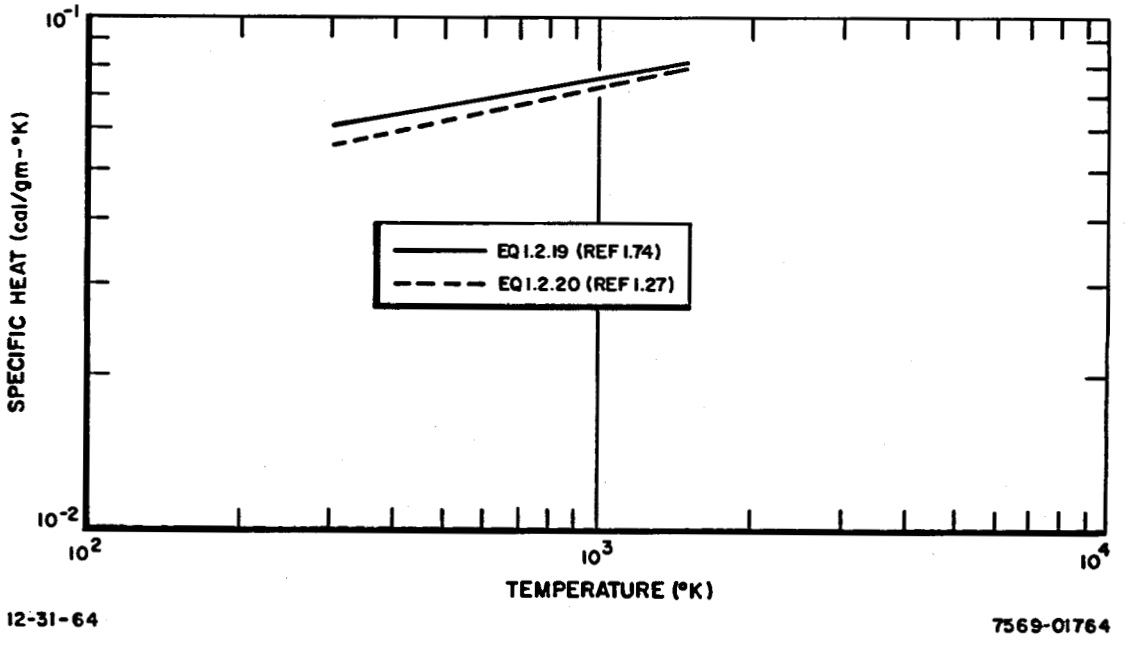

Figure 1.2.20. Specific Heat vs Temperature of UO_2

1.2.3.3 Thermal Expansion

Table 1.2.5 lists linear thermal expansion data[1.75] from arc-cast $UC_{1\pm x}$ samples illustrating the effects of carbon content and temperature. At 700 and 780°C, a difference in the thermal expansion behavior was observed between hypostoichiometric (carbon content less than 4.8 wt %) and hyperstoichiometric (carbon content greater than 4.8 wt %) samples which can be attributed to the α to β (670°C) and β to γ (780°C) phase transformations of free uranium located in the grain boundaries and within the grains of hypostoichiometric UC. A sharp increase in thermal expansion of hypostoichiometric UC above 850°C was observed by Mendez-Peñalosa,[1.75] as well as other authors,[1.76] and was also attributed to the presence of free γ phase uranium which has a higher thermal expansion coefficient. In addition, Mendez-Peñalosa postulated that the rapid increase near its melting point was due to a relief of the forces in the grain boundaries accumulated during the heating cycle and those present from the casting process. Changes in the properties of hyperstoichiometric UC above 1100°C were observed[1.75, 1.42] and may be attributed to the formation of U_2C_3.

Table 1.2.6 lists the available linear thermal expansion coefficient data on uranium-nitrogen compounds with 20°C as the reference temperature.

No extensive investigation has been conducted to obtain the linear thermal expansion of uranium-oxygen compounds. Table 1.2.7 presents the thermal expansion data that are currently available.

The data presented by Gronwald[1.70] were obtained by x-ray diffraction measurements. Dayton and Tipton[1.82] indicated that the thermal expansions of U_4O_9 and $UO_{2.40}$ were linear with temperature over the range reported.

TABLE 1.2.5

AVERAGE THERMAL EXPANSION OF ARC-CAST $UC_{1\pm x}$ SPECIMENS[1.75]

Temperature (°C)	Expansion (%)								
	Carbon Content of Sample (wt %)								
	4.35	4.43	4.59	4.71	4.9	5.04	5.05	5.08	5.24
12-100	0.09	0.09	0.09	0.08	0.08	0.08	0.08	0.08	0.08
12-200	0.19	0.19	0.19	0.19	0.19	0.19	0.19	0.18	0.18
12-300	0.29	0.29	0.29	0.29	0.29	0.29	0.29	0.29	0.29
12-400	0.40	0.40	0.40	0.40	0.40	0.40	0.40	0.39	0.40
12-500	0.52	0.51	0.51	0.51	0.51	0.51	0.51	0.50	0.52
12-600	0.64	0.63	0.62	0.62	0.62	0.62	0.62	0.60	0.64
12-700	0.76	0.76	0.75	0.74	0.74	0.74	0.74	0.70	0.76
12-800	0.90	0.90	0.87	0.85	0.85	0.85	0.85	0.83	0.89
12-900	1.05	1.10	1.01	0.97	0.97	0.98	0.97	0.94	1.02
12-1000	-	-	-	-	1.10	1.10	1.10	1.08	1.15
12-1200	-	-	-	-	1.35	1.35	1.35	1.30	1.42
12-1400	-	-	-	-	1.61	1.61	1.62	1.55	1.70
12-1600	-	-	-	-	1.89	1.89	1.89	1.80	1.99
12-1800	-	-	-	-	2.17	2.17	2.18	2.07	2.27
12-2000	-	-	-	-	2.46	2.46	2.46	2.34	-

TABLE 1.2.6

LINEAR THERMAL EXPANSION COEFFICIENTS OF UN AS A FUNCTION OF TEMPERATURE

Temperature (°C)	Coefficient 10^{-6} cm/cm-°C	Reference
20 - 1200	9.7	1.78, 1.79
20 - 1200	9.5	1.62
20 - 1600	10.1	1.78, 1.79
20 - 1600	9.9	1.62

TABLE 1.2.7

AVERAGE LINEAR THERMAL EXPANSION OF URANIUM-OXYGEN COMPOUNDS

Compound	Temperature (°C)	Expansion (%)	Reference
UO_2	20 - 400	0.34	1.70
UO_2	20 - 720	0.81	1.70
UO_2	20 - 940	0.99	1.70
UO_2	25 - 500	0.45	1.80
UO_2	25 - 1000	1.09	1.80
UO_2	25 - 1200	1.43	1.80
UO_2(ρ = 7.2 gm/cc)	400 - 900	0.50	1.81
$UO_{2.13}$(ρ = 8.54 gm/cc)	400 - 900	0.50	1.81
U_4O_9	25 - 700	0.63	1.82
$UO_{2.40}$	25 - 700	0.63	1.82

1.2.3.4 Thermal Shock Resistance

Preliminary investigations have been conducted to determine the thermal shock resistance of uranium-carbide compounds. Samples containing from 4.47 to 4.67 wt % C and quenched from temperatures between 2370 and 3450°F showed no apparent detrimental effects. The quenching medium was Dow Corning No.704 diffusion pump oil, outgassed under vacuum and initially at room temperature. Approximately 25 sec elapsed before boiling (420°F) ceased during specimen quench.[1.139] Another test was conducted by thermal cycling from a base temperature, after the first cycle, of 1000°F. Table 1.2.8 summarizes the results. The results showed that fuel instability due to cracking can be caused by thermal cycling (nonuniform temperature). It was also discovered that with the initial heating and cooling cycles, the fuel specimens sustained a permanent increase in length. This effect was also shown to a lesser degree on the second heating and cooling cycle. Tests are underway to study this fuel growth phenomenon.[1.140]

No data have been found which illustrate the thermal shock resistance of UN.

The presence of thermal gradients and thermal shock will produce cracking in UO_2 fuel elements, generally in a radial direction though circumferential cracking also occurs. The axial and circumferential normal stresses at the surface of a cylindrical pellet exposed to a uniform heat generation rate have been expressed as:[1.133]

$$\sigma_t = \sigma_z = \left(\frac{E}{1 - \mu}\right)\left(\frac{\alpha q b^2}{8k}\right) , \qquad \ldots(1.2.21)$$

where

σ_t = transverse stress

σ_z = axial stress

E = modulus of elasticity

μ = Poisson's ratio

α = coefficient of thermal expansion

q = heat generation rate

b = pellet radius

k = thermal conductivity

TABLE 1.2.8

EFFECT OF THERMAL CYCLING ON URANIUM-CARBON COMPOUNDS(1.140)

wt % C	Number of Cycles	Maximum Temperature (°F)	Maximum ΔT (°F/in.)	Maximum Diameter Change (%)
4.54	11	1350	950	1.3
4.55	13	2500	4000	2.0*
4.67	28	2600	4950	8.0*
4.90	100	2000	3600	*

*Ends extensively cracked, maximum change not measurable.

1.2.4 Chemical – Compatiblity

The compatibility of uranium carbides with gases, liquids, and solids, is summarized in Tables 1.2.9 through 1.2.11, respectively. The reaction of uranium carbides with solids are characterized by a temperature range below which no perceptible reaction occurs and above which reaction occurs at a catastrophic rate.[1.1]

TABLE 1.2.9

COMPATIBILITY OF URANIUM CARBIDES WITH GASES

Gas	Remarks
Air or O_2	Freshly cast UC oxidizes slowly at 500°C; however, reactive (aged) UC ignites in air at 370°C and in O_2 at 275°C. The rate in O_2 is five times that in air with the same partial pressure.[1.93,1.94] Bulk uranium carbide begins to oxidize in oxygen at about 300°C. An initial rapid reaction is followed by a slower reaction, probably due to the first forming oxide being adherent and somewhat protective.[1.93] $UC_2 + O_2$ reaction follows a parabolic rate law to 400°C with U_3O_8 the only solid product as determined by x-ray analysis.[1.84]
Carbon Dioxide	Between 350 and 670°C, UC reacts with CO_2 to form UO_2 and CO. Above 670°C free carbon is also formed.[1.95] The reaction rate at 500°C is greater than and similar to U and CO_2 reacting at 700 to 1000°C.[1.85]
Helium	Uranium carbides are decarburized or oxidized depending upon the partial pressure of the oxygen imposed on the system as an impurity in helium at temperatures of about 1000°C or above.[1.1]
Hydrogen	Uranium dicarbide and hydrogen react to form uranium monocarbide and methane above 700°C.[1.100] Decarburization stops at stoichiometry.[1.98]
Nitrogen	UC reacts with N_2 to form U_2N_3 and carbon below 650°C. Above 650°C U_2N_3 decomposes to UN plus N_2. The reaction rate varies with composition with the minimum rate occurring at slightly hypostoichiometric. The reaction rate also varies with nitrogen pressure; it varies to the 3/4 power of N_2 pressure. Aged UC has a higher reaction rate by a factor of 28 than freshly melted UC.[1.90] UC_2 plus N_2 reaction follows a parabolic rate law to 600 to 800°C with UN_x ($x > 1.5$) as the product.[1.84]
Miscellaneous[1.91,1.92]	$UC_2 + Cl_2 \xrightarrow{350°C} UCl_4 + CCl_4$ $UC_2 + F_2 \xrightarrow{30°C}$ no reaction $UC_2 + F_2 \xrightarrow{>30°C}$ explosion + UF_4 $UC_2 + H_2S \xrightarrow{600°C}$ ignition + US_2 $UC_2 + NH_3 \xrightarrow{\text{red heat}}$ partly decomposed UC_2

TABLE 1.2.10

COMPATIBILITY OF URANIUM CARBIDES WITH LIQUIDS

Liquid	Remarks
Liquid Metals	UC in contact with NaK at 590°C for 12 weeks showed no reaction;[1.60] for one month in NaK at 800°C no reaction occurred.[1.27] Oxygen present as an impurity in sodium and NaK oxidize uranium carbides at temperatures of 600°C and above.[1.1] UC is wetted by and bonds to iron, cobalt, nickel, and uranium.[1.5]
Miscellaneous	UC reacts with water at 80°C to form a gas containing by volume 11% H_2, 86% methane, 2% ethane, and 0.6% propane. At 90°C the reaction rate is faster. UC_2 produces less total gas with less methane but more hydrogen and ethane.[1.88] UC powder reacts with propane and butane at 650°C. At 700 to 800°C it reacts with methane and ethane.[1.98]

TABLE 1.2.11

COMPATIBILITY OF URANIUM CARBIDES WITH SOLIDS

Solid	Remarks
Aluminum	Slight reaction at 600°C and above.[1.1]
Beryllium	Reacts to form UBe_{13} at 700°C and above.[1.1]
Chromium	No reaction to 1000°C.[1.87]
Copper	No reaction at 1000°C.[1.1]
Graphite	Slight reaction at 1600°C.[1.1]
Inconel	Slight reaction at 800°C.[1.1]
Inconel X	Formed liquid eutectic at 820°C.[1.1]
Iron	No reaction to 1000°C.[1.87]
Magnesium	No reaction at 600°C.[1.1]
Molybdenum	Slight reaction at 1200°C.[1.1]
Nickel	Endebrock[1.1] reports rapid reaction at 1000°C (see Inconel X), while Borchardt[1.87] reports no reaction to 1000°C.

TABLE 1.2.11 (continued)

Solid	Remarks
Nichrome V	Melted at 1100°C (see Inconel X).[1.1]
Niobium	Slight reaction at 1100°C,[1.1] no reaction to 1000°C.[1.87]
Niobium + 4 at. % Titanium	Formed a liquid phase at 1200°C.[1.1]
Silicon	Reacts to form USi_3 at 1000°C.[1.1]
Mild Steel	Slight reaction at 1000°C.[1.1]
Type 304SS	No reaction with stoichiometric UC to 870°C; slight carburization of stainless by U_2C_3 and UC_2 at 550°C.[1.1]
Tantalum	Rapid reaction at 1800°C.[1.1]
Titanium	Slight reaction at 1100°C.[1.1]
Tungsten	Endebrock[1.1] reports rapid reaction at 1800°C, while Barnes, et al.,[1.86] reports no reaction with UC held at 1900°C for 120 min.
Zirconium	Slight reaction at 800°C.[1.1]
Zircaloy-2	Slight reaction at 820°C.[1.1]

Very little data are available on the compatibility of uranium nitrides with gases and liquids. Table 1.2.12 summarizes the data available. No data exist on the compatibility of uranium nitrides with solids.

TABLE 1.2.12

COMPATIBILITY OF URANIUM NITRIDES WITH GASES AND LIQUIDS

Substance	Remarks
Air	Catastrophic with UN above 150°C.[1.1]
Hydrogen	No reaction with UN up to 800°C.[1.1]
Nitrogen	Will probably form higher nitrides with UN up to 1300°C;[1.1] see Section 1.2.1.1.
Oxygen	Reacts with UN at 50°C; rapid reaction occurs at temperatures greater than 200°C.[1.101]
Water	Reacts with UN at 30°C; rapid reaction occurs at temperatures greater than 200°C.[1.101] Newkirk,[1.102] reports no reaction with UN at 100°C.

The compatibility of uranium oxides with gases, liquids, and solids is summarized in Tables 1.2.13 through 1.2.15, respectively.

TABLE 1.2.13

COMPATIBILITY OF URANIUM OXIDES WITH GASES

Gas	Remarks
Air	UO_2 combines with the oxygen (air) to form U_3O_8 and interstitial O_2.[1.103]
H_2	UO_2 is reduced with reaction being zero ordered with respect to the fraction UO_2 remaining.[1.104,1.105]
HF	UO_2 is reduced to $UF_4 + H_2O$.[1.106]

TABLE 1.2.14

COMPATIBILITY OF URANIUM OXIDES WITH LIQUIDS

Liquid	Remarks
BrF_3	UO_2 reacts to form $UF_6 + Br_2 + O_2$, an explosive.[1.107]
H_2SO_4	UO_2 is dissolved with a rate that is linear with time, agitation, H^+ pressure, and O_2 pressure.[1.138]
Liquid Metal	High density UO_2 in 600°C NaK for 72 hr showed no reactions.[1.36] However, Nichols[1.27] states that variable results with NaK occur in static tests.
Water	No reaction with UO_2 up to 315°C.[1.36]
Miscellaneous	No reaction between UO_2 or U_3O_8 and methane, acetylene, or benzene.[1.108]

TABLE 1.2.15

COMPATIBILITY OF URANIUM OXIDES WITH SOLIDS

Solids	Remarks
Aluminum	Harlow[1.109] indicates no reaction up to 1100°F (593°C) for 5000 hr with UO_2. However, Nichols[1.27] states that UO_2 reacts slowly with Aℓ at 500°C. At 615°C x-ray diffraction reveals that $UAℓ_3$, $UAℓ_4$, or $Aℓ_2O_3$ is formed by UO_2 with Aℓ.[1.110]
Beryllium	UO_2 does not react with Be to 600°C.[1.27]
Calcium	Reacts with UO_2 at 850°C to form U and CaO.[1.111]
Carbon	Decomposes to UC and CO_2 or CO.[1.112,1.113]
Chromium-base alloys	No reaction with UO_2 to 2000°F.[1.1]
Copper	Reacts to melting point.[1.27]
Gold	Reacts to melting point.[1.27]
Iron-base alloys	No reaction with UO_2 to 2000°F.[1.1]
Molybdenum	First reaction at 2155°C.[1.1]
Nickel	Reacts slowly with UO_2 at 1400°C.[1.27]
Nickel-base alloys	No reaction at 2000°F; reacts at 2500°F.[1.1]
Niobium	Reacts with UO_2 at 1000°C.[1.27]
Niobium-base alloys	No reaction to 2300°F.[1.1]
Rhenium	Very slight reaction at 925°C; fast reaction at 2295°C.[1.1]
Silver	Reacts to melting point.[1.27]
Stainless steel	No reaction at 2400°F.[1.1]
Tantalum	First reaction at 2295°C; fast reaction at 2420°C.[1.1]
Tungsten	First reaction at 1785°C; fast reaction at 2065°C.[1.1]
Zirconium	Reaction at 1500°F.[1.1] Nickols[1.27] indicates a reaction occurring above 1800°C.
Miscellaneous	No reaction with $Aℓ_2O_3$, MgO, and BeO to 1800°C and SiO_2 to 1600°C.[1.20]

1.3 Mechanical Properties

1.3.1 Short Time

1.3.1.1 Tensile Properties

Room temperature dynamic tensile properties of uranium + 4.8 wt % carbon, cold pressed and sintered from UC powder, with 75 to 95% of theoretical density (T. D.) are shown in Table 1.3.1. Table 1.3.2 presents modulus of elasticity results for as-cast uranium carbides as a function of carbon content and temperature.

TABLE 1.3.1

ROOM TEMPERATURE TENSILE PROPERTIES OF URANIUM + 4.8 wt % CARBON (Reference 1.114)

Bulk Density, % T.D.	Young Modulus, 10^6 psi	Shear Modulus, 10^6 psi	Poisson's Ratio, $\mu = 1/2[(E/G)-2]$
75-95	25	9.7	0.289
80	-	-	0.182
85	-	-	0.241
90	-	-	0.286
95	-	-	0.304

TABLE 1.3.2

YOUNG'S MODULUS OF AS-CAST URANIUM CARBIDES

Material (wt % C)	Temperature (°C)	Young's Modulus, 10^6 psi	Reference
U + 4.8	20	29.5	1.114
U + 7.0	20	29.0	1.114
U + 5.0	20	29.6	1.115
U + 5.0	500	28.8	1.115
U + 5.0	1000	27.2	1.115
U + 5.0	1500	20.7	1.115
U + 5.0	1700	14.8	1.115

The available tensile properties of uranium mononitride are presented in Table 1.3.3. These properties were determined by dynamic measurements on UN produced by isostatic hot pressing to a fully dense material.

TABLE 1.3.3
TENSILE PROPERTIES OF UN AT ROOM TEMPERATURE
(Reference 1.62)

Material	Young's Modulus, 10^6 psi	Shear Modulus, 10^6 psi	Poisson's Ratio
UN	30.9-31.1	14-14.3	0.1

A summary of the available room temperature tensile properties of UO_2 is presented in Table 1.3.4. The effect of temperature on the modulus of elasticity, dynamically measured, of UO_2 sintered to approximately 95% of theoretical density is shown in Figure 1.3.1.

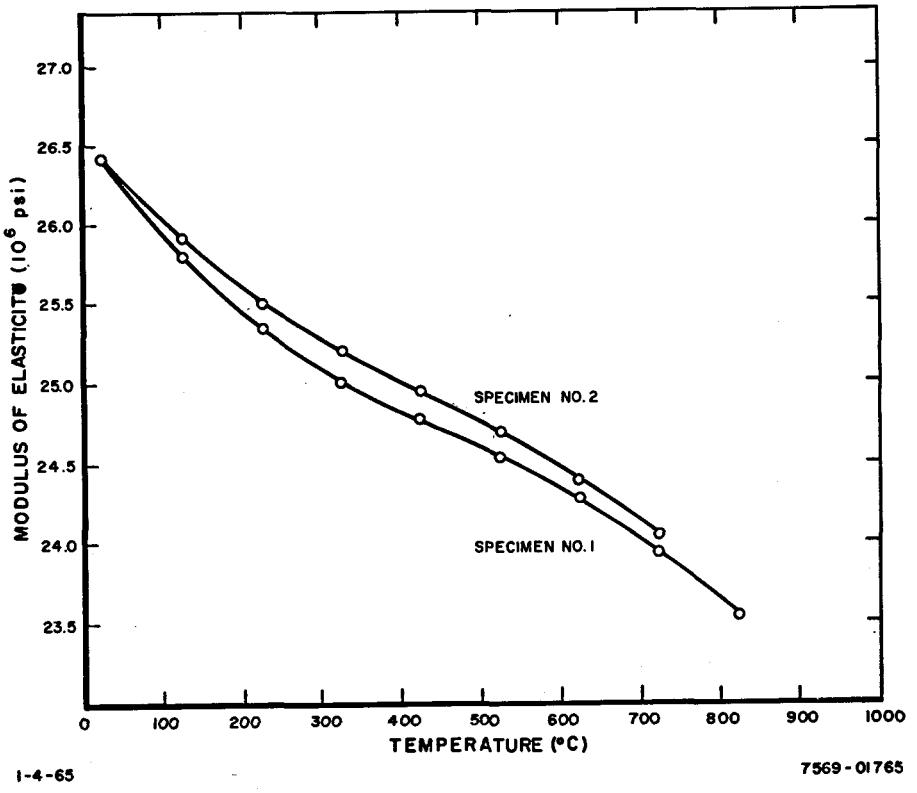

Figure 1.3.1. Modulus of Elasticity vs Temperature of UO_2 in Vacuum (Reference 1.118)

TABLE 1.3.4

ELASTIC PROPERTIES OF UO_2 AT ROOM TEMPERATURE[1.117]

Type of UO_2	Bulk Density (% T.D.)	Young's Modulus* (10^6 psi)			Shear Modulus† (10^6 psi)	Poisson's Ratio§		Bulk Modulus** (10^6 psi)	
		E_L	E_{FW}	E_{FL}		μ_L	μ_{FW}	K_L	K_{FW}
MCW cold-pressed UO_2 sintered at 1750°C in hydrogen (oxygen/uranium atom ratio = 2.02)	94.6	28.0	28.1	28.0	10.8	0.302	0.306	23.5	24.1
NH_3-precipitate cold-pressed UO_2 sintered at 1750°C in hydrogen	93.0	26.4	25.2	26.7	10.2	0.291	-	21.1	-

* E_L = Young's modulus calculated from the longitudinal resonant frequency.
E_{FW} = Young's modulus calculated from the flatwise flexural vibration.
E_{FL} = Young's modulus calculated from the edgewise flexural vibration.
†Shear modulus calculated from the torsional resonant frequency.
§ $\mu = (E/2G) - 1$.
** $K = (E/3(1 - 2\mu)$.

1.3.1.2 Transverse Rupture Strength

Room temperature transverse rupture strength data are given in Figure 1.3.2 for as-cast uranium carbides. After one month of storage in dry air the transverse rupture strength for UC (4.8 wt % carbon) decreased from 10,000 to 7,100 psi; after 1 hr of storage in water, it decreased from 10,000 to 2,400 psi.[1.115] The effect of temperature on the transverse rupture strength, determined in three point bending, of cold pressed and sintered U + 4.8 wt % C powder is presented in Table 1.3.5. Table 1.3.6 presents additional transverse rupture data on as-cast uranium carbides which illustrate the effect of temperature and carbon content. The hyperstoichiometric (excess carbon from stoichiometric) uranium carbide contained surface cracks which probably accounted for its lower strength as compared to the hypostoichiometric (deficient carbon) at room temperature. The healing of these cracks, crack blunting, and UC_2 transformation to U_2C_3 may have caused the increase in strength with temperature of the hyperstoichiometric uranium carbide.

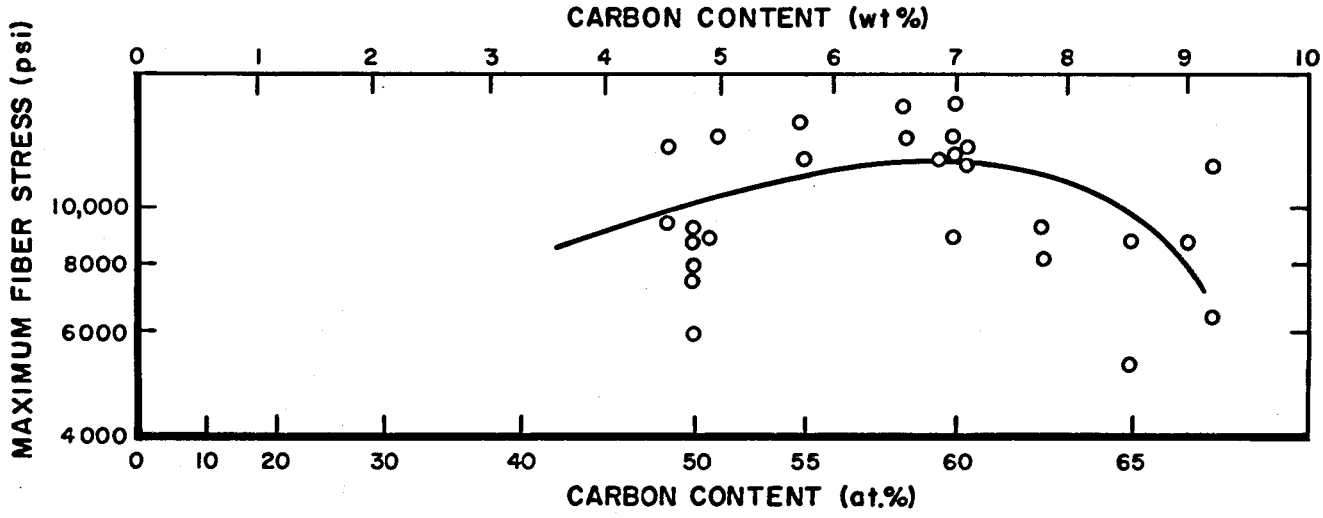

Figure 1.3.2. Room Temperature Transverse Rupture Strength of As-Cast Uranium Carbides (Reference 1.115)

TABLE 1.3.5

EFFECT OF TEMPERATURE ON THE TRANSVERSE RUPTURE STRENGTH OF COLD PRESSED AND SINTERED UC POWDER
(Reference 1.114)

Temperature (°C)	Theoretical Density (%)	Transverse Rupture Strength (10^3 psi)
25	81-83	23
800	84-87	17.6
1000	83	10
1200	83-91	Plastic

TABLE 1.3.6

TRANSVERSE RUPTURE STRENGTH IN THREE-POINT BENDING OF URANIUM CARBIDES
(Reference 1.119)

Carbon Composition* (wt %)	Strength† (Average of 6-9 Tests) (psi)			
	25 °C	600 °C	900 °C	1100 °C
4.0	-	>40,000§	-	-
4.3	32,000	32,340	6,840††	1,180††
4.5	31,700	21,470	4,550††	1,510††
4.7	-	25,190**	4,250††	2,620††
4.8	14,800	15,380	13,930	21,920
5.0	14,070	20,850	19,430	28,300
5.2	15,400	23,960	22,180	31,460

*Grain size 0.06 to 0.1 mm
†Cross head speed 0.0012 in./minute
§Exceeded capacity of Instron
**Average of three tests
††Stress at which plastic bending occurred instead of brittle fracture.

No data are available on the transverse rupture strength of UN.

Table 1.3.7 lists modulus of rupture data of UO_2 specimens made from electric-furnace fused UO_2 and from four varieties of chemically prepared UO_2. The specimens were broken by quarter-point loading with stress applied in 1000 psi increments at 20 second intervals.[1.73] Belle[1.73] illustrated with data that sintering time and surface treatment (untreated, ground with 400 grit Al_2O_3, and/or annealed at 500°C) did not appreciably affect the modulus of rupture, but the modulus was slightly higher at 1000°C test temperature than at room temperature. The effect of sintering temperature on the modulus of rupture in four point bending of sintered UO_2 is illustrated in Figure 1.3.3.

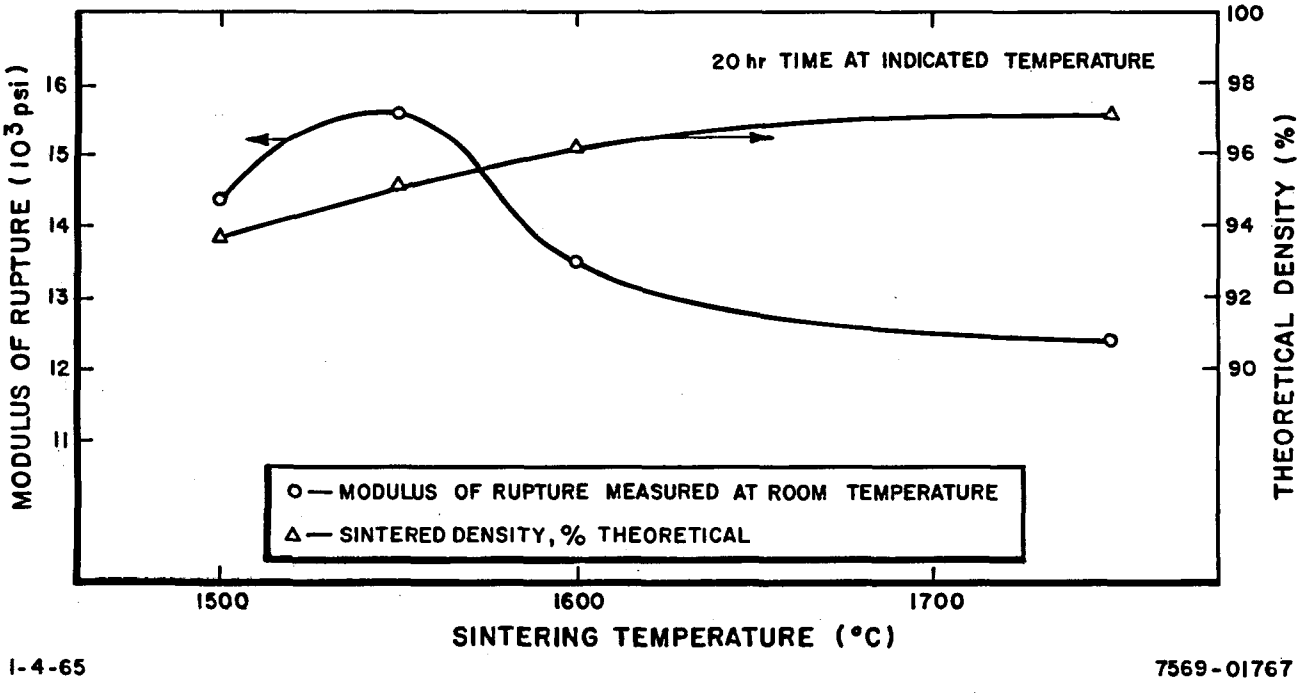

Figure 1.3.3. Modulus of Rupture and Sintered Density of UO_2 as a Function of Sintering Temperature (Reference 1.118)

TABLE 1.3.7

BEND STRENGTH AND BULK DENSITY OF DIFFERENT UO_2 CERAMICS [1.73]

Starting UO_2 Powder	Sintering Conditions*			Strength Data			
	Atmosphere	Temperature (°C)	Time (hr)	Number of Specimens	Average Modulus of Rupture (psi)	Standard Deviation (psi)	Bulk Density (gm/cm^3)
	At Room Temperature						
Fused, 0 to 5μ†	Argon	2000	1/2	4	11,990	2,370	10.10
Fused, 5 to 10μ	Argon	2000	1/2	4	9,480	1,180	9.68
Fused, 10 to 15μ	Argon	2000	1/2	6	10,270	1,040	9.14
Fused, 15 to 20μ	Argon	2000	1/2	4	8,610	1,380	8.48
Fused, 0 to 5μ	Helium	2000	1/2	9	12,920	1,261	9.89
Steam oxidized§	Helium	2000	1	8	7,340	560	8.34
Hydrogenated steam oxidized§	Helium	2000	1	7	9,580	637	8.82
Peroxide precipitated§	Helium	2000	1	6	12,400	1,610	10.04
Ammonia precipitated§	Helium	1900-2000	1	12	11,100	1,230	9.84
Steam Oxidized + 0.75 wt % TiO_2	Helium	1900	1	7	12,700	2,180	9.66
Hydrogenated steam oxidized + 0.50 wt % TiO_2	Helium	1800	1	6	14,500	3,180	10.10
Peroxide precipitated + 0.25 wt % TiO_2	Helium	1600	1	7	10,400	2,800	10.39
Peroxide precipitated + 0.2 wt % aluminum stearate	Helium	2000	1	8	12,700	1,730	10.37
Ammonia precipitated + 0.2 wt % aluminum stearate	Helium	2000	1	11	10,870	1,164	10.26
	At 1000°C						
Fused, 0 to 5μ	Argon	2000	1/2	3	17,980	900	10.02
Fused, 5 to 10μ	Argon	2000	1/2	4	15,790	1,050	9.56
Fused, 10 to 15μ	Argon	2000	1/2	6	12,590	3,170	9.17
Fused, 15 to 20μ	Argon	2000	1/2	4	8,280	1,080	8.48
Fused, 0 to 5μ	Helium	2000	1/2	9	14,900	2,020	9.89
Steam oxidized	Helium	2000	1	7	7,700	897	8.34
Hydrogenated steam oxidized	Helium	2000	1	8	10,800	1,210	8.81
Peroxide precipitated	Helium	2000	1	7	21,700	3,770	10.05
Ammonia precipitated	Helium	1900-2000	1	12	9,380	1,440	9.85
Steam oxidized + 0.75 wt % TiO_2	Helium	1900	1	7	15,600	846	9.62
Hydrogenated steam oxidized + 0.50 wt % TiO_2	Helium	1800	1	8	19,500	1,480	10.13
Peroxide precipitated + 0.25 wt % TiO_2	Helium	1600	1	6	13,600	3,060	10.39
Peroxide precipitated + 0.2 wt % aluminum stearate	Helium	2000	1	15	11,800	1,820	10.36
Ammonia precipitated + 0.2 wt % aluminum stearate	Helium	2000	1	16	9,380	1,770	10.30

*Forming: Preformed in a steel mold and then hydrostatically repressed at 45,000 psi; no binder used.
Sintering: Tungsten setter plates, inductively heated, graphite susceptor furnace.
Finishing: Specimens ground and lapped to 1/8 by 1/4 by 1-1/4 in.
†Norton Company electric-arc fused UO_2.
§Prepared by ORNL.

1.3.1.3 Compressive Strength

Room temperature compressive strength and modulus of elasticity in compression data for as-cast uranium carbides are listed in Table 1.3.8. The effect of temperature on the compressive strength of fully dense uranium carbide single crystals (4.7 to 4.9 wt % carbon) with minor substructure is shown in Figure 1.3.4. The crystals were prepared by electron beam, floating zone refining of cast rods, and hydrogen reduction of the rods to the desired composition. The samples containing UC_2 retained some of that phase at the test temperature and this seems to strengthen the UC matrix. Compression testing using the sudden change of strain rate technique gave an activation energy for flow of 70,000 to 80,000 cal/mole for samples being single phase (≤ 4.8 wt % carbon) between 1500 and 2000°C.[1.120]

Figure 1.3.5 illustrates the effect of temperature on the flow and recovery properties of nearly stoichiometric arc-cast uranium carbide (~4.75 wt % carbon). The samples were tested in compression using a stress-relaxation technique. An activation energy for flow of 74,000 cal/mole between 1500 and 1900°C was found.[1.121]

No data on the compressive strength properties of UN are available.

The effect of particle size on the room temperature compressive strength of fused UO_2 specimens is illustrated in Table 1.3.9. Specimens having a length to diameter ratio of 1:1 fractured at a slightly higher stress.[1.122]

TABLE 1.3.8

ROOM TEMPERATURE COMPRESSIVE MODULUS OF ELASTICITY AND RUPTURE STRENGTHS OF URANIUM CARBIDES (Reference 1.115)

Carbon Content (wt %)	Rupture Strength, 10^3 psi	Modulus, 10^6 psi
4.8	54.5	31.5
4.8	45.0	-
4.8	80.0	-
4.8	46.4	-
4.8	40.6	-
4.8	35.3	26.4
4.8	39.6	32.5
4.8	67.5	27.6
Average	51.1	29.5
7.0	85.4	-
7.0	67.6	-
7.0	63.4	-
7.0	60.4	-
7.0	52.6	32.1
7.0	64.7	25.9
Average	65.7	29.0

TABLE 1.3.9

ROOM TEMPERATURE COMPRESSIVE STRENGTH OF FUSED UO_2 (Reference 1.122)

Grain Size (μ)	Length/Diameter Ratio of Sample	Average Compressive Strength, 10^3 psi
0-5	2:1	140
10-15	2:1	70
15-20	2:1	60

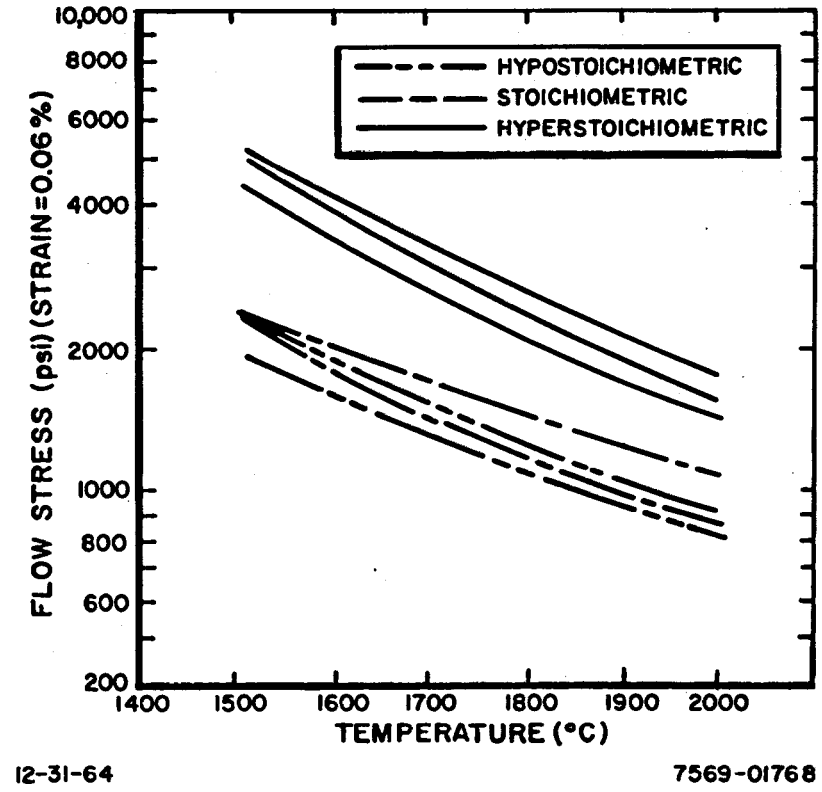

Figure 1.3.4. Flow Stress vs Temperature for Uranium-Carbon Crystals (Reference 1.120)

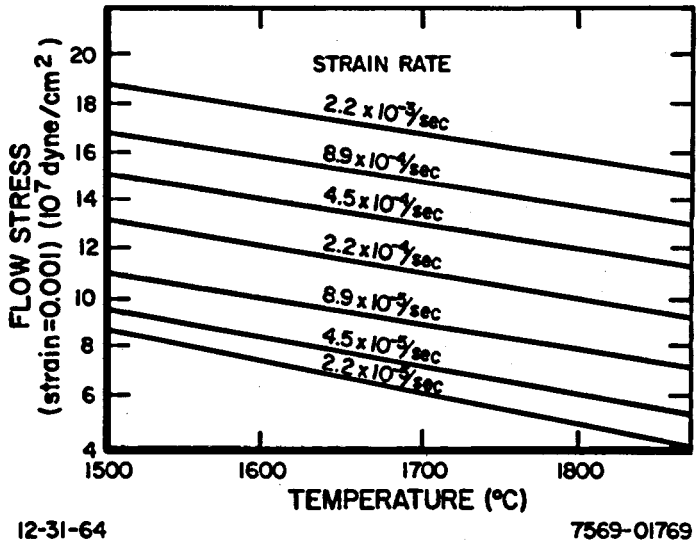

Figure 1.3.5. Flow Stress Data at Various Temperatures and Various Strain Rates for U + 4.75 wt % C (Reference 1.121)

1.3.1.4 Hardness

Room temperature hardness[1.123] of sintered U + 4.82 wt % C as a function of actual density is listed in Table 1.3.10. The effect of carbon content on the room temperature hardness of as-cast uranium carbides[1.115] is listed in Table 1.3.11. The effect of temperature on the hardness of as-cast uranium carbides is shown in Figure 1.3.6. All results were within 10% of the curve drawn in the figure, with no variation with carbon content on hardness for sample containing 4.5, 4.8, and 5.1 wt % carbon.[1.124] Additional data illustrating the effect of temperature and carbon content on hardness of uranium-carbon compounds are given in Table 1.3.12. Table 1.3.13 illustrates the effect of temperature and carbon content on the Vickers hardness (same as diamond pyramid hardness values) of as-cast uranium carbides at higher temperature than in Figure 1.3.6. Tests were conducted in a vacuum using a ZrO_2 indentor rod and a 1.0 kg load.[1.4]

Dynamic hardness properties for fully dense UN as a function of temperature are summarized in Table 1.3.14. The UN samples were made using isostatic hot pressing techniques.[1.62]

TABLE 1.3.10

ROOM TEMPERATURE VICKERS HARDNESS NUMBER FOR SINTERED UC
(Reference 1.123)

Density (gm/cc)	VHN (kg/mm^2)
10.2	550 ± 50
10.8	700 ± 50

TABLE 1.3.11

ROOM TEMPERATURE DIAMOND PYRAMID HARDNESS OF AS-CAST URANIUM CARBIDES
(Reference 1.115)

Material	DPH (kg/mm^2)
U + 4.8 wt % C (UC)	700
U + 7.0 wt % C (UC + UC_2)	750
U + 7.0 wt % C* (U_2C_3)	1100
U + 9.0 wt % C (UC_2)	500

*Material was annealed

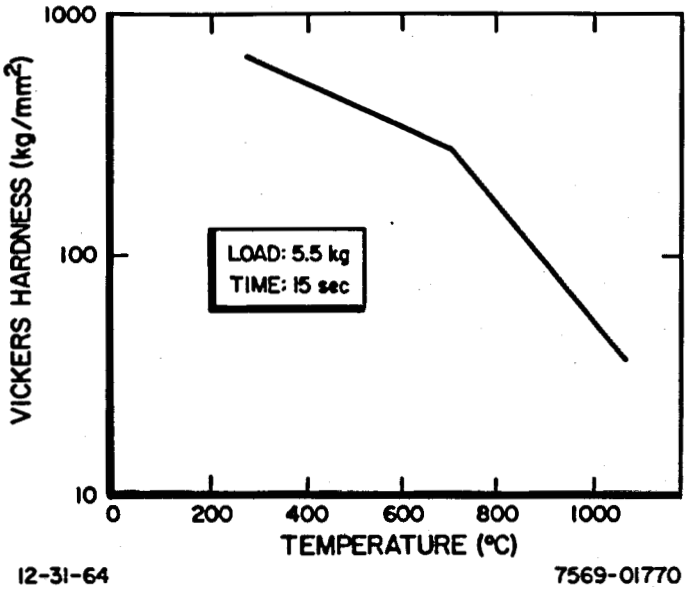

Figure 1.3.6. Hardness Variation With Temperature of As-Cast Uranium Carbides (Reference 1.124)

TABLE 1.3.12

DIAMOND PYRAMID HARDNESS NUMBER AS A FUNCTION OF TEMPERATURE AND CARBON CONTENT OF AS-CAST URANIUM-CARBON COMPOUNDS (Reference 1.142)

Temperature (°C)	DPH, kg/mm^2 (0.4 kg load)							
	Sample Number							
	1[a]	2[a]	3[b]	4[c]	5[d]	6[e]	7[f]	8[g]
25	1050	950	700	713	770	865	720	540
500	550	940	480	405	505	470	400	400
700	320	400	300	123	147	203	136	250
800	210	250	270	53	73	115	97	230

(a) 4.59- 4.63 wt % C; impurities – 0.39 wt % Si, 0.24-0.27 wt % Mo
(b) 4.76-4.81 wt % C; impurities – 100-160 ppm O and 880-920 ppm N
(c) 3.94 wt % C; impurities – 100 ppm O and 770 ppm N
(d) 4.19 wt % C; impurities – 100 ppm O, 250 ppm N
(e) 4.60 wt % C; impurities – 200 ppm O, 180 ppm N, and 800 ppm metallic impurities
(f) 4.75 wt % C; impurities – 50 ppm O, 130 ppm N, and 500 ppm metallic impurities
(g) 4.85 wt % C; single crystal; 1:0:0 orientation; high purity with less than 500 ppm of impurities

TABLE 1.3.13

VICKERS HARDNESS OF URANIUM CARBIDES AS A FUNCTION OF HIGH TEMPERATURE AND CARBON CONTENT (Reference 1.4)

Temperature (°C)	VHN* kg/mm² (1.0 kg load)					
	Sample (5 wt % C)		Sample (7 wt % C)		Sample (9 wt % C)	
	1	2	3	4	5	6
1000	780	374	†	†	679	185
1100	270	95	318	115	464	105
1200	130	30	49	43	340	66
1300	70	16	17	38	274	51
1400	40	12	8	11	203	40
1500	22	10	2	7	163	21

*Hardness numbers are averages of five measurements at each temperature.
†Indentations too small for accurate measurements.

TABLE 1.3.14

DIAMOND PYRAMID HARDNESS OF FULLY DENSE UN AS A FUNCTION OF TEMPERATURE (Reference 1.62)

Temperature (°C)	DPH (kg/mm²)
25	500 - 600
650	275
760	224
800	169
870	164
900	143
980	130
1000	123
1090	116
1100	107
1200	81
1300	64
1400	53

The effect of load on the microhardness of UO_2 is shown in Figure 1.3.7. Unannealed UO_2 single crystals prepared by arc fusion often are slightly deficient in oxygen (hypostoichiometric) and contain small inclusions of U and UN. Annealing in a hydrogen atmosphere removes these inclusions and decreases the hardness, as shown in Figure 1.3.7. The effect of oxygen content on the hardness of uranium oxides are shown in Figure 1.3.8. The samples were annealed at 900°C for 67 hr and quenched single phase UO_{2+x}. The data plotted in the figure are an average of 15 hardness impressions. The one data point shown from Lambertson and Handwerk[1.126] was obtained from an inclusion free sample of electrically fused UO_2. No load was specified.

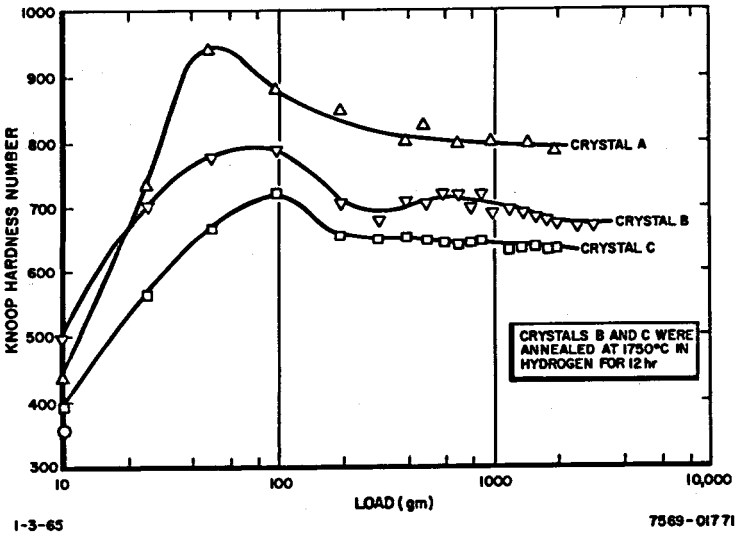

Figure 1.3.7. Microhardness of Uranium Dioxide (Reference 1.125)

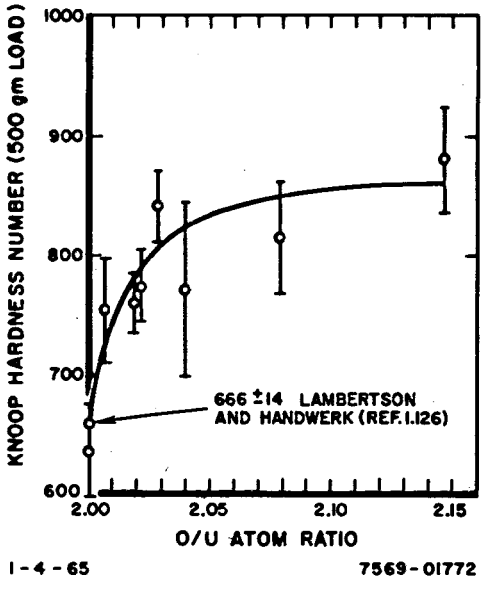

Figure 1.3.8. Effect of Oxygen Content on Hardness of UO_{2+x} Solid Solution (Reference 1.73)

1.3.2 Long Time – Creep

A few measurements have been made on the creep strength of unirradiated as-cast uranium-carbon compounds which are given in Figure 1.3.9 and Table 1.3.15.[1.143]

No data are available on the creep strength of UN. Figure 1.3.10 illustrates the effect of grain size and density on the plastic behavior of UO_2 during three point loading. The samples were prepared by pressing and sintering 2 hr at 1650°C, giving a six micron grain size and a 96% theoretical density. Longer sintering times at higher temperatures were used to obtain larger grain sizes and higher densities. Creep behavior showed grain boundary cracking. Slip along boundaries was assumed.[1.127] Figures 1.3.11 and 1.3.12 show the effect of excess oxygen and temperature, respectively, on the creep behavior of UO_{2+x}. Specimens showed grain boundary sliding during creep. Excess oxygen inhibits intercrystalline cracking found on stoichiometric uranium dioxide.[1.128] The effect of load time and oxygen content on the creep strength during bending is shown in Figure 1.3.13. Specimens were obtained by sintering in nitrogen at 1450°C for 2 hr followed by reduction in hydrogen at 1200°C for 2 hr. Sintered $UO_{2.00}$ becomes plastic only above ~1600°C, but $UO_{2.06}$ or $UO_{2.16}$ with density of >95% theoretical can be plastically deformed at about 800°C.[1.129]

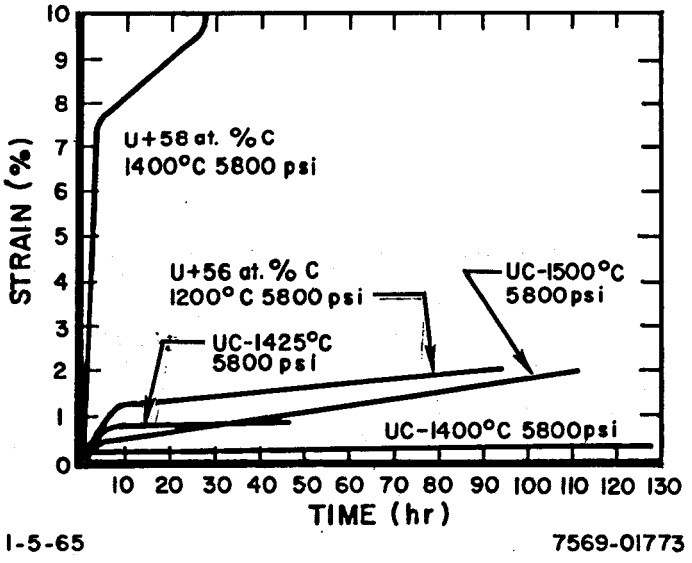

Figure 1.3.9. Creep Curves of Uranium-Carbon Compounds (Reference 1.143)

TABLE 1.3.15

CREEP RATE DATA FOR URANIUM-CARBON COMPOUNDS
(Reference 1.143)

Carbon Content		Nominal Temperature (°C)	Stress ($lb_f/in.^2$)	Test Duration (hr)	Creep Rate (% hr)	
(at. %)	(wt %)				Average	Minimum
58	6.7	1400	5800	97	0.24	0.085
56	6.5	1200	5800	94	0.025	0.010
50.5	4.8	1400	5800	128	0.0025	0.001
50.5	4.8	1500	5800	111	0.02	0.013
50.5	4.8	1425	5800	46	0.018	0.002

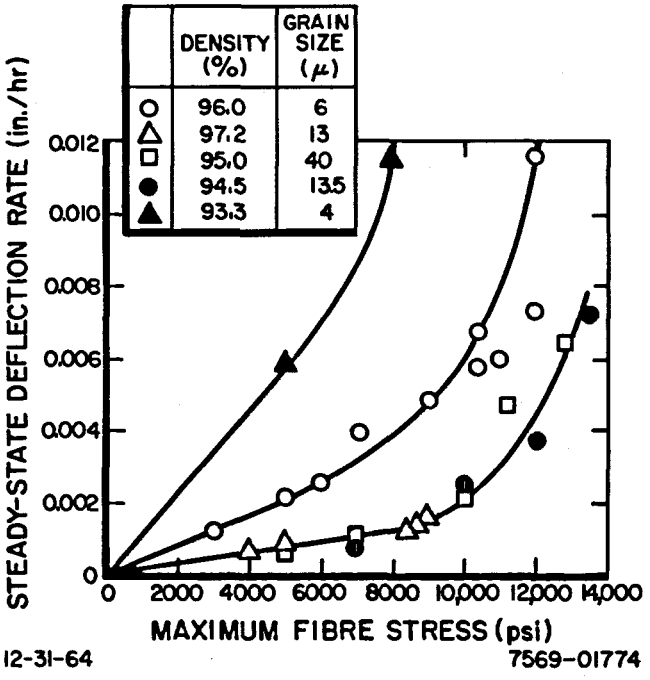

Figure 1.3.10. Effect of Grain Size and Density on Plastic Behavior of Stoichiometric UO_2 at 1400°C (Reference 1.127)

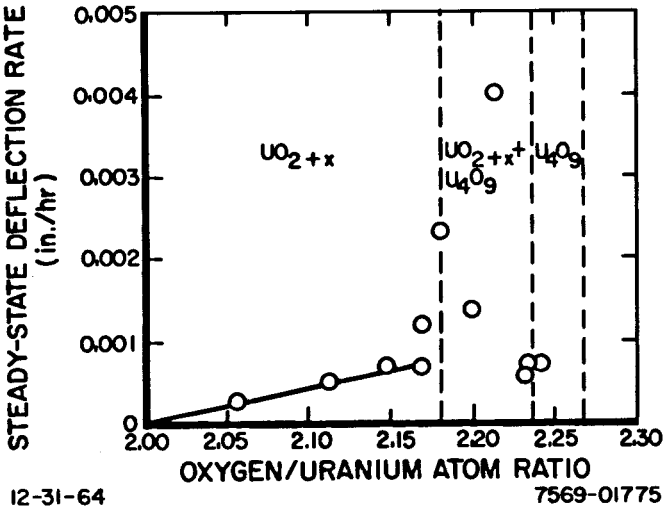

Figure 1.3.11. Steady-State Deflection Rates at 975°C (Specimens tested under a maximum fibre stress of 5000 psi) (Reference 1.128)

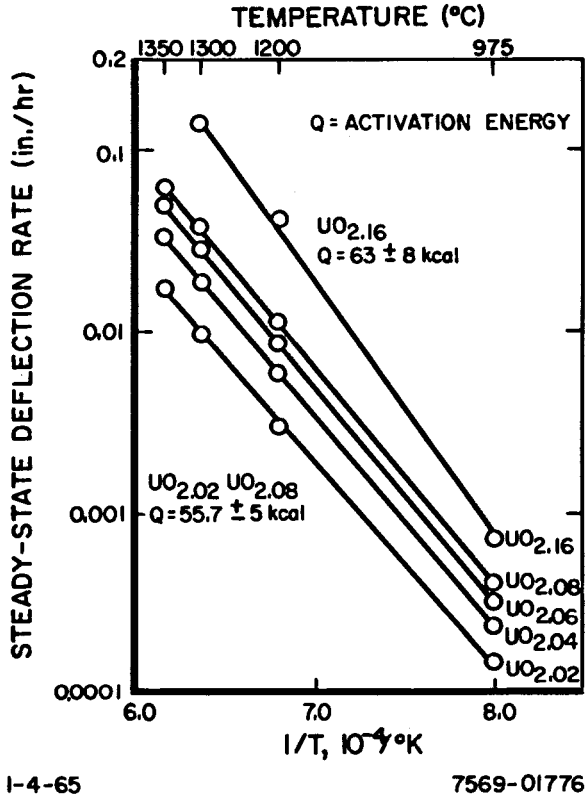

Figure 1.3.12. Arrhenius Plot for Non-Stoichiometric Uranium Dioxide (Maximum fibre stress, 5000 psi) (Reference 1.128)

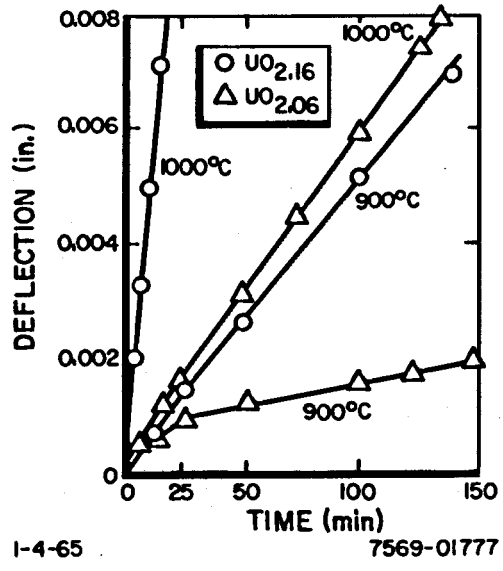

Figure 1.3.13. Creep Behavior of $UO_{2.06}$ and $UO_{2.16}$ as a Function of Temperature and Time With a 1200 gm Load (Reference 1.129)

1.4 Irradiation Properties

1.4.1 Nuclear – Cross Sections

Table 1.4.1 gives the absorption and scattering cross sections of UC, UN, and UO_2.

TABLE 1.4.1

ABSORPTION AND SCATTERING MACROSCOPIC CROSS SECTIONS OF UC, UN, AND UO_2
(Reference 1.130)

Material	Σ_a, cm^{-1}	Σ_s, cm^{-1}
UC	22.68	0.491
UN	23.70	0.692
UO_2	16.63	0.448

1.4.2 Radiation Behavior

1.4.2.1 Radiation Changes

Table 1.4.2 lists irradiation stability data on as-cast UC samples. Capsule AI-5-1, NAA-48-1, -2, -3, and -6 contained UC samples bonded with NaK in stainless steel tubes; the remaining capsules listed in the table were bonded with Na in stainless steel tubes. In general, fission gas release is assumed to be practically all by recoil and to be independent of temperature. Fission gas release in excess of 1% is believed due to extensive cracking. Cracking occurs in all the UC fuels during irradiation, but is thought to be less severe in U-rich (hypostoichiometric) fuels because of the U-phase at the grain boundaries. The changes in diameter do not follow the changes in density because of radial and axial cracking.[1.135]

Table 1.4.3 presents data on the radiation stability of UN, made by hot pressing powder techniques and obtaining approximately 100% theoretical density.

Figure 1.4.1 illustrates the effect of burnup (fission flux) on the dimensional stability of approximately 99% dense UO_2. However, Eichenberg, et al.,[1.133] points out that there is no evidence of any changes in microstructure or density during irradiation, other than those due to thermal effects. Under a thermal gradient the grains in a UO_2 fuel rod grow in a columnar manner. Bradbury[1.134] reports that sintered pellets of UO_2 irradiated at high heat ratings showed void formation along the axis of the fuel cylinder, a center region adjacent to the void with large radially oriented grains, an intermediate region of equiaxed grain growth, and an outer region with the original sintered structure. Large thermal gradients existed in this cylinder.

TABLE 1.4.2
PROPERTY CHANGES OF UC DUE TO IRRADIATION

Capsule	Carbon Content (wt %)	Average Irradiation Temperature (°F)		Burnup (Mwd/MTU)*	Fission Gas Release	Diameter Change (%)	Length Change (%)	Density Change (%)	Reference
		Center	Surface						
AI-3-1	4.4 to 4.7	1800	1250	7,500	1.58	2 to 5†	2.5 to 3	-	1.135
AI-3-4	4.8 to 5.0	1750	1200	16,600	0.18	1.8	§	-	1.135
AI-3-5	4.2 to 4.4	2110	1350	13,000 to 14,000	-	3.8 to 7.6	11.8 to 21.5	-	1.136**
AI-5-1	4.8 to 5.0	-	-	7,500	0.06	0.8	8.4	-	1.135
NAA-48-1	4.8 to 5.0	1730 to 2150	1050 to 1280	9,100	-	1 to 4	-	-	1.135
NAA-48-2	4.8 to 5.0	900 to 1530	560 to 920	23,900	1.3	0.6 to 5.0	-	-	1.135
NAA-48-3	4.8 to 5.0	1520	910	19,000	7.0	3.7	-	-	1.135
NAA-48-6	4.8 to 5.0	1750	1060	6,400	0.74	3.2 to 4.4	0.6	-	1.135
BRR-2	5 to 5.5	600	660	700	Negligible	0.16 to 0.20	-	0.29 to 0.45	1.135
BMI-23-1	5.2	980 to 1350	540 to 770	1,500	0.04	0.3 to 0.4	-	0.7 to 2.5	1.135
BMI-23-2	5.0 to 5.3	1060 to 1380	620 to 760	5,000	0.12	0.9	-	0.6 to 2.5	1.135
BMI-23-3	5.0	1080 to 1180	620 to 760	1,000	-	0.8	-	1.8	1.135
BMI-23-4	5.2	800 to 1250	460 to 760	23,000	-	1.2 to 1.4	-	3.4 to 4.4	1.135
BMI-23-5	4.5 to 4.6	1250 to 1330	720 to 880	5,000	0.04	0.8 to 1.2	-	2.4 to 1.6	1.135
BMI-23-6	4.5 to 4.8	800 to 1600	500 to 850	5,000	0.04	0.48	-	1.15 to 1.57	1.135
BRR-5	5.0	590 to 880	430 to 720	4,700	-	-	-	1.2	1.4
BRR-5	6.7	590 to 880	430 to 720	7,100	-	1.0	-	1.3	1.4
BRR-5	5.0	590 to 880	430 to 720	4,000	-	0.9	-	1.2	1.4
BRR-6	5.0	730 to 980	490 to 740	6,900	-	0.6	-	1.2	1.4
BRR-6	5.0	730 to 980	490 to 740	6,800	-	-	-	1.7	1.4
BRR-6	5.0	940 to 1070	680 to 810	7,300	-	0.2	-	0.6	1.4
BRR-6	5.0	-	-	5,600	-	0.2	-	0.9	1.4
BRR-6	5.0	-	-	5,900	-	-	-	0.3	1.4
BRR-6	5.0	-	-	6,300	-	0.2	-	0.7	1.4

*Megawatt days/Metric ton of uranium contained in the UC.
†Fuel was cracked. There were surface microcracks and a few large axial cracks in two out of six samples.
§Samples were broken. No length measurements could be made.
**It was recommended to use UC with at least 4.55 wt % C at central temperatures below 2000°F.

TABLE 1.4.3

STRUCTURE CHANGES AND FISSION GAS RELEASE OF UN DURING IRRADIATION
(Reference 1.131)

Test Number	Burnup, (at. % U)	Temperature (°C)		Fission Gas Release (%)	Structure Changes
		Surface	Center		
BMI-40-1	0.14	75	120	—	—
BMI-40-4	0.33	105	200	—	Broke into large pieces
BMI-40-5	1.40	230	650	—	Broke into large pieces
BMI-40-6	2.30	390	1260	0.4 - 0.6	Cracking, bubbles at grain boundaries

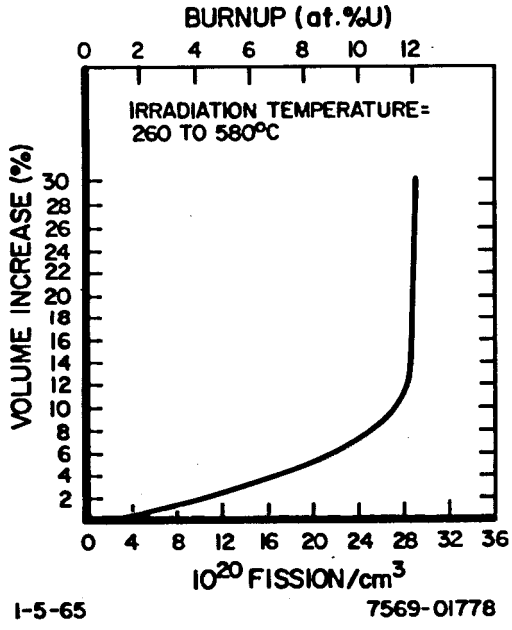

Figure 1.4.1 Effect of Irradiation to High Burnup on Dimensional Stability of UO_2 (Reference 1.132)

1.4.2.2 Property Changes

Increases in the electrical resistivity and in the lattice strain due to irradiation of UC have been observed. An increase in electrical resistivity of 2.5% was observed at a flux of 6×10^{17} thermal nvt, while an increase of over 150% at a burnup of 1.3×10^{18} fissions/cm^3 was observed.[1.1]

Wullaert[1.131] reports that on UN samples, made by hot pressing to approximately 100% density, the hardness increased from 600 to 800 DPH during irradiation to burnup ranging from 0.14 to 2.3 at. % U.

Ross[1.137] reported a change in thermal conductivity in 92% dense sintered UO_2 at 60°C after various exposure levels. The thermal conductivity saturated at a value of 30% less than that of unirradiated UO_2 for a fission density of less than 5×10^{16} fissions/cm^3 and remained unchanged to exposures of 6.7×10^{18} fissions/cm^3. However, upon annealing the samples to 1000°C for 1 hr, complete recovery of the decreased thermal conductivity due to exposure to 2×10^{16} fissions/cm^3 was noticed. With irradiation exposures over 10^{18} fissions/cm^3 the recovery was only about 50% complete.[1.73] Increasing the annealing temperature above 1000°C does not seem to increase the percentage of recovery to the thermal conductivity of unirradiated UO_2. Belle[1.73] reports that the room temperature hardness of 98% dense UO_2 increased from 625 to 830 DPH after receiving irradiation exposures of 2×10^{20} fissions/cm^3.

REFERENCES

1.1 R. W. Endebrock, Editor, "Properties of Fuels for High Temperature Reactor Concepts," BMI 1598 (November 1962)

1.2 F. A. Rough and A. A. Bauer, "Constitution of U and Th Alloys," BMI-1300 (June 2, 1958)

1.3 F. A. Rough and W. Chubb, "Progress on the Development of Uranium Carbide Type Fuels," BMI-1441 (May 31, 1960)

1.4 F. A. Rough and W. Chubb, "Progress on the Development of Uranium Carbide Type Fuels," BMI-1554 (November 1961)

1.5 R. Hallse, "Uranium Carbides - Their Properties and Preparations," NAA-SR-MEMO-2041 (August 22, 1957)

1.6 A. E. Austin, "Carbon Positions in Uranium Carbide," Acta Crystallographica 12, 159 (1959)

1.7 J. Henney, D. T. Livey, and N. A. Hill, "Some Effects of Oxygen and Nitrogen as Impurities in the Equilibria in the Uranium-Carbon System," AERE-R-4176 (January 1963)

1.8 J. M. Leitmaker and W. G. Witteman, "Dissociation Pressure of UC_2," J. Chem. Phys. 36, 1443 (1962)

1.9 L. Litz, A. B. Garrett, and F. C. Croxton, "Preparation and Structure of the Carbides of Uranium," J. Am. Chem. Soc. 70, 1918 (1948)

1.10 R. E. Rundle, et al., "The Structure of the Carbides, Nitrides, and Oxides of Uranium," J. Am. Chem. Soc. 70, 99-105 (1948)

1.11 I. Higashi, "Determination of the Lattice Constants of UC and UC_2," Kikagaku Kenkyusho Hokoku 37, 271-5 (1961)

1.12 J. Williams and R. A. Sambell, Jr., "The Variation of Unit Cell Edge of UC in Arc Melted U-C Alloys," J. Less Common Metals, 2, 352-6 (1960)

1.13 R. F. Stoops and J. V. Hamm, "Study of Phase Relationships in the U-C-O System," NCSC-2663-9 (September 1962)

1.14 M. W. Mallett, A. F. Gerds, and D. A. Vaughan, "Uranium Sesqucarbide," J. Electrochem Soc. 98, 505-9 (1951)

1.15 W. G. Witteman and M. G. Bowman, "Studies Within the System UC-UC_2," Fourth Uranium Carbide Meeting - Boston (1963)

1.16 R. W. Dayton and C. R. Tifton, "Progress Relating to Civilian Applications," BMI-1149 (December 1, 1956)

1.17 L. F. Ferguson, R. S. Street, and T. N. Waters, "High Temperature X-ray Diffraction Studies," AERE-M-819 (January 1961)

1.18 R. J. Ackermann, "The High Temperature, High Vacuum Vaporization and Thermodynamic Properties of UO_2," ANL-5482 (September 14, 1955)

1.19 J. Belle, "Properties of UO_2," A/Conf/15/p/2404 (1958)

1.20 J. R. Johnson, et al., "Technology of UO_2 as a Reactor Material," Am. Ceram. Soc. Bull. 36, 112-7 (1957)

1.21 H. W. Newkirk and J. L. Bates, "The Melting Points of UO_2, UC, and UN," HW-59468 (March 4, 1959)

1.22 R. E. Rund, N. C. Baeziger, and A. S. Wilson, "X-ray Study of the Uranium-Oxygen System," MDDC-1273 (June 3, 1947)

1.23 J. Weissbait, P. E. Blackburn, and E. A. Gulbrauesen," Further Studies on the Mechanism of Oxidation of UO_2," AECU-3729 (June 6, 1957)

1.24 R. Hashiguchi, et al., "Electrical Resistivity and Lattice Constants of UO_2," Trans. Nat'l. Research Inst. Metals (Tokyo) 2 No. 1, 1-5 (1960)

1.25 L. E. J. Roberts, "The Actmide Oxides," Second International Conference on Peaceful Uses of Atomic Energy, Proc. 28, 215-22 (1958)

1.26 N. F. H. Bright, "Examination of a Reddish Colored Sample of UO_2," MD-TR-833-CC

1.27 R. W. Nichols, "Ceramic Fuels, Properties and Technology," Nuc. Eng. 3, 327-33 (1958)

1.28 J. S. Anderson, et al., "The Properties and Microstructure of UO_2," AERE-C/R-886 (August 19, 1952)

1.29 M. W. Mallet, A. F. Gerds, and H. R. Nelson, "The Uranium Carbon System," J. Electrochem. Soc. 99, 197-204 (1952)

1.30 L. Brewer, L. A. Bromley, and P. W. Gilles, "Thermodynamic Properties and Equilibria at High Temperatures of Uranium Halides, Oxides, Nitrides, and Carbides," MDDC-1543 (September 1945)

1.31 P. Chiotti, "Experimental Refractory Bodies of High Melting Nitrides, Carbides, and UO_2," J. Am. Ceram. Soc. 35, 123-30, (1952)

1.32 M. J. Snyder and W. H. Duckworth, "Properties of Some Refractory Uranium Compounds," BMI-1223 (September 9, 1957)

1.33 T. C. Ehlert and J. L. Margrave, "Melting Point and Spectral Emissivity of UO_2," J. Am. Ceram. Soc. 41, 330 (1958)

1.34 L. G. Wisngi and S. W. Pijanowski, "The Thermal Stability of UO_2," KAPL-1702 (November 1, 1957)

1.35 W. A. Lambertson and F. H. Gunzel, "Refractory Oxide Melting Points," AECD-3465 (October 22, 1952)

1.36 W. A. Lambertson and J. H. Handwerk, "Fabrication and Physical Properties of UO_2 Bodies," ANL-5053 (February 1956)

1.37 F. A. Rough and W. Chubb, "Progress on the Development of Uranium Carbide Fuels," BMI-1370 (August 21, 1959)

1.38 S. Fijishiro, "Dissociation Pressure of UC_2," Nippon Genshiryoku Gakkaishi 3, 913-7 (1961)

1.39 P. A. Vozzella, A. D. Miller, and M. A. DeCrescente, "The Thermal Decomposition of UC," PWAC-378 (January 15, 1962)

1.40 R. J. Ackermann, P. W. Gilles, and R. J. Thom, "High Temperature Thermodynamic Properties of UO_2," J. Chem. Phys. 25, 1089-97 (1956)

1.41 R. J. Ackermann, R. J. Thom, C. A. Alexander, and M. Tetenbaum, "Free Energies of Formation of Gaseous Molybdenum, Tungsten, and Uranium Trioxide," presented at the Am. Chem. Soc. Meeting (April 1959)

1.42 W. Chubb and R. F. Dickerson, "Properties of Uranium Carbides," Am. Ceram. Soc. Bull. 41, 564-9 (1962)

1.43 F. A. Rough and R. F. Dickerson, "Uranium Carbides - Fuel of the Future," Nucleonics 18, No. 2, 74-77 (1960)

1.44 D. L. Keller, "Quarterly Progress Report to Joint US-EURATOM Research and Development Board on Development of Uranium Mononitride for the Period Ending June 30, 1961," EUR/AEC-77 (1961)

1.45 R. E. Taylor, "Electrical Resistivity of UC," Unpublished Data - Atomics International, A Division of North American Aviation, Canoga Park, California (December 1963)

1.46 L. N. Grossman, J. G. Wilson, and F. Ziskind, "Thermal Properties of UC," US/UK Research Newsletter No. 14 (1962)

1.47 R. W. Dayton and C. R. Tipton, "Progress Relating to Civilian Applications," BMI-1357 (July 1, 1959)

1.48 D. L. Keller, "Quarterly Progress Report to Joint US-EURATOM Research and Development Board on Development of Uranium Mononitride for the Period Ending June 30, 1961," EUR/AEC-77 (1961)

1.49 R. R. Hasiguti and A. R. Kiyoura, "Fundamental Researches in Physical Metallurgy of Nuclear Fuels in Japan," Second International Conference on the Peaceful Uses of Atomic Energy, Proceedings 6, 34-41 (1958)

1.50 W. H. Howland and L. F. Epstein, "Semiconductivity of UO_2," KAPL-M-WHH-1 (March 6, 1952)

1.51 B. J. Seddon, "Uranium Ceramics Data Manual, Properties of Interest in Reactor Design," DEG-Report 120 (R) 1960 p 18

1.52 R. K. Willardson, J. W. Moody, and H. J. Goering, "The Electrical Properties of Uranium Oxides," BMI-1135 (September 25, 1956)

1.53 W. Tryebiatowski, R. Troc, and J. Leciyewicz, "Magnetic Properties of Some Uranium Nitrides and Carbides," BULL ACAD POLON SPI SER SCI CHIM, 10, 395-8 (1962)

1.54 J. K. Dawson and M. W. Lister, "A Magnetic Susceptibility Study of the U-O System," AERE-C/R-447 (February 1950)

1.55 A. A. Accary and R. Caillat, "Development of Ceramic Fuel Elements in France," H. Hauser and J. Schuman Editors, Rhemhold Publ. Corp., N. Y. (1959)

1.56 D. J. Brown and J. J. Stobo, "Preparation and Properties of UC," Powder Met. in the Nuclear Age Plansee Proc. 1961, Rentle/Tyrol, Metallwork Plansee A6, 279-293

1.57 R. S. Carpenter, "Thermal Conductivity of Hypostoichiometric UC," NAA-SR-TDR-8168 (February 27, 1963)

1.58 V. C. Howard, "Thermal Conductivity of UC," IGR-TM/C-0164 (May 1958)

1.59 A. Secrest, E. Foster, and R. F. Dickerson, "Preparation and Properties of UC Castings," BMI-1309 (January 2, 1959)

1.60 C. A. Smith and F. A. Rough, "Properties of Uranium Carbide," NAA-SR-3625 (June 1, 1959)

1.61 A. Boettcher and G. Schneider, "Some Properties of UC," Second Geneva Conference on the Peaceful Uses of Atomic Energy, Proceedings 6, 561 (1958)

1.62 E. Speidel and D. L. Keller, "Fabrication and Properties of Hot Pressed Uranium Mononitride," BMI 1633 (May 1963)

1.63 J. C. Hedge and I. B. Fieldhouse, "Measurement of the Thermal Conductivity of UO_2," AECU-3381 (September 1956)

1.64 W. D. Kingery, et al., "Thermal Conductivity X: Data for Several Pure Oxide Materials Corrected for Zero Porosity," J. Am. Ceram. Soc., 37, 107 (1954)

1.65 R. W. Dayton and C. R. Tipton, "Progress Relating to Civilian Applications," BMI-1294 (October 1, 1958)

1.66 O. J. C. Runnak, "UO_2 Fuel Elements," CRL-55 (January 28, 1959)

1.67 T. Mukaibo, et al., "The Measurement of the Specific Heat of UC Above Room Temperature," IAEA Symposium SM-26/28 (May 1962)

1.68 O. H. Krikorian, "Estimation of High Temperature Heat Capacities of Carbides," UCRL-6785 (February 6, 1962)

1.69 A. Tripler, M. Snyder, and W. H. Duckworth, "Further Studies of Sintered Refractory Uranium Compounds," BMI-1313 (January 27, 1959)

1.70 D. F. Gronwold, "High Temperature X-ray Studies on Uranium Oxides in the UO_2-U_3O_8 Region," J. Morg. & Nucl. Chem. 1, 357-70 (1955)

1.71 J. S. Anderson, "Recent Work on the Chemistry of Uranium Oxides," Bull. Soc. Chem. France 20, 781-788 (1953)

1.72 B. E. Schaner, "Metallographic Determination of the UO_2 - U_4O_9 Phase Diagram," J. Nuclear Materials 2, 110-120 (1960)

1.73 J. Belle, Editor, "Uranium Dioxide: Properties and Nuclear Applications," Naval Reactors, Division of Reactor Development, USAEC (July 1961)

1.74 J. A. Stavrotakis and H. N. Barr, "Appraisal of Uranium Oxides," TID-5150 (August 3, 1953)

1.75 R. Mendez-Peñalosa, "Thermal Expansion of UC," NAA-SR-8538 (September 30, 1963)

1.76 "Fuel Cycle Development Program," NYO-2695 (November 1961)

1.77 W. R. Kerr, "Literature Survey - Uranium Mononitride," NAA-SR-TDR-7208 (March 1962)

1.78 D. L. Keller, "Quarterly Progress Report to Joint US-EURATOM Research and Development Board," EUR/AEC-169, BMI-X-178 (October 1, 1961)

1.79 K. M. Taylor and C. H. McMurtry, "Synthesis and Fabrication of Refractory Uranium Compounds," ORO-400 (February 1961)

1.80 O. H. Krikorian, "Thermal Expansion of High Temperature Materials," UCRL-6132 (September 6, 1960)

1.81 P. Murray and R. W. Thackray, "The Thermal Expansion of Sintered UO_2," AERE-M/M-22 (1955)

1.82 R. W. Dayton and C. R. Tipton, "Progress Relating to Civilian Applications," BMI-1226 (October 1, 1957)

1.83 J. D. Farr, et. al., "Preparation of UC and Its Heat of Formation," J. Phys. Chem. 63, 1455-6 (1959)

1.84 W. M. Albrecht and B. G. Kohl, "Reaction Rates of Uranium Compounds," A/Conf/15/P/710 (1958)

1.85 J. E. Antill, et. al., "Compatibility of UO_2, UC, and U With CO_2," AERE-M/M-158 (1957)

1.86 E. Barnes, et. al., "Preparation, Fabrication, and Properties of UC and U-UC Cernets," AERE-M/R-1958 (May 14, 1956)

1.87 H. J. Borchardt, "Observations of Reactions of Uranium Compounds," J. Inorg. Nuc. Chem., 12, 113 (1959)

1.88 M. J. Bradley and L. M. Ferris, "Processing UC Reactor Fuels," ORNL-3101 (August 1961)

1.89 R. W. Dayton and C. R. Tipton, "Progress Relating to Civilian Applications," BMI-1238 (December 1957)

1.90 L. A. Hayson, "Reprocessing of UC by a Nitride-Carbide Cycle. I Kinetics of Nitride Formation," NAA-SR-8388 (October 31, 1963)

1.91 H. Moissan, "Study of Uranium Carbide," Compt. Rand 122, 274 (1896)

1.92 H. Moissan, "Reactions of Uranium Carbide," Soc. Chem. France Paris 17, 14 (1897)

1.93 E. W. Murbach, "Oxidation of UC," NAA-SR-TDR-5494 (July 14, 1960)

1.94 E. W. Murbach, "Oxidation of Reactive UC," NAA-SR-6331 (July 15, 1961)

1.95 E. W. Murbach and W. D. Turner, "Oxidation of UC by CO_2," NAA-SR-7482 (December 30, 1962)

1.96 P. Murray and J. Williams, "Ceramic and Cermet Fuels," A/Conf/15/P/318 (1959)

1.97 F. D. Rosen, "The Reaction of UC Powder With Water Vapor," NAA-SR-TDR-7249 (March 28, 1962)

1.98 T. Sano, et. al., "Production of UC II Reaction Between Uranium Powder and Some Hydrocarbons," Nippon Genshiryoku Gakkaishi 2, 285-90 (1960)

1.99 B. A. Webb, "UC Compatibility With 304 Stainless Steel," NAA-SR-TDR-6190 (March 9, 1961)

1.100 L. Silverman, "The High Temperature Chemical Reactivities of the Uranium Carbides," NAA-SR-MEMO-4269 (August 1959)

1.101 K. E. Francis and N. Hodge, "Purification of Nitrogen by the Formation of Uranium Nitride," AERE-R-3710 (October 1961)

1.102 H. W. Newkirk, "Chemical Reactivity of UC and UN With Water at 100°C," HW-59408 (April 1960)

1.103 P. Murray, et al., "UO_2 as a Reactor Fuel," TID-7546 (November 1957)

1.104 W. R. De Hollander, "A Kinetic Study of the Reduction of Uranium Oxides with Hydrogen," HW-46685 (November 8, 1956)

1.105 T. R. P. Gibbs, "The Dissociation Pressure and Nature of Uranium Hydride and the Preparation of Transition Metal Hydrides," NYO-3913 (February 26, 1953)

1.106 E. K. Teter, "UF_4 Production by Continuous Methods," MCW-179 (April 11, 1947)

1.107 R. E. Greene and G. S. Petit, "Fluorination of UO_2 with BrF_3 for Mass Spectrometer Assaying," K-1137 (August 25, 1954)

1.108 J. Guon, "Reaction of UO_2 and UF_4 With Gaseous Hydrocarbons," NAA-SR-TDR-5040 (March 2, 1960)

1.109 R. A. Harlow, "Compatibility Between UO_2 and Aluminum Powdered Metallurgy Alloys at T = 650-1100°F," NAA-SR-TDR-6988 (January 3, 1962)

1.110 M. L. Picklesimer, "The Reaction of UO_2 With Aluminum," CF-56-8-135 (August 7, 1957)

1.111 R. H. Meyers, R. G. P. Mayo, and R. G. Bellamy, "Production of Uranium Powder by the UO_2-Ca Route," AERE-M/R-862 (February 8, 1952)

1.112 R. M. Powers, et al., "Carbothermic Reduction of UO_2," SCNC-241 (June 27, 1957)

1.113 W. G. Smiley, "Oxidation-Reduction Reprocessing of UC Reactor Fuels. I Carbothermic Reduction of UO_2," NAA-SR-6976 (March 15, 1962)

1.114 K. M. Taylor and C. H. McMurtry, "Synthesis and Fabrication of Refractory U Compounds," ORO-400 (May 1959)

1.115 F. A. Rough and W. Chubb, "Progress on Development of UC-Type Fuels," BMI-1488 (December 1960)

1.116 Annual Technical Progress Report, Part VII, NAA-SR-5350 (April 1, 1960)

1.117 S. M. Lang, "Properties of High Temperature Ceramics and Cermets, Elasticity and Density at Room Temperature," National Bureau of Standards, Monograph 6 (March 1960)

1.118 J. Belle and B. Lustman, "Properties of UO_2," WAPP-184 (September 1957)

1.119 G. G. Bentle and R. M. Kniefel, "The Fracture Strength of Cast UC," NAA-SR-9006 (September 1963)

1.120 G. G. Bentle, F. E. Ekstrom, and R. Chang, "The Plastic Deformation of UC Crystals," NAA-SR-8108 (September 1963)

1.121 R. Chang, "The Flow and Recovery Properties of Nearly Stoichiometric UC and the Mechanism of Work Hardening of Crystalline Solids," NAA-SR-6481 (March 1962)

1.122 M. D. Burdick and H. S. Parker, "Effect of Particle Size on Bulk Density and Strength Properties of UO_2 Specimens," Journal of American Chemical Society, 39, 181-187 (1956)

1.123 A. Boettcher and G. Schneider, "Some Properties of UC," Paper No. 964, Second Geneva Conference, Geneva, Switzerland (1958)

1.124 D. J. Brown and J. J. Stobo, "Properties of Uranium Carbides," Transact. of Brit. Cer. Soc., 62, 2, pp 177-182 (February 1963)

1.125 W. E. Roake, "Irradiation Alternation of Uranium Dioxide," HW 73072 (March 1962)

1.126 W. A. Lambertson and J. H. Handwerk, "The Fabrication and Physical Properties of Urania Bodies," ANL-5053 (February 1956)

1.127 W. R. Irvine and R. H. Martinson, Journal of Nuclear Materials, 7, p 133 (1962)

1.128 W. M. Armstrong and W. R. Irvin, "Creep Deformation of Non-stoichiometric Uranium Dioxide," Journal of Nuclear Materials, 9, No. 2, p 121 (1963)

1.129 R. Scott, et al., "The Plastic Deformation of Uranium Oxides Above 800°C," Journal of Nuclear Materials, 1, No. 1, p 39 (1959)

1.130 "Nucleonics Data Sheet," Nucleonics p 115 (August 1962)

1.131 R. A. Wullaert, "Radiation Stability of UN," BMI-1638 (June 1963)

1.132 M. Bleiberg, Progress Report, December 1960 to July 1961, WAPD-MRP-89-93 (1960-61)

1.133 J. D. Eichenberg, et al., "Effects of Irradiation on Bulk UO_2," TID-7546 (November 1957)

1.134 B. T. Bradbury, "Microstructural Changes Produced in UO_2 During Irradiation and Under the Influence of High Temperature Gradients," Journal of British Ceramic Society, Vol. 62 (February 1963)

1.135 R. D. Hahn, "A Study of Uranium Carbide and Cladding Materials for High Temperature Sodium-Cooled Reactors," NAA-SR-7696 (March 1963)

1.136 R. D. Hahn and J. F. Leirich, "High Temperature Irradiation Behavior of Uranium Carbide Fuels," NAA-SR-TDR-8241 (November 1963)

1.137 A. M. Ross, "The Dependence of the Thermal Conductivity of Uranium Dioxide on Density Microstructure, Stoichiometry, and Thermal Neutron Irradiation," CRFD-817 (September 1960)

1.138 T. L. Mackay and M. E. Wadsworth, "Kinetics of Dissolution of UO_2 in H_2SO_4," AECU-3660 (September 15, 1957)

1.139 E. E. Ritchie, Unpublished Data, Atomics International, A Division of North American Aviation, Canoga Park, California (December 7, 1964)

1.140 R. D. Hahn, Unpublished Data, Atomics International, A Division of North American Aviation, Canoga Park, California (January 27, 1964)

1.141 "Implications of U-N Phase System for UN Fuel," Nucleonics, Vol 22, No. 1, p 64 (January 1964)

1.142 G. G. Bentle and R. M. Kniefel, Unpublished Data, Atomics International, A Division of North American Aviation, Canoga Park, California (December 1962)

1.143 J. J. Norreys and M. J. Wheeler, "Compressive Creep and Some Physical Properties of Uranium Monocarbide," Trans. British Ceramic Society 62, p 183 (1963)

2.0 CERAMIC DISPERSIONS

2.1 Compositions

Properties for only two dispersions (Al_2O_3-UO_2 and BeO-UO_2) are presented in this handbook, because ample data on other dispersions were not found. The Al_2O_3-UO_2 dispersions have a eutectic at 1900° ± 10°C and 48.3 wt % UO_2. BeO-UO_2 dispersions have a eutectic at 2170 ± 20°C and 83.6 wt % UO_2; dispersions containing from 2 to 80 wt % UO_2 have been successfully fabricated and irradiated.

2.2 Physiochemical Properties

2.2.1 Physical

2.2.1.1 Phase Diagrams and Structure

Phase diagrams for the systems $Al_2O_3 + UO_2$ and $BeO + UO_2$ were worked out experimentally and presented in Figures 2.2.1 and 2.2.2 respectively. The UO_2 was reported to contain less than 430 ppm of metallic impurities and to have an O/U ratio of very close to 2. The Al_2O_3 and BeO employed were finely divided commercial grades whose purity equalled or exceeded 99.9%. The investigators found no compound and no solid solution formation in either system at temperatures from 800 to 1800°C in composition range from 10 to 90 mol % of Al_2O_3 or BeO. Both systems showed simple eutectics. For $Al_2O_3 + UO_2$ the eutectic composition and temperature was about 75 mol % Al_2O_3 and 1915 ± 15°C respectively; for $BeO + UO_2$, about 63 mol % BeO and 2150 ± 10°C.

The crystalline structure of a dispersion will contain crystalline structures of the individual compounds. The grain growth of both components of $BeO + UO_2$ dispersions have been reported to occur above 1600°C. There is marked recrystallization of BeO above 2050°C.[2.19]

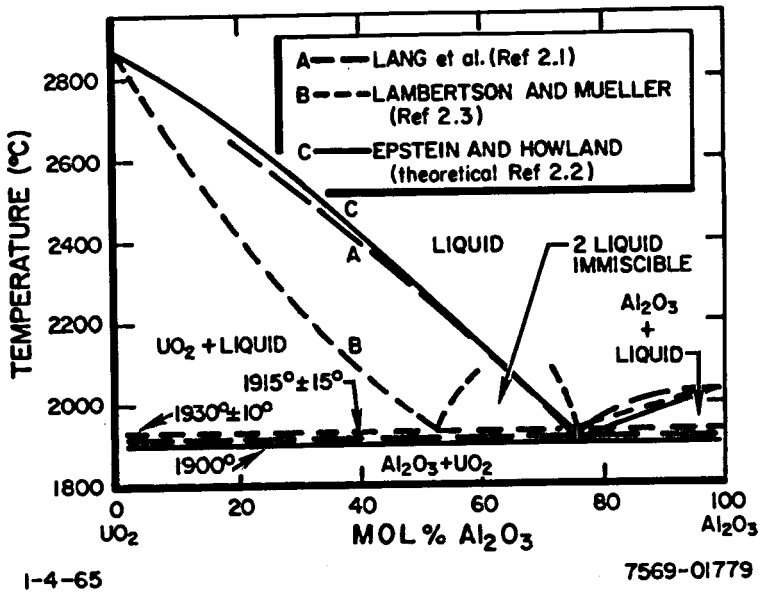

Figure 2.2.1. Phase Diagram of Al_2O_3 + UO_2 Dispersion System (Reference 2.1)

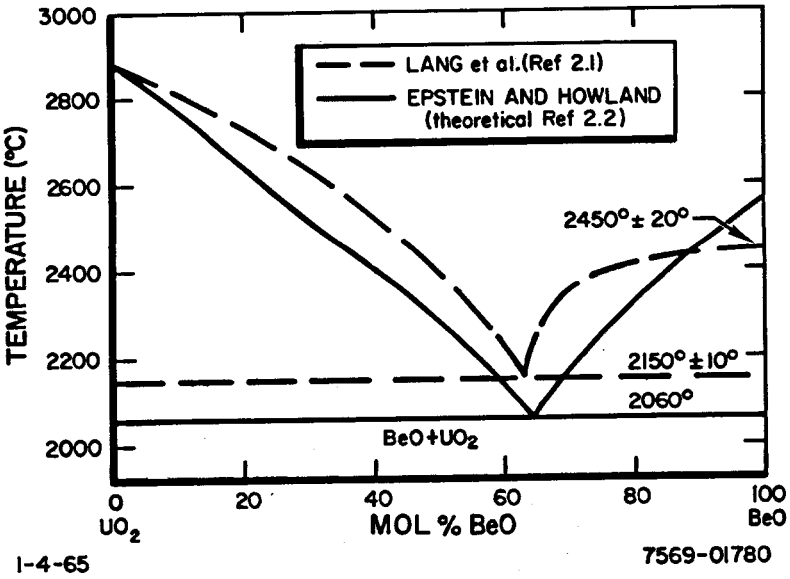

Figure 2.2.2. Phase Diagram of BeO + UO_2 Dispersion System (Reference 2.1)

2.2.1.2 Density

The theoretical density of Al_2O_3+UO_2 dispersions at room temperature can be calculated using the following equation with ρ_d (dispersion density) in units of gm/cc,

$$\rho_d = \left(\frac{\text{vol \% } UO_2}{100}\right)(10.96) + \left(\frac{\text{vol \% } Al_2O_3}{100}\right)(4.00) \quad . \qquad \ldots(2.2.1)$$

The theoretical density of BeO+UO_2 dispersions at room temperature can be calculated using the following equation with ρ_d in units of gm/cc,

$$\rho_d = \left(\frac{\text{vol \% } UO_2}{100}\right)(10.96) + \left(\frac{\text{vol \% BeO}}{100}\right)(3.03) \quad . \qquad \ldots(2.2.2)$$

2.2.2 Electrical – Electrical Resistivity

Figure 2.2.3 illustrates the effect of UO_2 content and particle size on the electrical resistivity of Al_2O_3+UO_2 dispersion at room temperature. No data are available for BeO+UO_2 dispersions.

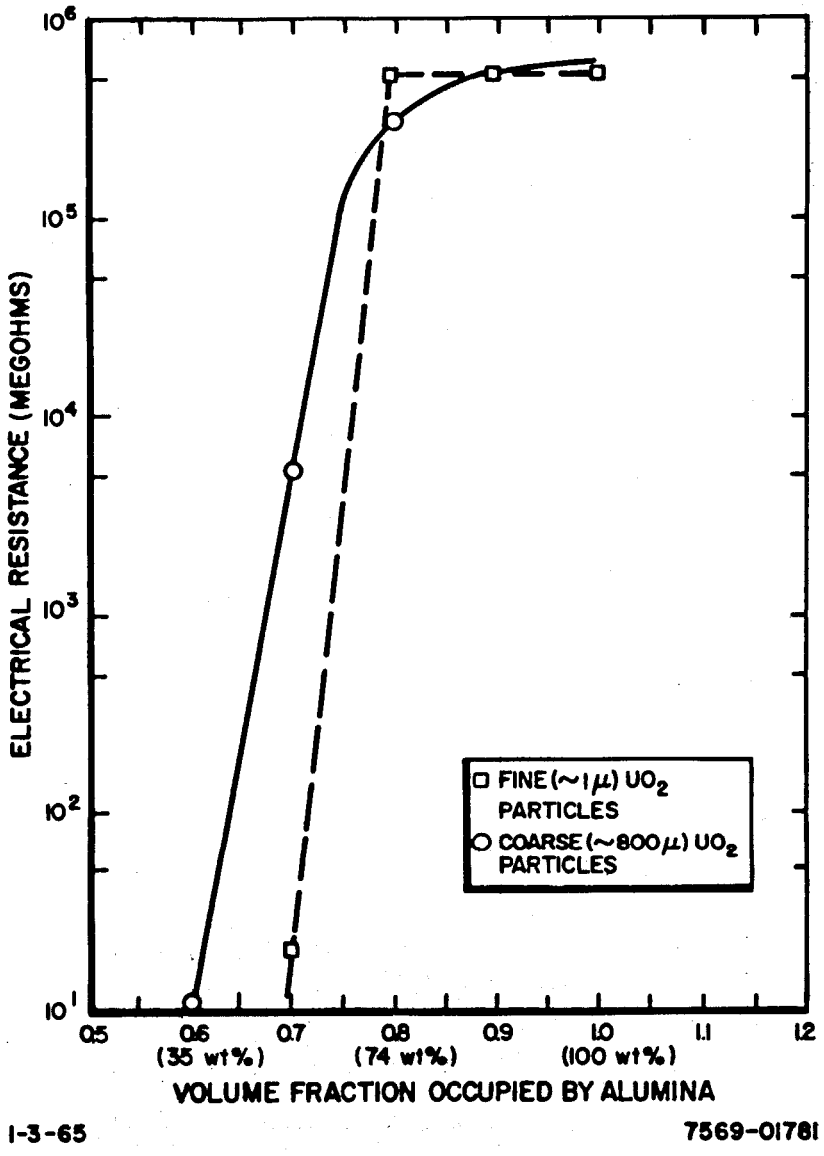

Figure 2.2.3. Electrical Resistance vs Composition for $Al_2O_3 + UO_2$ Pellets (Reference 2.19)

2.2.3 Thermal

2.2.3.1 Thermal Conductivity

No thermal conductivity data are available for Al_2O_3+UO_2 dispersions. Compacts of UO_2 and UO_2 containing up to 20 vol % (about 6.43 wt %) of BeO and sintered to about 95% of theoretical density were used to obtain theoretical conductivity measurements at temperatures up to 1000°C. These results are presented in Figure 2.2.4 and indicate that the 20 vol % addition of BeO approximately doubled the conductivity of the UO_2 compact.[2.4] This figure also presents thermal conductivity values for lower UO_2 weight percentages. No information on specimen preparation purity or the size ranges of the constituent oxides are available from these lower UO_2 wt % specimens.[2.5] In addition, these results indicate a contradictory trend in conductivity changes as the amount of UO_2 in the dispersion increases.

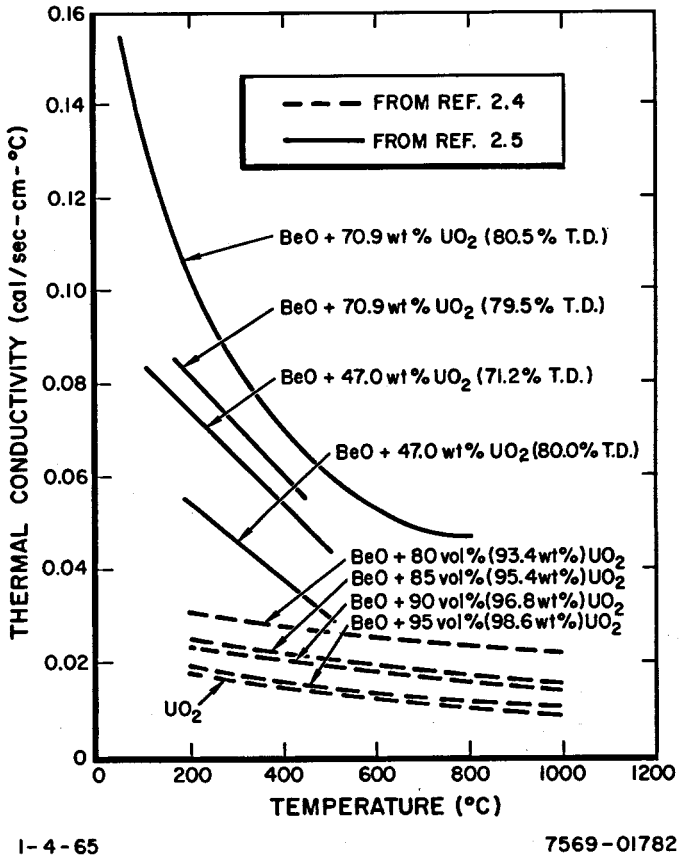

Figure 2.2.4. Thermal Conductivity of BeO + UO_2 Dispersions vs Temperature and Composition

2.2.3.2 Thermal Expansion

No data are available for Al_2O_3-UO_2 dispersions. Figure 2.2.5 illustrates the effect of temperature on the thermal expansion of cold-pressed and sintered (1850°C) BeO + 70.9 wt % UO_2. These values were measured between 100 and 400°C with a Gaertner interferometer. The bulk density of the specimen was approximately 80% of theoretical. Expansion data for UO_2 and BeO are included for comparison.[2.6] Figure 2.2.6 gives thermal expansion values as a function of temperature of hot-pressed BeO, UO_2 and BeO + UO_2 mixture. Mixtures of BeO were up to 10 wt % (about 3 vol %) of UO_2 with hot-pressed in graphite dies to bulk densities exceeding 98% of theoretical. No data were available on carbon contamination or O/U ratio of the UO_2 with gm in reference 2.7. Thermal expansion measurements up to 800°C showed UO_2 additions having negligible effect on the thermal expansion of BeO. Table 2.2.1 contains coefficient of linear thermal expansion data on compacts of UO_2 and UO_2 containing up to 20 vol % (about 6.43 wt %) of BeO which were sintered to about 95% of theoretical density. These data up to 1100°C indicate that BeO additions have negligible effect, within the limits of experiments on the thermal expansion.

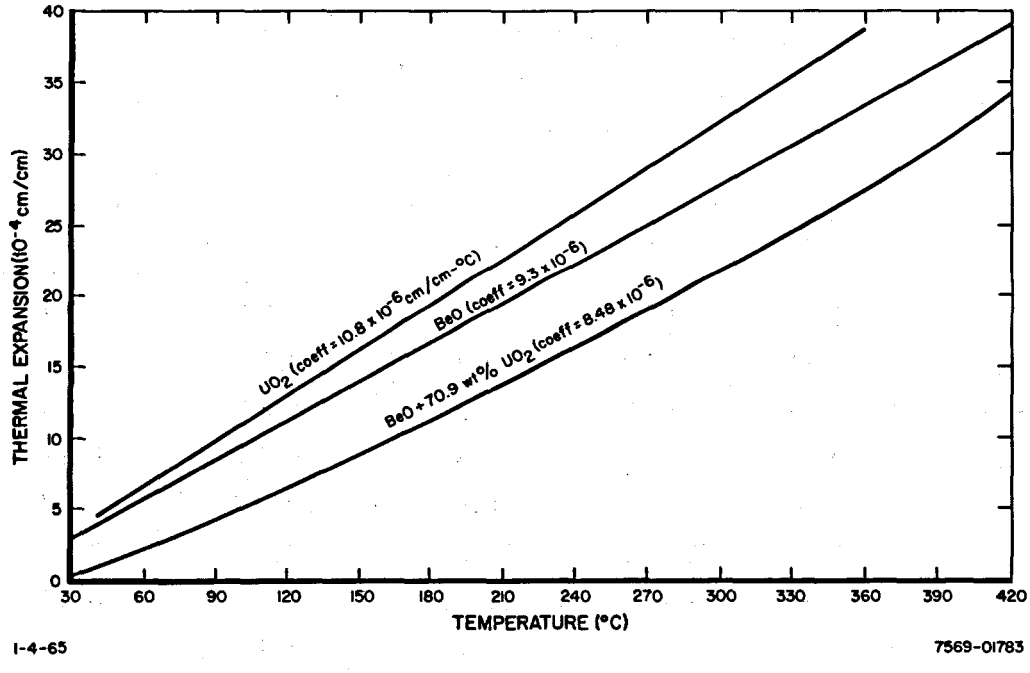

Figure 2.2.5. Thermal Expansion of BeO + 70.9 wt % UO_2 for Low Temperatures (Reference 2.6)

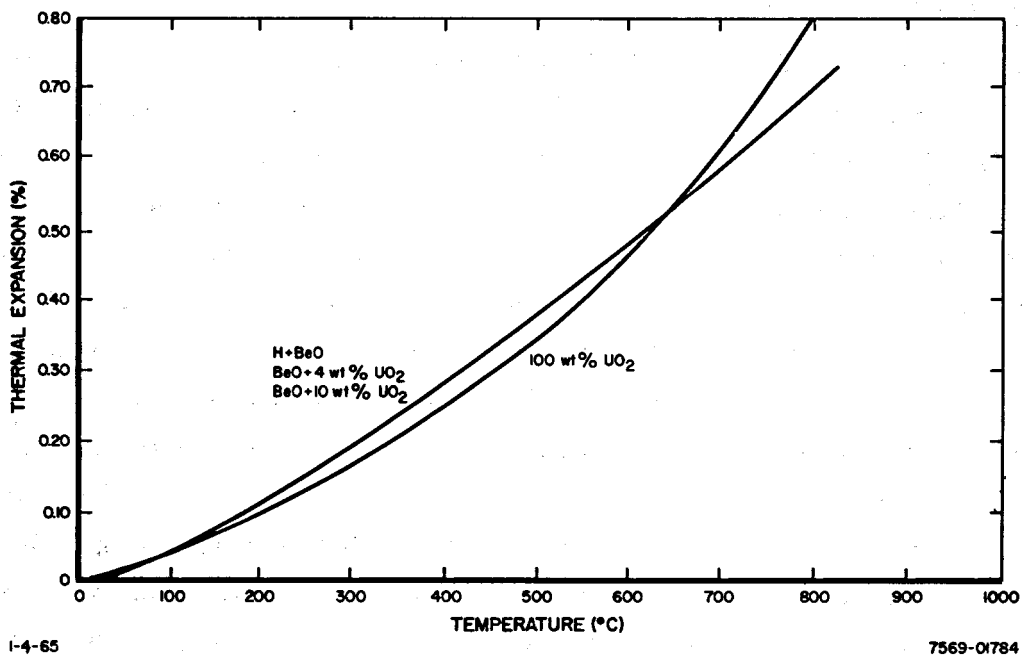

Figure 2.2.6. Thermal Expansion of Hot Pressed H-BeO, UO_2, and BeO-UO_2 Mixture (Reference 2.7)

TABLE 2.2.1

COEFFICIENTS OF THERMAL EXPANSION OF UO_2, BeO, AND BeO + UO_2 DISPERSION COMPACTS (Reference 2.4)

Temperature Range (°C)	Coefficient of Linear Thermal Expansion* (10^{-6} cm/cm-°C)					
	UO_2	5 Vol % BeO	10 Vol % BeO	15 Vol % BeO	20 Vol % BeO	BeO
20 to 200	9.13	9.06	8.96	8.88	8.98	7.1
20 to 400	9.55	9.50	9.32	9.22	9.09	8.6
20 to 600	9.83	9.75	9.54	9.60	9.49	9.6
20 to 800	10.04	10.14	9.80	9.80	9.82	10.3
20 to 1000	10.27	10.39	10.07	10.03	10.07	10.9
20 to 1100	10.36	10.41	10.16	10.16	10.13	-
400 to 800	10.51	10.75	10.26	10.36	10.52	-
800 to 1100	11.36	11.31	11.25	11.10	-	-

*Estimated accuracy ± 0.2 x 10^{-6} cm/cm-°C

2.3 Mechanical Properties — Short Time

The tensile modulus of rupture for Al_2O_3 + 33 wt % UO_2 (60% T. D.) is in the range of 1900 to 3300 psi.[2,20] Tensile and compressive properties of BeO-UO_2 dispersions are summarized in Table 2.3.1.

TABLE 2.3.1

MECHANICAL PROPERTIES OF BeO-UO_2 DISPERSIONS AT ROOM TEMPERATURE (Reference 2.19)

UO_2 Content, (wt %)	% of Theoretical Density	Young's Modulus, 10^6 psi	Bending Strength, 10^3 psi	Compressive Strength, 10^3 psi
2	98	—	27.6	—
10	98	—	32.8	—
10	91.5	49.3	—	188
10	88.4	44.2	—	155

2.4 Irradiation Properties

2.4.1 Nuclear Cross Sections

Table 2.4.1 illustrates the effect of UO_2 content on the macroscopic absorption and scattering cross sections for thermal neutrons of BeO + UO_2 dispersions. Calculations were performed assuming absorption and scattering properties of individual compounds being retained when mixed together to form the dispersion fuels.

TABLE 2.4.1

CALCULATED THERMAL ABSORPTION AND SCATTERING CROSS SECTIONS OF BeO + UO_2 DISPERSIONS

UO_2 Content		Cross Sections of Dispersion	
Vol %	Wt %	Σ_a, cm^{-1}	Σ_s, cm^{-1}
0	0	0.000599	0.798
10	28.65	1.66	0.763
20	47.45	3.33	0.728
30	60.72	4.99	0.693
40	70.60	6.65	0.658
50	78.23	8.32	0.623
60	84.31	9.98	0.588
70	89.26	11.64	0.553
80	93.38	13.30	0.518
90	96.85	14.97	0.483
100	100.00	16.63	0.448

2.4.2 Radiation Behavior

Table 2.4.2 illustrates the effect of neutron irradiation on the density of Al_2O_3 + 21 wt % UO_2. Bleiburg[2.9] indicated there was a loss of diffraction pattern and no grain boundaries were visible in Al_2O_3 after 10^{20} fissions/cm^2. Figure 2.4.1 illustrates the effect of uranium burnup on the density of Al_2O_3 + 21 wt % UO_2 after irradiation.

Pellets containing BeO and 48.3 wt % (19.1 vol %) of UO_2 particles (125 microns in diameter), and having an enrichment of about 30% were encapsulated and irradiated by flux of about 0.3×10^{14} nv thermal unperturbed. The average sintered bulk density was about 93.8% of theoretical. The estimated specimen temperature during irradiation was between 2200 and 2300°F. The integrated thermal flux was about 3×10^{20} nvt; the fission density was estimated as 2×10^{20} fissions/cm^3 per pellet (10^{21} fissions/cm^3 of UO_2); the irradiated compact (BMI-31-3) was closed after reactor exposure, and the BeO was separated from the UO_2. The BeO powder was analyzed by X-ray diffraction using the Debye-Sherrer method. No change was found in the lattice parameter, c, spacing as a result of irradiation. A lattice parameter, a, was increased by 0.74%. Dimensions and densities of the irradiated pellets were measured. Comparison with previous experiments conducted by Johnson[2.11] is shown in Table 2.4.3. Statistical analysis of dimensional data show that there was essentially no change in the dimensions of the pellets. Strength of these pellets before and after irradiation is presented in Table 2.4.4. The data shown indicate that the strength was decreased by about 21% as a result of the neutron exposure.

Table 2.4.5 illustrates the effect of irradiation on the density and fuel thickness of BeO + UO_2 dispersions containing from 25.3 to 59 wt % UO_2. The effect of irradiation on the mechanical properties of a BeO + UO_2 dispersion is illustrated in Table 2.4.6

TABLE 2.4.2

IRRADIATION EFFECT ON DENSITY OF Al_2O_3 + 21 wt % UO_2
(Reference 2.9)

Material	Burnup, 10^{20} fissions/cc	at. % U^{235}	Thickness Change (%)	Irradiation Temperature (°C)	Density Change (%)
Al_2O_3 + 21 wt % UO_2	2.7	14	+10	290	-18.5
	2.3	12	+10	290	-19.5
	1.3	6.5	+10	290	-17.9
	10.8	55	+10	290	-19.7
	6.9	35	+10	290	-18.8
	5.3	36	+10	290	-17.4

TABLE 2.4.3

DIMENSIONS AND DENSITIES OF BeO + 19.1 VOLUME % UO_2 FUEL PELLETS BEFORE AND AFTER IRRADIATION
($\sim 2 \times 10^{20}$ fissions/cm^3 of pellet)
(Reference 2.11)

Pellet No.	Diameter			Length			Measured Density		
	Pre-irradiation (in.)	Post-irradiation (in.)	Change (%)	Pre-irradiation (in.)	Post-irradiation (in.)	Change (%)	Pre-irradiation (g/cm^3)	Post-irradiation (g/cm^3)	Change (%)
15171-50-6	0.2218	0.2223	+0.2	0.2494	0.2515	+1.0	4.38	-	-
15171-50-7	0.2226	0.2225	-0.05	0.2499	0.2510	+0.5	4.36	-	-
15171-50-10	0.222	0.2225	+0.2	0.2485	0.2505	+1.0	4.35	-	-
15171-50-12	0.2223	0.2225	+0.1	0.2508	0.2505	-0.1	4.35	-	-
15171-50-13	0.222	0.2203	-1.0	0.2503	0.2503	0	4.42	4.37	-1.
15171-50-14	0.2241	0.2221	-1.0	0.2493	0.2501	+0.4	4.32	4.30	-0.
15171-50-17	0.2229	0.222	-0.4	0.2501	0.2505	+0.2	4.32	4.33	+0.15
15171-50-24	0.2227	0.2223	-0.2	0.2510	0.251	0	4.32	4.33	+0.15

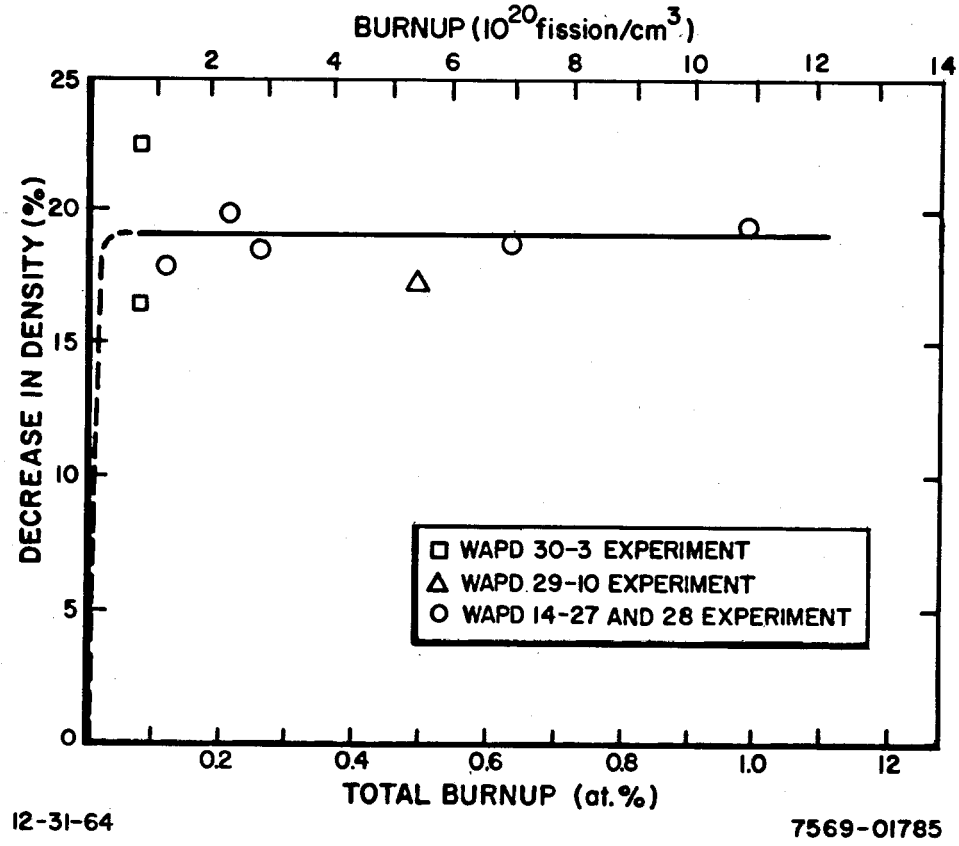

Figure 2.4.1. Increase in Volume of Al_2O_3 + 21 wt % UO_2 on Irradiation (Reference 2.10)

TABLE 2.4.4

CRUSHING STRENGTH OF BeO + UO_2 FUEL PELLETS FROM BMI-31-3 CAPSULE (~2 x 10^{20} fissions/cm^3 of pellet) (Reference 2-11)

Unirradiated Pellets (psi)	Irradiated Pellets (psi)
93,800	91,500
86,500	58,600
78,500	55,400
86,300 (average)	68,500 (average)

TABLE 2.4.5

EFFECT OF IRRADIATION ON DENSITY AND FUEL THICKNESS OF BeO + UO_2 DISPERSIONS

Material	Density (%)	Burnup (10^{20} fission/cm^3)	U^{235} Content (at. %)	Irradiation Temperature (°F)	UO_2 Structure	Fission Gas Release (%)	Fuel Thickness Change (%)	Density Change (%)	Reference
BeO + 25.3 wt % UO_2	96	11.1	–	890	fine*	19.9	+27.3	–	2.17
BeO + 28.2 wt % UO_2	96	13.5	59	550	coarse†	3	+3.0	–	2.12, 2.13, 2.14
BeO + 28.7 wt % UO_2	90	12.1	–	930	coarse	6.9	+5.8	–	2.17
BeO + 29.9 wt % UO_2	96	13.0	51	550	extra fine§	8	+15.0	–	2.12, 2.13, 2.14
BeO + 30.1 wt % UO_2	91	10.7	–	830	coarse	–	+10.5	–	2.17
BeO + 34.6 wt % UO_2	96	13.0	43	550	coarse	3	+8 (cracked)	–	2.12, 2.13, 2.14
BeO + 34.6 wt % UO_2	96	13.0	43	550	extra fine	8	–	–	2.12, 2.13, 2.14
BeO + 48 wt % UO_2	89	0.5	1.6	840	coarse	0.4	–	–	2.16
BeO + 59 wt % UO_2	97	0.8	2	890	coarse	0.001	+0.5	-0.8	2.15
BeO + 59 wt % UO_2	97	0.8	2	775	coarse	0.001	+0.2	-1.8	2.15
BeO + 65 wt % UO_2	89	10	15	550	coarse	–	+1.7	–	2.12, 2.13, 2.14

*50 micron diameter particle size
†150 micron diameter particle size
§< 4 micron diameter particle size

TABLE 2.4.6

EFFECT OF IRRADIATION ON THE MECHANICAL PROPERTIES OF $BeO + UO_2$ DISPERSIONS (Reference 2.18)

Material wt % UO_2	Density (%)	UO2 Structure	Burnup (10^{18} fissions/cm^3)	U^{235} Content (at. %)	Irradiation Temperature (°C)	Linear Expansion (%)	Thermal Resistance Change (%)	Elastic Modulus Change (%)	Compressive Strength Change (%)	Bending Strength Change (%)
2	91.5	fine*	2.2	1.75	250	0.51	+475	-21.6	-19	-
2	91.5	fine	5.3	4.27	250	0.60	+525	-25.0	-12	-
2	91.5	fine	8.9	7.18	250	0.60	+592	-28.3	-18	-
2	93.1	fine	2.2	1.75	250	0.48	+575	-17.8	-	-
2	93.1	fine	5.4	4.27	250	0.66	+604	-27.5	-	-
2	93.1	fine	9.1	7.18	250	0.65	+656	-27.9	-	-
10	87.5	fine	1.1	1.77	600	0.61	+414	-23.9	-32	-
10	87.5	fine	2.3	3.61	600	0.74	+465	-25.1	-30	-
10	87.5	fine	3.9	6.22	600	0.78	+566	-28.3	-28	-
10	93.2	fine	1.2	1.77	600	0.59	-	-	-27	-
10	93.2	fine	2.4	3.61	600	0.62	+554	-23.3	-23	-
10	93.2	fine	4.2	6.22	600	0.81	+616	-30.7	-28	-

*<4 microns diameter particle size

REFERENCES

2.1 S. M. Lang, et al., "High Temperature Reactions of UO_2 with Various Metal Oxides," NBS-C-568, United States Department of Commerce, National Bureau of Standards (February 1956)

2.2 L. F. Epstein and W. H. Howland, "Binary Mixtures of UO_2 and Other Oxides," Journal of American Ceramic Society, 36, p 334 (1953)

2.3 W. A. Lambertson and M. H. Mueller, "Uranium Oxide Phase Equilibrium Systems: I - $UO_2 + Al_2O_3$," J. American Ceramic Society, 36, p 329 (1953)

2.4 "Fabrication of UO_2 and UO_2 + BeO Mixed Pellets," Final Report, December 15, 1960 to April 30, 1962, EURAEC-369, Battelle Institute e.v., Frankfurt am Main (1962)

2.5 L. R. McCreight, "Thermal Conductivity Data for Some Nuclear Fuels," KAPL-822 (October 1952)

2.6 L. R. McCreight, "Thermal Expansion Measurements of Six Fuel Materials," KAPL-M-LRM-7 (January 1952)

2.7 K. Kida, S. Nishigaki, and R. Ueda, "Study on the Fabrication of the BeO + UO_2 Sintered Body by Means of Vacuum Hot Pressing," J. of the Atomic Energy Society of Japan, 3, no. 3, p 200 (1961)

2.8 P. O. Budnikov, "Binary Phase Diagrams for $UO_2 + Al_2O_3$, UO_2 + BeO, and UO_2 + MgO," Paper 2193, Geneva Conf. 1958, Geneva, Switzerland

2.9 M. L. Bleiburg, K. M. Berman, W. Yeniscavich, "Fission Fragment Damage to Crystal Structures," J. Nucl. Mat., Vol. 2, No. 2, p 129 (1960)

2.10 D. E. Johnson and J. M. Tobin, Proceedings of BeO Meeting, ORNL, TID-7602, Pt. 1 (December 1960)

2.11 D. E. Johnson, "Stability of BeO-UO_2 Reactor Fuel Material During Irradiation," GA-2065 (March 31, 1961)

2.12 A. Albreckt and K. Mandeville, "Storage of Energy in BeO," Phys. Rev. 101, 4, p 1250 (1956)

2.13 Pressurized Water Reactor Project Progress Report, January-February 1960, WAPD-MRP-84, pp 72-73

2.14 Pressurized Water Reactor Project Progress Report, October-December 1959, WAPD-MRP-83, p 69

2.15 Army Gas-Cooled Reactor Systems Program Progress Report, April-June 1960, IDO-28558, p 163

2.16 R. W. Dayton and C. R. Tipton, Jr., Progress Relating to Civilian Applications During July 1959, BMI 1366

2.17 Bettis Technical Review, Reactor Technology, WAPD-BT-20, p 7 (September 1960)

2.18 J. R. Gilbreath and A. C. Simpson, "The Effect of Reactor Irradiation on the Physical Properties of BeO," Paper 621, Geneva Conf. 1958, Geneva, Switzerland

2.19 R. W. Endebrock, Editor, "Properties of Fuels for High-Temperature Reactor Concepts," BMI-1598 (November 1962)

3.0 CERMETS

3.1 Composition

Properties for only three cermets (Mo-UC, -UN, and -UO_2) are presented in this handbook due to the fact that data found on other cermets were insufficient. Cermets containing 60 to 80 vol % UC, 60 to 90 vol % UN, or 60 to 90 vol % UO_2 dispersed in molybdenum have been successfully fabricated.

3.2 Physiochemical Properties

3.2.1 Physical – Density

Calculated densities (external dimension divided by weight) of molybdenum-uranium carbide cermets range from 12.27 to 12.95 gm/cm^3 over a 60 to 90 vol % (65.5 to 90.9 wt %) UC loading.[3.1] The theoretical density of Mo + UC cermets can be calculated using the following equation with ρ_c (cermet density) in units of gm/cc,

$$\rho_c = \left(\frac{\text{vol \% Mo}}{100}\right)(12.25) + \left(\frac{\text{vol \% UC}}{100}\right)(13.63) \quad . \qquad \ldots(3.2.1)$$

Calculated density of Mo + 80 vol % (82.4 wt %) UN was found to be 13.5 gm/cc.[3.1] The theoretical density of molybdenum-uranium carbide cermets can be calculated using the following equation with ρ_c in units of gm/cc.

$$\rho_c = \left(\frac{\text{vol \% Mo}}{100}\right)(12.25) + \left(\frac{\text{vol \% UN}}{100}\right)(14.32) \quad . \qquad \ldots(3.2.2)$$

Calculated density of Mo + 80 vol % (82 wt %) UO_2 was found to be 10.81 gm/cc.[3.1] The theoretical density of molybdenum-uranium oxide cermets can be calculated using the following equation with ρ_c in units of gm/cc,

$$\rho_c = \left(\frac{\text{vol \% Mo}}{100}\right)(12.25) + \left(\frac{\text{vol \% } UO_2}{100}\right)(13.96) \quad . \qquad \ldots(3.1.3)$$

3.2.2 Electrical – Electrical Resistivity

Figure 3.2.1 illustrates the effect of temperature on the electrical resistivity of molybdenum-uranium carbide cermets.

The effect of temperature on the electrical resistivity of Mo + 80 vol % UN cermet is illustrated in Figure 3.2.2.

Results on the effect of temperature on the electrical resistivity of Mo + 80 vol % UO_2 cermet are given in Figure 3.2.3.

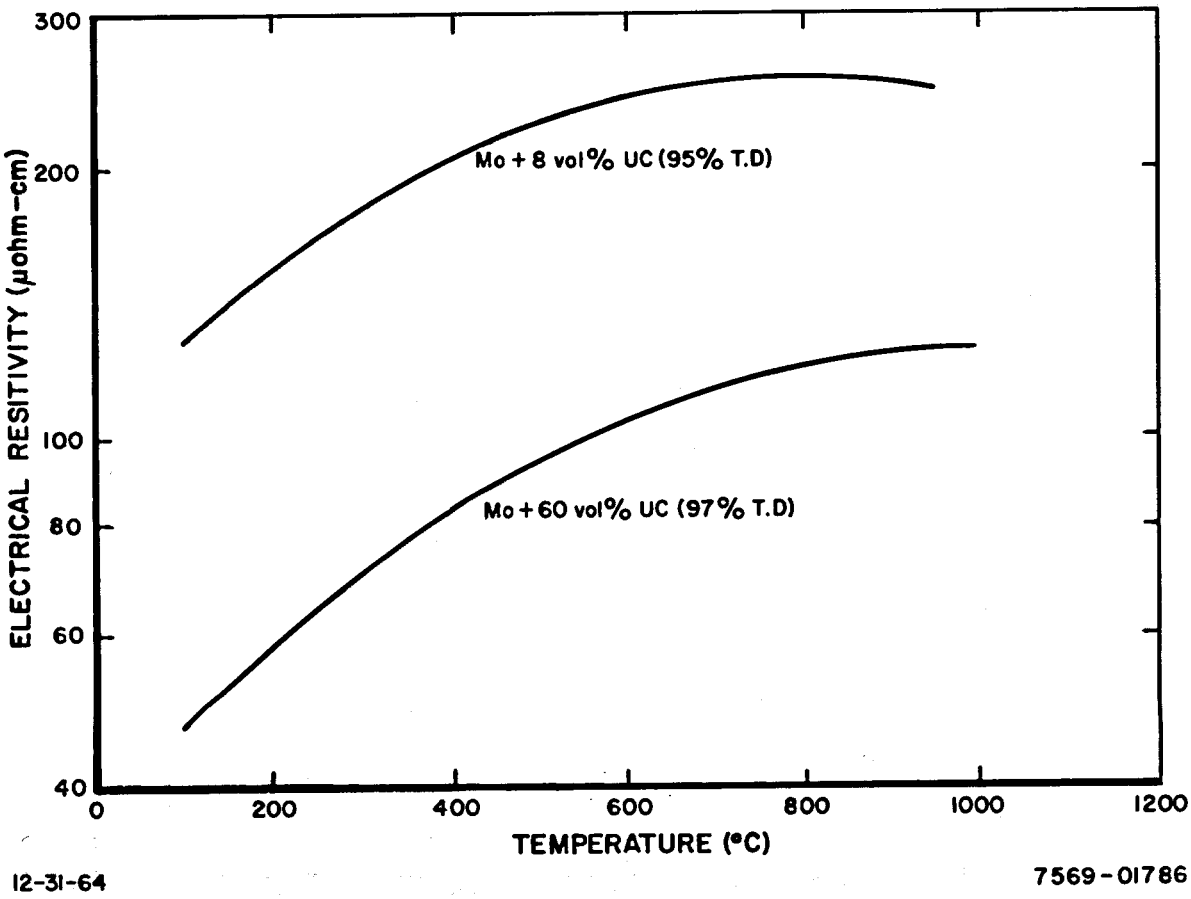

Figure 3.2.1 Electrical Resistivity of Mo-UC Cermets
(Reference 3.1)

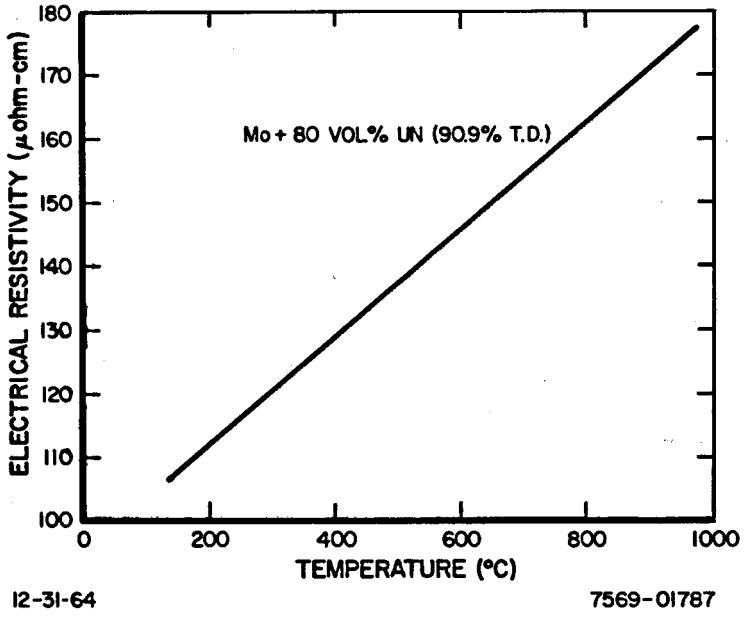

Figure 3.2.2. Electrical Resistivity of Mo-UN Cermet (Reference 3.1)

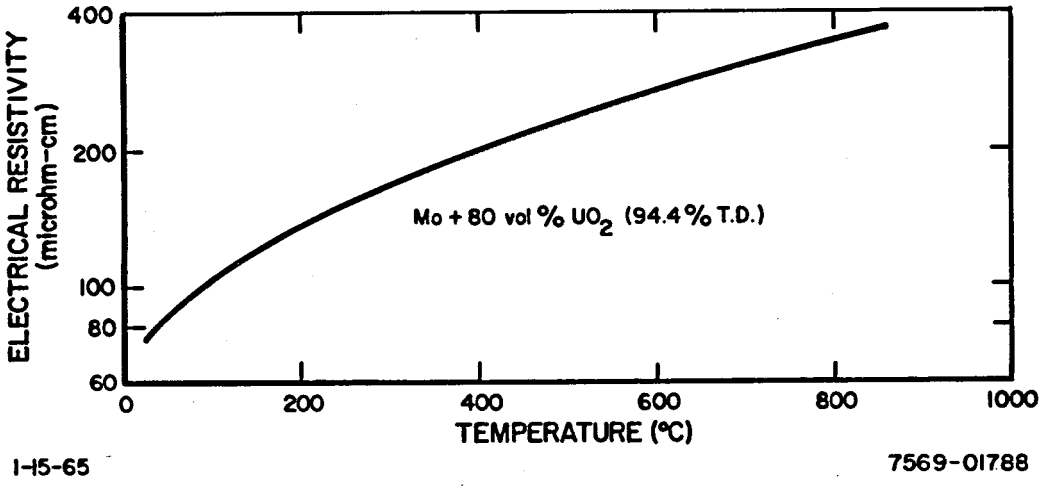

Figure 3.2.3. Electrical Resistivity of Mo-UO_2 Cermet (Reference 3.1)

3.2.3 Thermal

3.2.3.1 Thermal Conductivity

Figure 3.2.4 illustrates the effect of temperature and UC content on the thermal conductivity of molybdenum-uranium carbide cermets. Figure 3.2.5 presents thermal conductivity results for a Mo + 80 vol % UN cermet, as well as a Mo + 80 vol % UO_2 cermet.

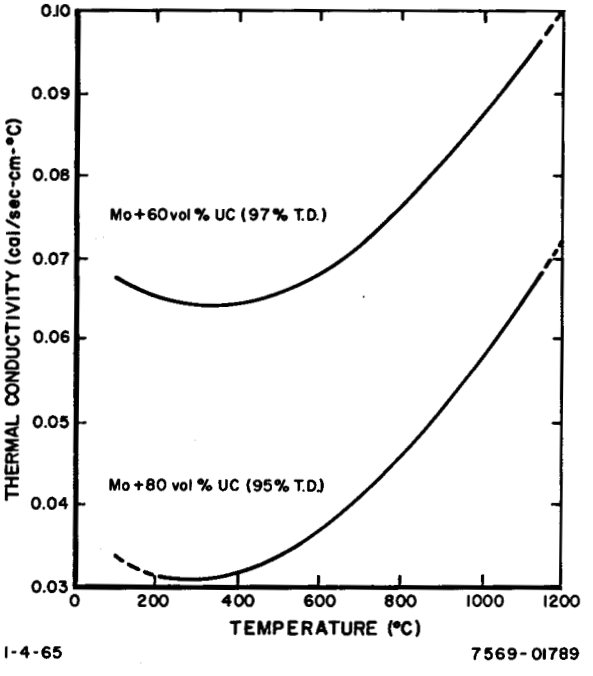

Figure 3.2.4. Thermal Conductivity of Mo-UC Cermets (Reference 3.1)

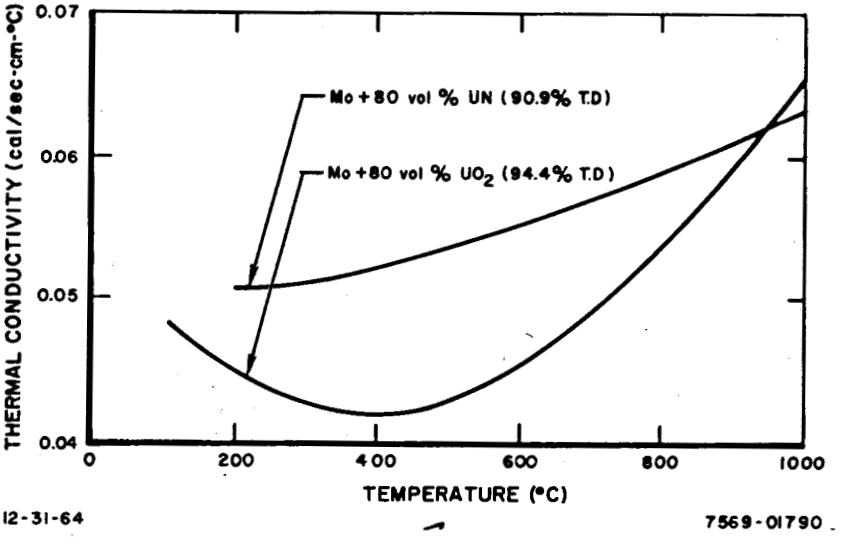

Figure 3.2.5. Thermal Conductivity of Mo-UN and Mo-UO_2 Cermets (Reference 3.1)

3.2.3.2 Thermal Expansion

The mean linear thermal expansion coefficient for a Mo + 80 vol % UC cermet having a density of 95% theoretical over the temperature range of 20 to 950°C was found to be 7.2 to 7.6 x 10^{-6} cm/cm-°C. A Mo + 60 vol % UC cermet with a 97% T. D. had a coefficient of 6.4 to 6.8 x 10^{-6} cm/cm-°C over the same temperature range.[3.1]

The mean linear thermal expansion coefficient of Mo + 80 vol % UN cermet having a 90.9% T. D. was measured to be 9.1 to 9.5 x 10^{-6} cm/cm-°C over the temperature range of 20 to 950°C.[3.1]

Mo + 80 vol % UO_2 cermet (94.4% T. D.) had a mean linear thermal expansion coefficient of 8.8 to 9.2 x 10^{-6} cm/cm-°C over the temperature range of 20 to 950°C. Over the same temperature range a Mo + 70 vol % UO_2 cermet (91.7% T. D.) had a coefficient of 7.9 to 8.3 x 10^{-6} cm/cm-°C.[3.1]

3.3 Mechanical Properties — Short Time

Table 3.3.1 presents results at room temperature on the Young's modulus, ultimate compressive strength, and compressive yield strength of molybdenum-uranium carbide cermets as a function of UC content and percent of theoretical density. The cermets were made using powder metallurgy techniques.

The available mechanical property data on Mo + 80 vol % UN cermet produced using powder metallurgy techniques are presented in Table 3.3.2.

Data on the modulus of rupture of Mo + 80 vol % UO_2 cermet are presented in Table 3.3.3. Figure 3.3.1 presents stress-strain data illustrating the compressive properties of a Mo + 80 vol % UO_2 cermet.

TABLE 3.3.1

COMPRESSIVE MECHANICAL PROPERTIES FOR Mo-UC CERMETS
(Reference 3.2)

UC Content (vol %)	Density (Percent of Theoretical)	Ultimate Compressive Strength (10^3 psi)	Young's Modulus (10^6 psi)	Yield Strength (10^3 psi)	
				0.1% Offset	0.2% Offset
60	95	139.5	28.8	114.5	113.8
60	98	111.7	25.5	73.9	80.0
80	95	95.1	27.8	93.5	-

TABLE 3.3.2

ROOM TEMPERATURE MECHANICAL-PROPERTY VALUES OBTAINED ON MOLYBDENUM CERMETS CONTAINING 80 VOLUME PERCENT UN (Reference 3.3)

UN Composition (vol. %)	Density (Percent of Theoretical)	Dynamic Modulus (10^6 psi)	Modulus of Rupture (psi)	Compressive Properties		
				Static Modulus (10^6 psi)	0.2 (% Offset Yield Strength, psi)	Ultimate Strength (psi)
80	93.9	30.24	26,200	33.1	118,000	152,000
80	93.9	29.66	24,900	30.2	110,000	140,000

TABLE 3.3.3

ROOM TEMPERATURE MODULUS OF RUPTURE DATA FOR Mo + UO_2 CERMETS (Reference 3.4)

UO_2 Content (vol %)	Theoretical Density (%)	Modulus of Rupture (10^3 psi)
80	91.6	12.0
80	90.7	13.8
80	88.5	12.1

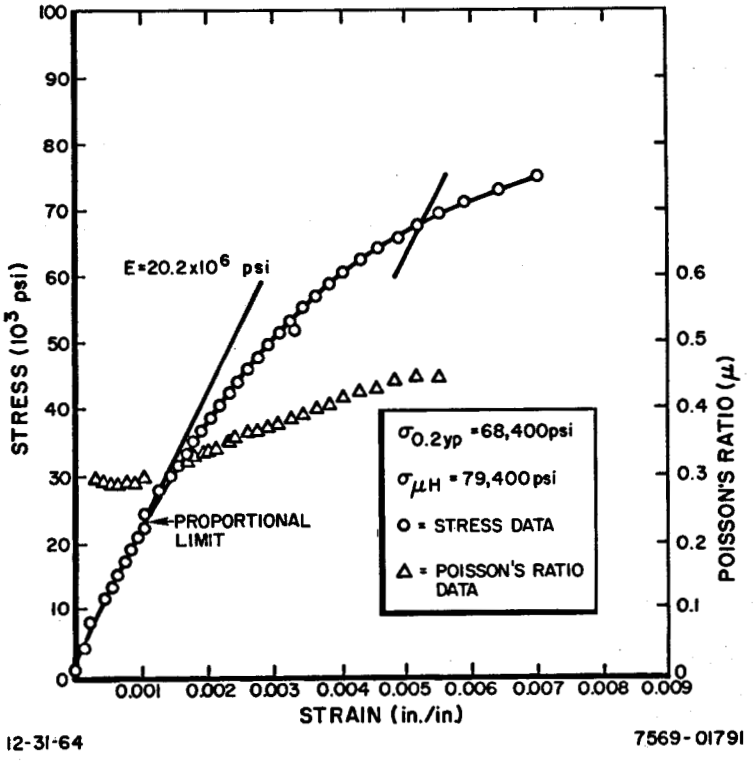

Figure 3.3.1. Compressive Test on a Mo + 80 vol % UO_2 Cermet With a Density 90.7% of Theoretical (Reference 3.4)

3.4 Irradiation Properties — Nuclear Cross Sections

Tables 3.4.1 to 3.4.3 contain thermal macroscopic absorption and scattering cross sections for Mo-UC, Mo-UN, and Mo-UO_2 cermets as a function of UC, UN, and UO_2 content, respectively. These cross sections were calculated assuming absorption and scattering properties of individual elements and compounds being retained when mixed together to form the cermet fuel.

TABLE 3.4.1

THERMAL ABSORPTION AND SCATTERING CROSS SECTIONS FOR Mo-UC CERMET

UC Content		Macroscopic Cross Section	
Vol %	Wt %	Σ_a, cm^{-1}	Σ_s, cm^{-1}
0	0	0.173	0.448
10	11.0	2.42	0.452
20	21.8	4.67	0.457
30	32.3	6.93	0.461
40	42.6	9.18	0.465
50	52.7	11.43	0.469
60	62.5	13.68	0.474
70	72.2	15.93	0.478
80	81.7	18.18	0.482
90	90.9	20.43	0.487
100	100.0	22.68	0.491

TABLE 3.4.2

THERMAL ABSORPTION AND SCATTERING CROSS SECTIONS FOR Mo-UN CERMET

UN Content		Macroscopic Cross Section	
(vol %)	(wt %)	$\Sigma_a(cm^{-1})$	$\Sigma_s(cm^{-1})$
0	0	0.173	0.448
10	11.5	2.53	0.472
20	22.6	4.88	0.497
30	33.4	7.23	0.521
40	43.8	9.58	0.546
50	53.9	11.94	0.570
60	63.7	14.29	0.594
70	73.2	16.64	0.619
80	82.4	18.99	0.643
90	91.3	21.35	0.668
100	100	23.70	0.692

TABLE 3.4.3

THERMAL ABSORPTION AND SCATTERING CROSS SECTIONS FOR Mo-UO_2 CERMET

UO_2 Content		Macroscopic Cross Section	
(vol %)	(wt %)	$\Sigma_a(cm^{-1})$	$\Sigma_s(cm^{-1})$
0	0	0.173	0.448
10	11.2	1.82	0.448
20	22.2	3.46	0.448
30	32.8	5.11	0.448
40	43.2	6.76	0.448
50	53.3	8.40	0.448
60	63.1	10.05	0.448
70	72.7	11.69	0.448
80	82.0	13.34	0.448
90	91.1	14.98	0.448
100	100	16.63	0.448

REFERENCES

3.1 R. W. Endebrock, Editor, "Properties of Fuels for High-Temperature Reactor Concepts," BMI-1598 (November 1962)

3.2 R. W. Dayton and R. F. Dickerson, "Progress Report Relating to Civilian Applications," BMI-1574 (March 1962)

3.3 R. W. Dayton and R. F. Dickerson, "Progress Report Relating to Civilian Applications," BMI-1577 (May 1962)

3.4 S. J. Paprocki, D. L. Keller, G. W. Cunningham, and D. E. Kizer, "Preparation and Properties of UO_2 Cermet Fuels," BMI-1487 (December 1960)

4.0 CLADDINGS

4.1 Introduction

Properties of eight refractory materials are presented in this handbook. These cladding materials are columbium (niobium), iridium, molybdenum, rhenium, tantalum, titanium, vanadium, and tungsten. They are discussed in the order of their symbols – Cb, Ir, Mo, Re, Ta, Ti, V, and W. No information on alloys composed of any combinations of these elements was included in this handbook because of the scarcity of data available and the many combinations of elements that could conceivably be useful as a high temperature cladding.

4.2 Physiochemical Properties

4.2.1 Physical

4.2.1.1 Crystal Structure

Table 4.2.1 presents the crystalline structure of eight refractory metals at room temperature.

TABLE 4.2.1

CRYSTALLINE STRUCTURE OF EIGHT REFRACTORY METALS AT ROOM TEMPERATURE (Reference 4.4)

Metal	Structure
Cb	body centered cubic
Ir	face centered cubic
Mo	body centered cubic
Re	close packed hexagonal
Ta	body centered cubic
Ti	close packed hexagonal
V	body centered cubic
W	body centered cubic

4.2.1.2 Density

Figure 4.2.1 presents the calculated density variation with temperature of Cb, Mo, Ti, and V. Figure 4.2.2 presents the calculated density variation of temperature of Ir, Re, Ta, and W. The density at various temperatures of these metals is calculated by assuming a 1 cm^3 of material at room temperature and using the linear thermal expansion to calculate the density at various temperatures.

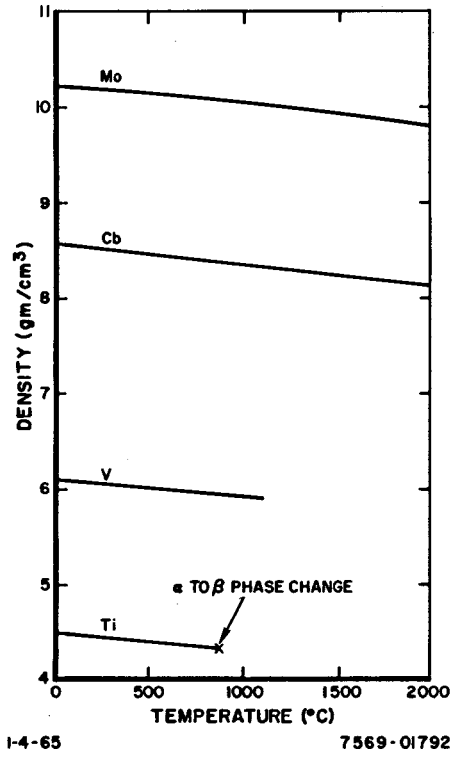

Figure 4.2.1. Calculated Temperature Effect on Density of Cb, Mo, Ti, and V

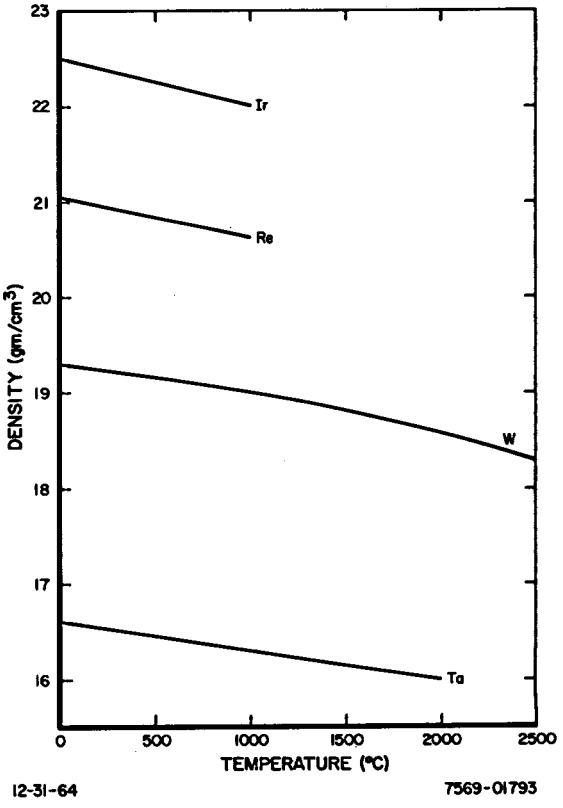

Figure 4.2.2. Calculated Temperature Effect on Density of Ir, Re, Ta, and W

4.2.1.3 Melting Point

The approximate melting points of 8 refractory metals considered in this handbook are presented in Table 4.2.2.

TABLE 4.2.2

APPROXIMATE MELTING POINTS OF EIGHT REFRACTORY METALS (Reference 4.16)

Metal	Melting Temperature (°F)
Cb	4474 ± 18
Ir	4449 ± 5
Mo	4730
Re	5755 ± 35
Ta	5425 ± 90
Ti	3035 ± 18
V	3450 ± 50
W	6170

4.2.2 Electrical

4.2.2.1 Electrical Resistivity

The effect of temperature on the resistivity of Ir, Ta, and Ti are presented in Figure 4.2.3. Only two values for Ir were found as a function of temperature. Very little data exist on this metal. Figure 4.2.4 presents the electrical resistivity of Cb, Mo, Re, V, and W as a function of temperature.

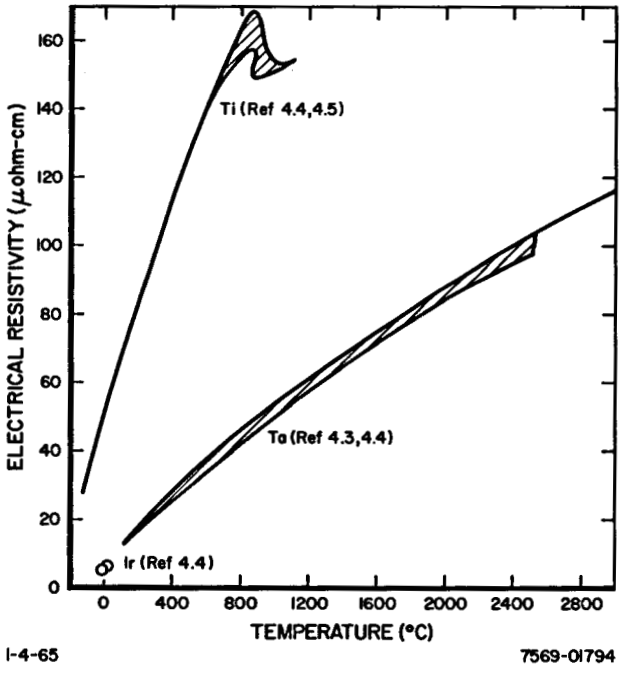

Figure 4.2.3. Electrical Resistivity of Ir, Ta, and Ti

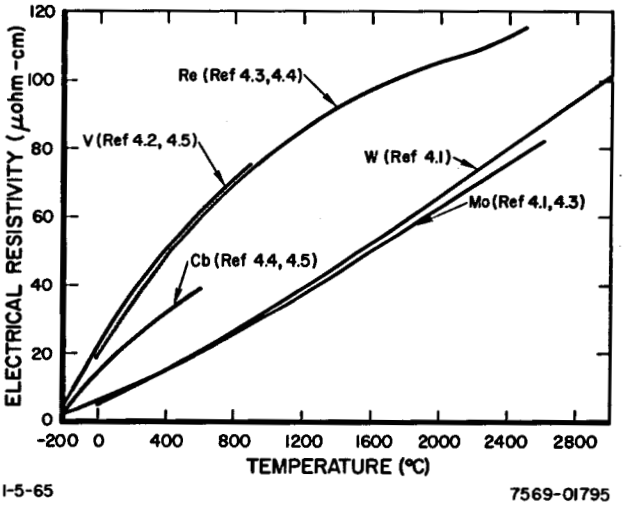

Figure 4.2.4. Electrical Resistivity of Cb, Mo, Re, V, and W

4.2.3 Thermal

4.2.3.1 Thermal Conductivity

The effective temperature on the thermal conductivity of Cb, Ir, Mo, Re, Ta, Ti, V, and W are presented in Figure 4.2.5. Again, very little data exist on Ir and Re metals.

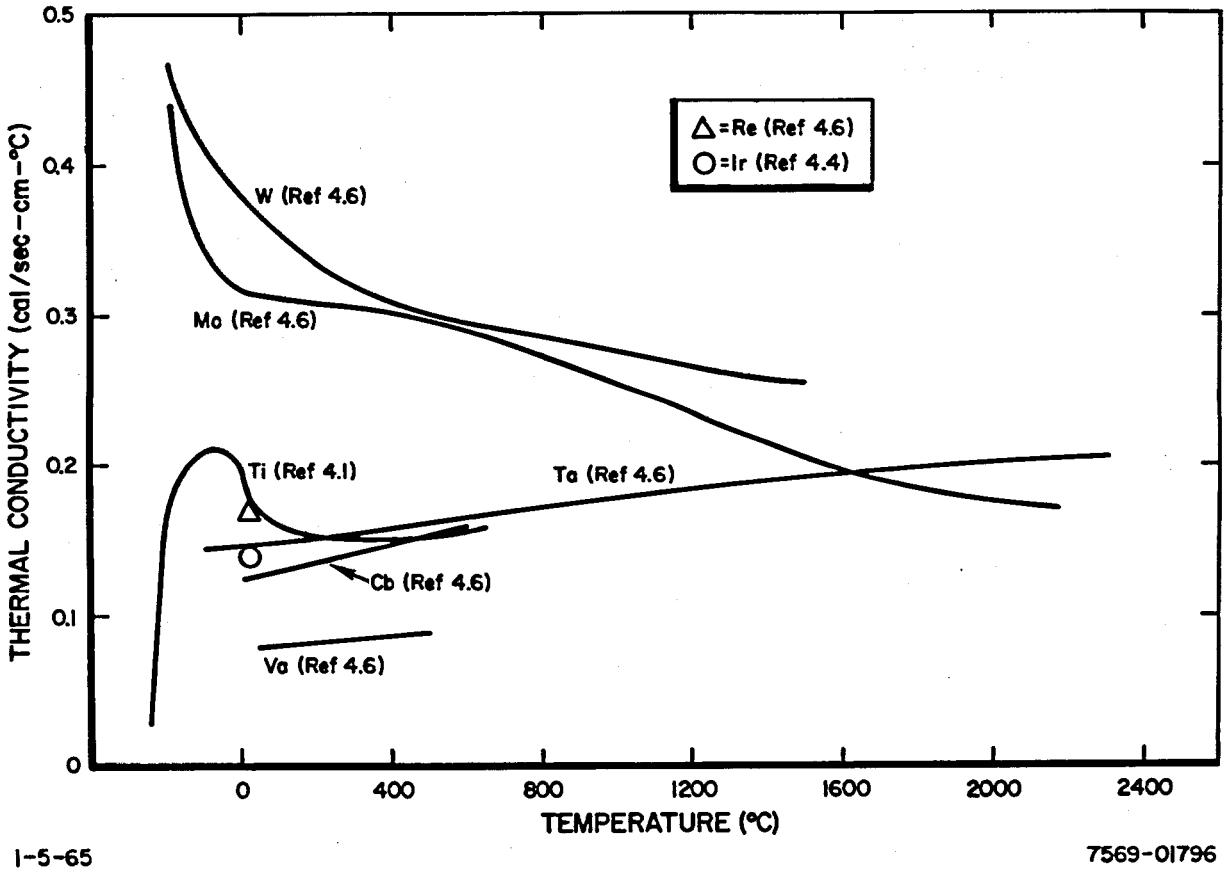

Figure 4.2.5. Thermal Conductivity of Cb, Ir, Mo, Re, Ta, Ti, V, and W

4.2.3.2 Specific Heat

The specific heat of Cb, Ta, V, and W as a function of temperature is presented in Figure 4.2.6. Figure 4.2.7 presents the effect of temperature of the specific heat properties of Mo, Re, Ir, and Ti.

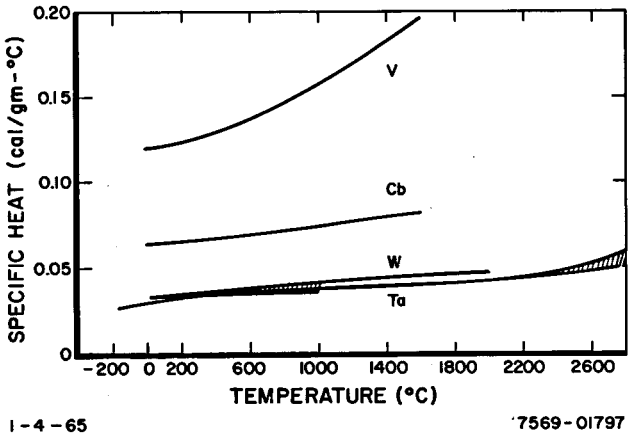

Figure 4.2.6. Specific Heat of Cb, Ta, V, and W
(Reference 4.1, 4.3, 4.4, 4.5)

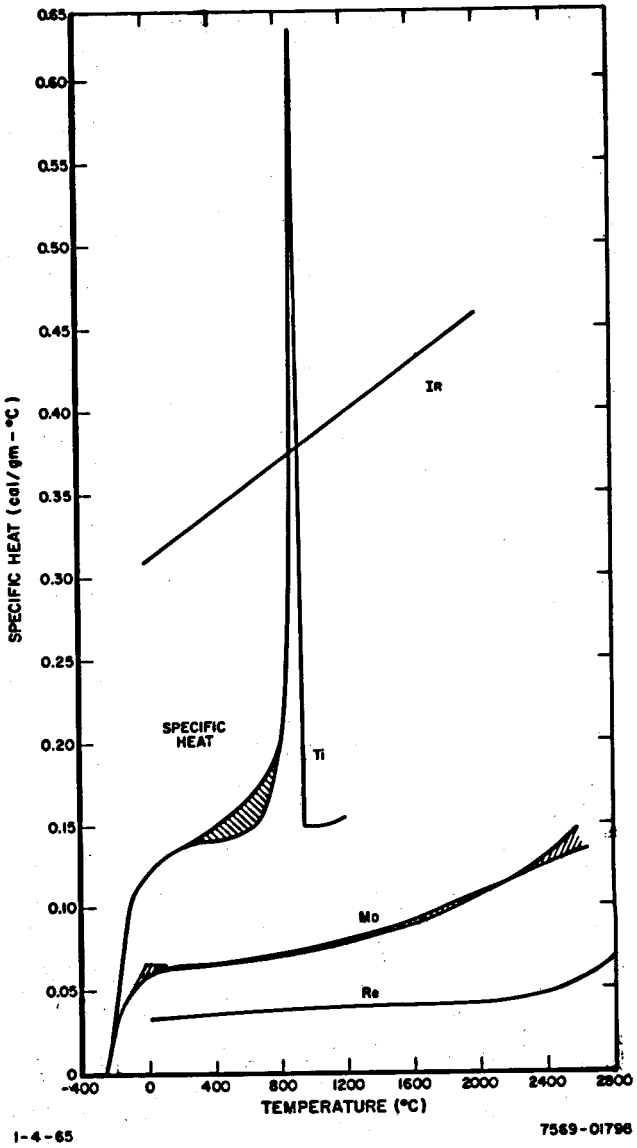

Figure 4.2.7. Specific Heat of Ir, Mo, Re, and Ti
(Reference 4.1, 4.3, 4.5, 4.7)

4.2.3.3 Thermal Expansion

The coefficient linear thermal expansion from room temperature for Cb, Mo, and V are presented in Figure 4.2.8 as a function of temperature. No data exist for Ir, Re, Ta, Ti, and W.

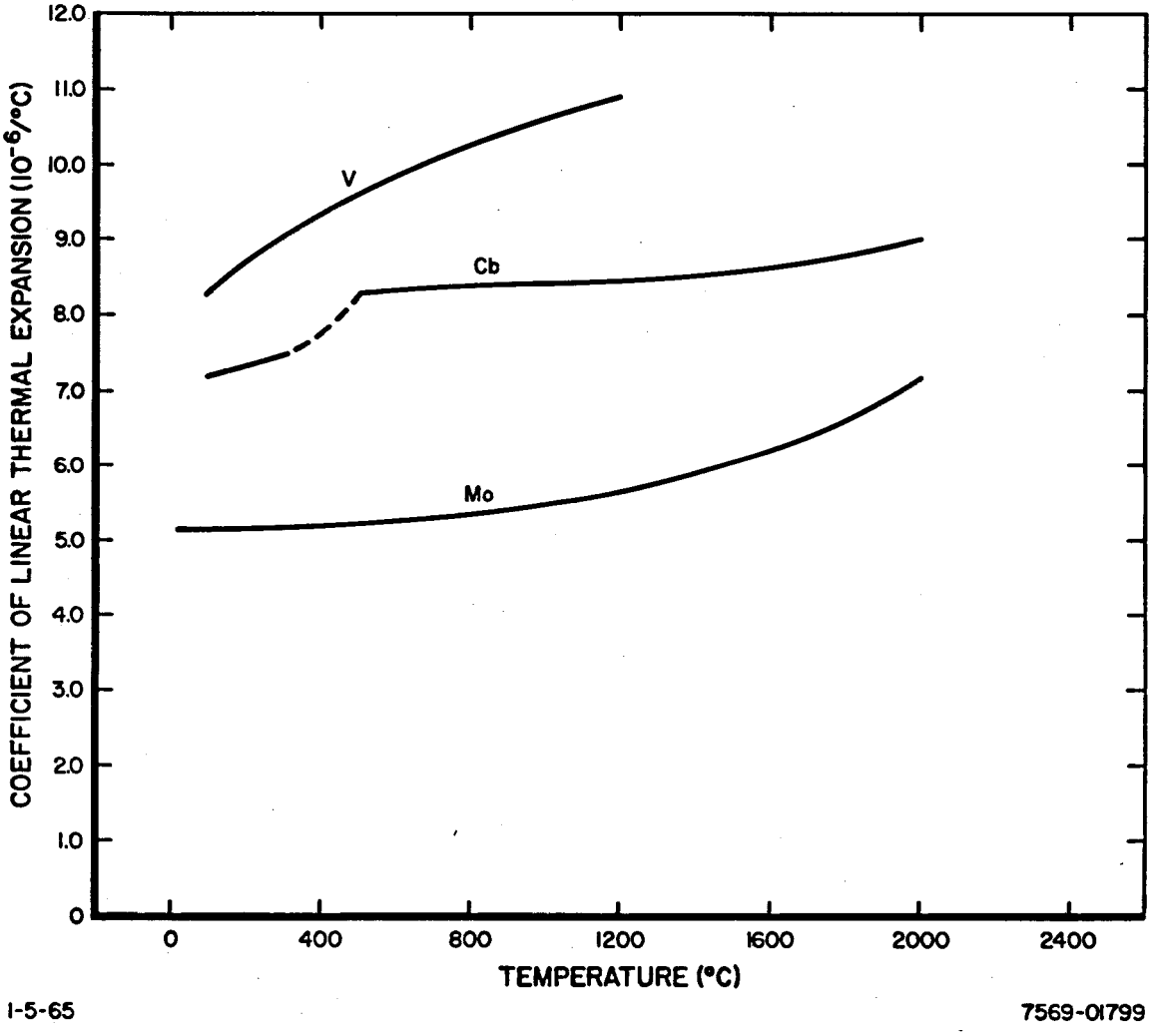

Figure 4.2.8. Coefficient of Linear Thermal Expansion From Room Temperature for Cb, Mo, and V (Reference 4.1)

4.2.4. Chemical

4.2.4.1 Hydrogen Permeation

Figure 4.2.9 contains the available data on the hydrogen permeation rate through refractory metals as a function of temperature. No data exist for Ir, Re, Ta, Ti, and V.

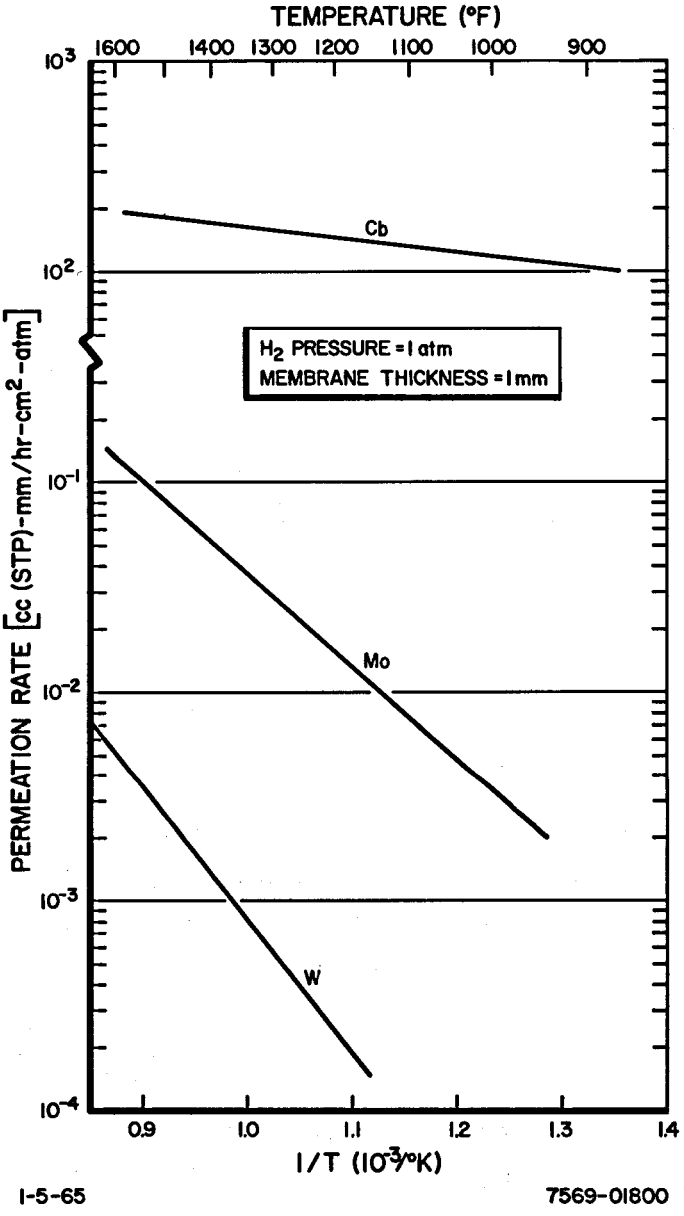

Figure 4.2.9. Hydrogen Permeation vs Temperature for Cb, Mo, and W Membranes (Reference 4.8)

4.2.4.2 Hydrogen Effects

Columbium (niobium) metal does not normally absorb hydrogen at room temperature. However, if it is first heated in hydrogen to a high temperature, the metal will continue to absorb hydrogen at room temperature until it approaches Nb $H_{0.86}$. The limiting formula appears to be Nb H. The solubility of hydrogen in niobium over the range 20 to 900°C is given in Table 4.2.3. The sample contained 98.5 wt % columbium and the remainder was tantalum. The pressure was 760 mm of Hg.[4.1]

TABLE 4.2.3
SOLUBILITY OF HYDROGEN IN NIOBIUM
(Reference 4.1)

Temperature (°C)	Solubility ($cm^3 H_2$/g Nb)	Temperature (°C)	Solubility ($cm^3 H_2$/g Nb)
20	(104.2)	500	47.4
200	(93.3)	550	29.7
300	88	600	18.5
350	83.6	700	9.7
400	76.8	800	6.1
450	65.6	900	4.0

Niobium is embrittled by heating in hydrogen and the products of reaction can be decomposed by heating in a vacuum. The rate of absorption is dependent upon the hydrogen pressure as well as ambient temperature. The rate of reaction being a function of the square root of the pressure.

Products formed at 300 and 350°C can be decomposed by evacuating at 342°C. Hydrides formed by reacting columbium and hydrogen at 700°C can be partially decomposed or evacuated to 10^{-6} mm at 700°C; however, the hydride formed at 900°C cannot be decomposed in a vacuum of 10^{-6} at 900°C. For operation in a hydrogen atmosphere, the safe operating temperature for columbium is limited to something below 1900°C because of grain growth dimensional changes and hydrogen embrittlement. Columbium hydride reacts in air, the ignition temperature being from 240 to 575°C in static air and from 310 to 610°C in dynamic air.[4.1]

No data exist on the effect hydrogen has on Ir, Mo, Re, and W.

It has been observed that the absorbed hydrogen makes a tantalum filament quite brittle and increases its electrical resistivity. Three phases of tantalum are formed with hydrogen. Up to about 12 at. % hydrogen, the structure is b.c.c. (alpha phase); between 31 and 35 at. % hydrogen, the structure is that of a closely packed hexagonal lattice (beta phase); and between 48 and 52 at. % a gamma phase is formed, which has the structure of a slightly deformed b.c.c. lattice.[4.9]

Only the hydrides of Li sodium and calcium have higher hydrogen content than Ti reaches. About 800°C the solubility of hydrogen in Ti follows the P-1/2 law. Absorption begins at 375°C and occurs at a rapid rate above 400°C. Figure 4.2.10 shows isotherms at four different temperatures illustrating the effect of hydrogen content in Ti on the hydrogen disposition pressure. The shape of the 600°C isotherm is accounted for by the pressure of two phases. It has been demonstrated by X-ray investigation that the solid solutions consist of a delta phase up to 35 at. %, and a beta phase for 50 at. % of hydrogen and iron. The alpha phase is a closely packed hexagonal lattice structure while the beta phase is a f.c.c. lattice structure. The maximum content of hydrogen in the solid solution corresponds to the formula Ti, $H_{1.75}$; and the density of the hydride is 3.91 as compared to the density of 4.52 grains per cm^3 for Ti. The decrease in density varies linearly with the hydrogen content and this fact indicates that the entrance of hydrogen atoms into interstitial sites in the metal lattice brings about an expansion of the lattice. It is important to observe that in Ti maximum absorption is obtained only after the metal has been heated and vacuumed for a prolonged period at a very high temperature. The metal, thus the gas, absorbs hydrogen very rapidly at a moderately high temperature. The absorption under these conditions is completely reversible. Absorption at lower temperature is usually affected by cooling the metal, which has been saturated at the higher temperatures in hydrogen.[4.9]

The maximum hydrogen content in V corresponds to the chemical composition $VH_{0.72}$, and the density of this solid solution is 5.30 as compared to 5.87 grams/cm^3 for V. Figure 4.2.11 shows isotherms for solutions of hydrogen in V. The isotherms are reversible and all of them follow the P-1/2 law.[4.9]

The rather sparse data on the strain rate dependence of tensile ductility of hydrided V are contained in Figure 4.2.12. Hydrogen seems to play the major role in the ductility temperature strain rate relationships. Only the data for the 0.15 atomic percent hydrogen reflect the thin strain rate dependence of V. The transition type plots of Figure 4.2.12 seem similar to the pattern of behavior for hydrogen charged steels.[4.10]

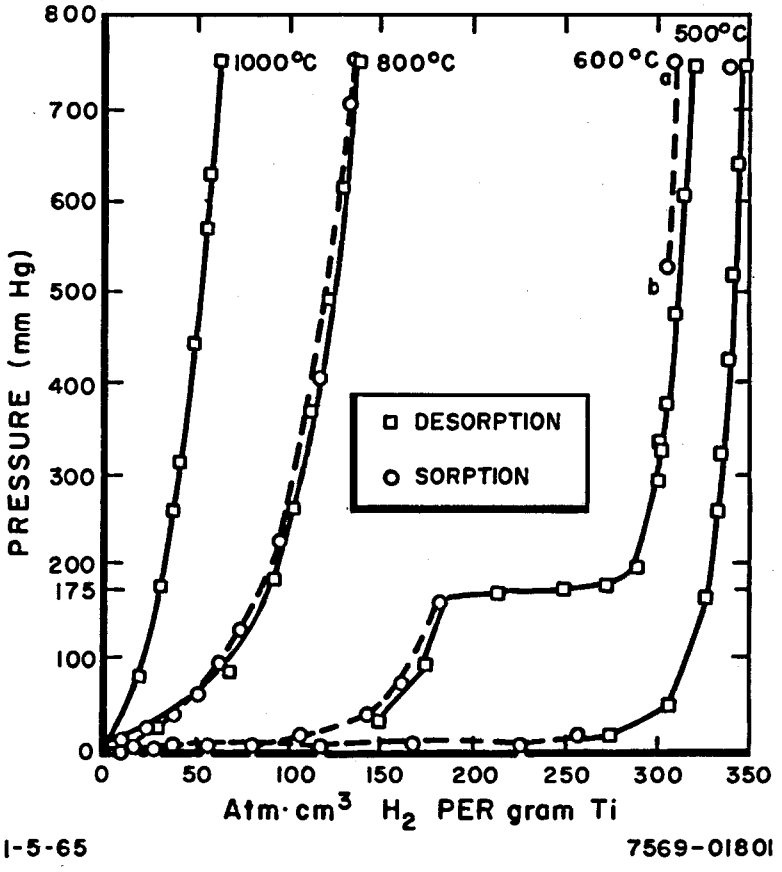

Figure 4.2.10. Isotherms at Four Different Temperatures for the System Hydrogen-Titanium (Reference 4.9)

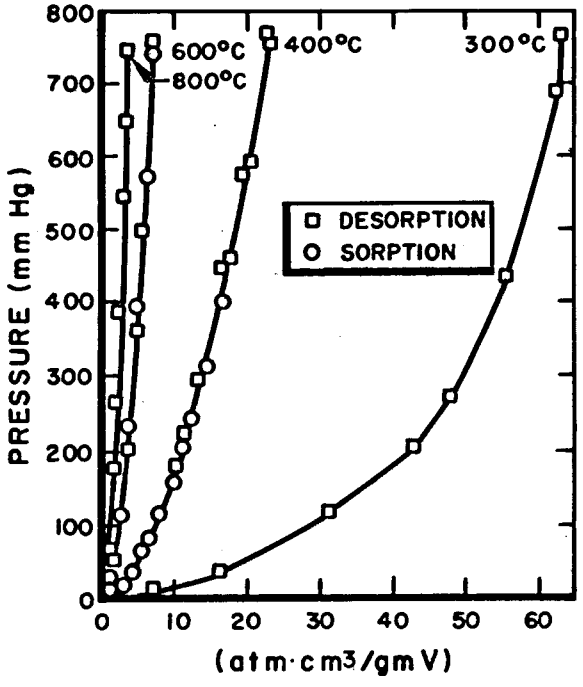

Figure 4.2.11. Isotherms at Four Different Temperatures for the System Hydrogen-Vanadium (Reference 4.9)

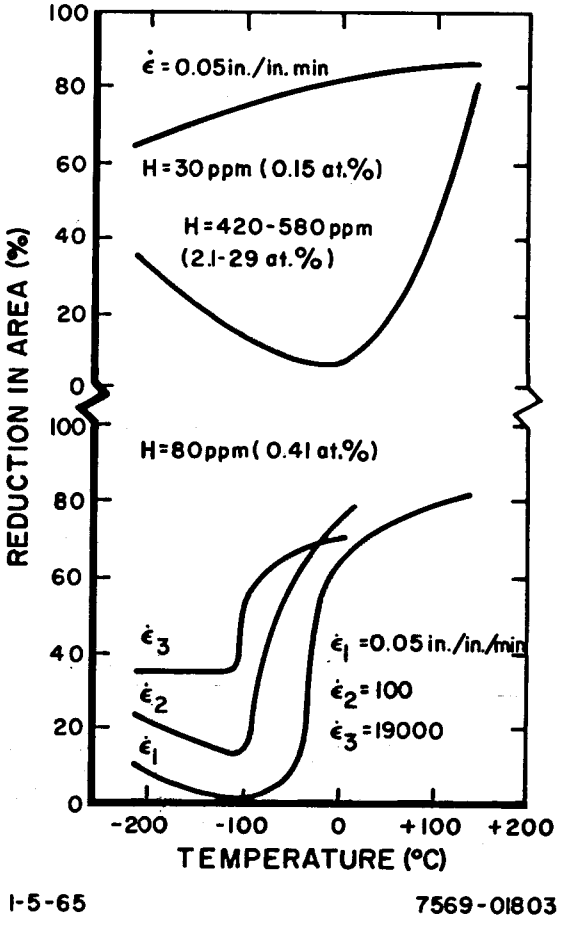

Figure 4.2.12. Tensile Ductility as a Function of Temperature, Strain Rate, and Hydrogen Content (Reference 4.10)

4.3 Mechanical Properties

4.3.1 Short Time

4.3.1.1 Tensile Properties

Figure 4.3.1 illustrates the ultimate tensile strength of properties of Cb as a function of temperature. The yield strength properties of Cb as a function of temperature are presented in Figure 4.3.2. The ultimate tensile strength of Mo as a function of relatively low temperatures is illustrated in Figure 4.3.3. Figure 4.3.4 illustrates the effect of relatively high temperature on the ultimate tensile strength of Mo as well as W. This figure also illustrates the effect of cold working and recrystallization at 3800°F on the ultimate tensile strength of Mo and W. Figure 4.3.5 presents ultimate tensile strength properties as well as the elongation properties as a function of temperature of Re. Ultimate tensile strength and yield strength properties of high purity Ta are presented in Figure 4.3.6 as a function of temperature. Also presented in this figure is the effect of many crystallizations of Ta on these properties. A wrought material was 95% cold rolled and stress relieved. The recrystallized material was held at 2190 for 1 hr after 75% cold rolling. Figure 4.3.7 presents elevated temperatures, ultimate and yield tensile properties of mill annealed alloyed Ti-55. Also presented in this figure is the effect of temperature on the elongation and reduction in area properties of Ti-55. For comparison of tensile strength properties, Figure 4.3.8 presents these properties as a function of temperature of mill-annealed Ti-40. Figure 4.3.9 presents strength and elongation properties of annealed high purity (99.9%) Ti. The ultimate tensile properties as a function of temperature of recrystallized V are presented in Figure 4.3.10. Figure 4.3.11 presents the yield strength properties of recrystallized V.

No data are available to illustrate the effect of temperature on the yield strength properties of Mo, Re, and W.

Figure 4.3.12 presents structure and dynamic modulus of elasticity properties of Cb as a function of temperature. The effects of temperature on the elastic modulus of Ir, Mo, Ta, and W are presented in Figure 4.3.13. The structure modulus of elasticity as a function of temperature of arc-cast Mo is presented in Figure 4.3.14. Figure 4.3.15 illustrates the effect of temperature on the Young's modulus of elasticity of Re. Additional data on the modulus of

elasticity of Ta are presented in Figure 4.3.16. The modulus of elasticity of Ti at various temperatures is presented in Figure 4.3.17. The effect of temperature on the dynamic modulus of elasticity of V is presented in Figure 4.3.18. No data exist to illustrate the effect of temperature on the modulus of elasticity with W.

The elongation properties of Cb in tension as a function of temperature is presented in Figure 4.3.19. Area reduction of Cb in tension as a function of temperature is presented in Figure 4.3.20. No data exist on the elongation and reduction in area properties as a function of temperature of Ir, Mo, Re, Ti, and W. The elongation property as a function of temperature of high purity Ta sheet is presented in Figure 4.3.21. Also presented in this figure is the effect of recrystallization of the elongation properties of Ta. The wrought material was 95% cold-rolled and stress relieved. Recrystallization material was held at 2190°F for 1 hr after 75% cold rolled. Figure 4.3.22 illustrates the effect of temperature on the tensile elongation property of recrystallization V. Figure 4.3.23 illustrates the effect of temperature on the reduction of area under tension of recrystallized V.

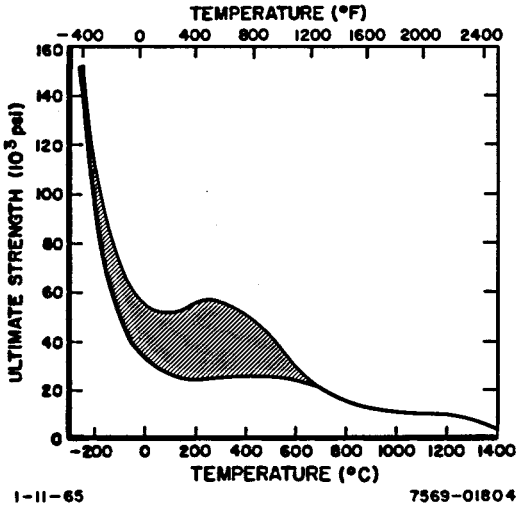

Figure 4.3.1. Ultimate Tensile Strength of Columbium vs Test Temperature (Reference 4.6)

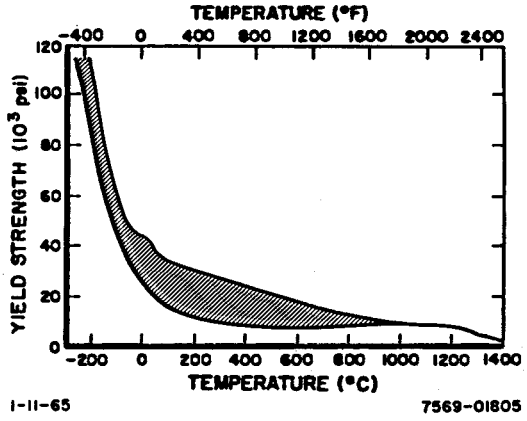

Figure 4.3.2. Yield Strength of Cb vs Temperature (Reference 4.6)

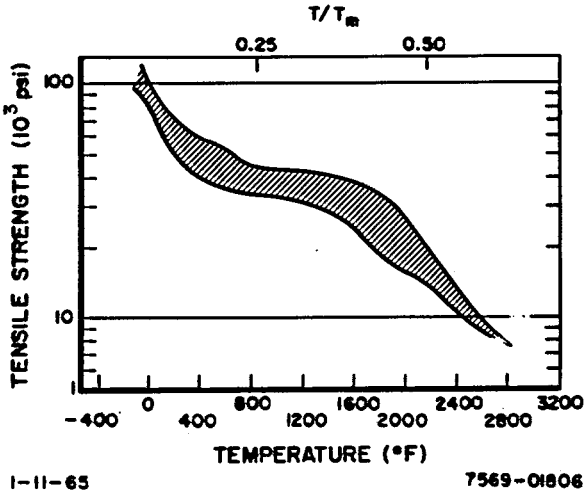

Figure 4.3.3. Effect of Low Temperatures on the Tensile Properties of Mo (Reference 4.13)

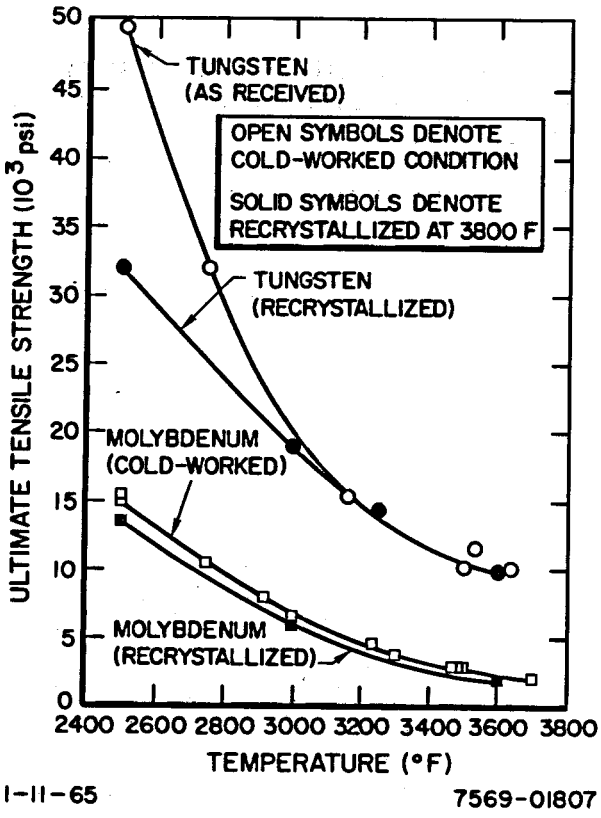

Figure 4.3.4. Tensile Strengths of Tungsten and Molybdenum-Base Materials in Cold-Worked and in Recrystallized Condition (Reference 4.14)

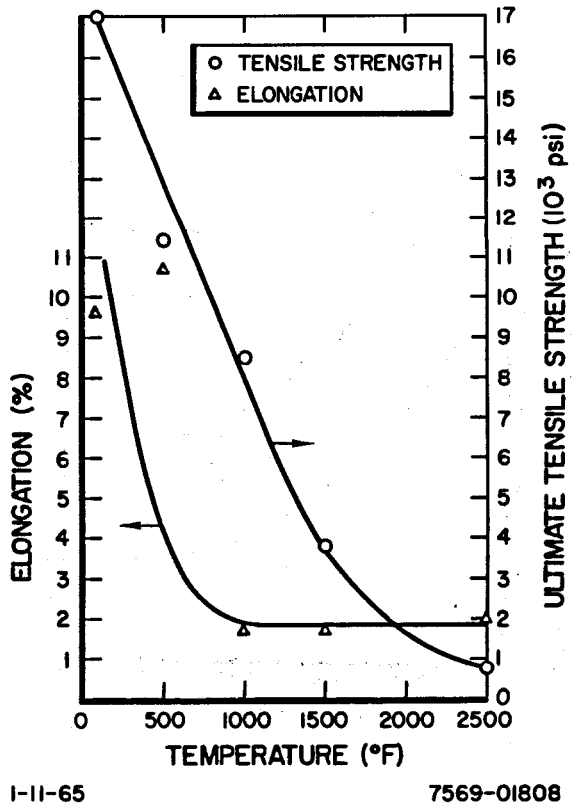

Figure 4.3.5. Ultimate Tensile Strength and Elongation of Rhenium vs Temperature (Reference 4.18)

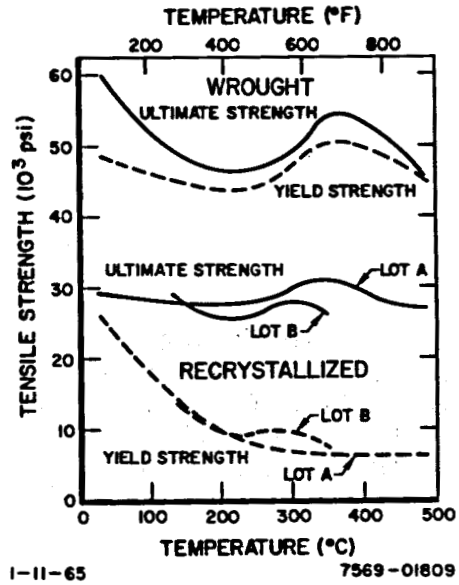

Figure 4.3.6. Tensile Strength of High-Purity Tantalum vs Temperature (Reference 4.12)

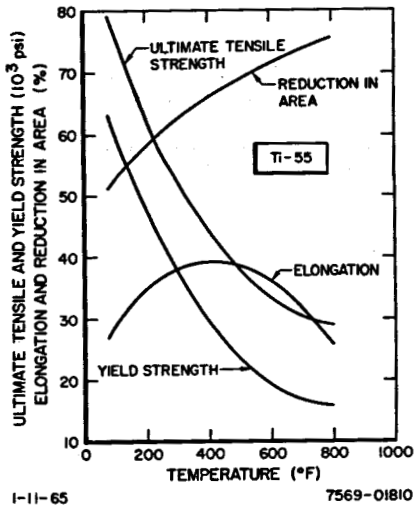

Figure 4.3.7. Elevated-Temperature Tensile Properties of Mill-Annealed Unalloyed Ti^{55} (Reference 4.11)

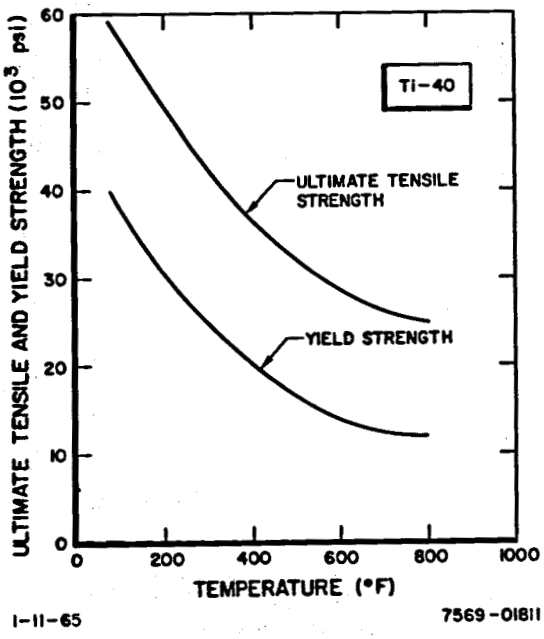

Figure 4.3.8. Elevated-Temperature Tensile Properties of Mill-Annealed Unalloyed Ti^{40} (Reference 4.11)

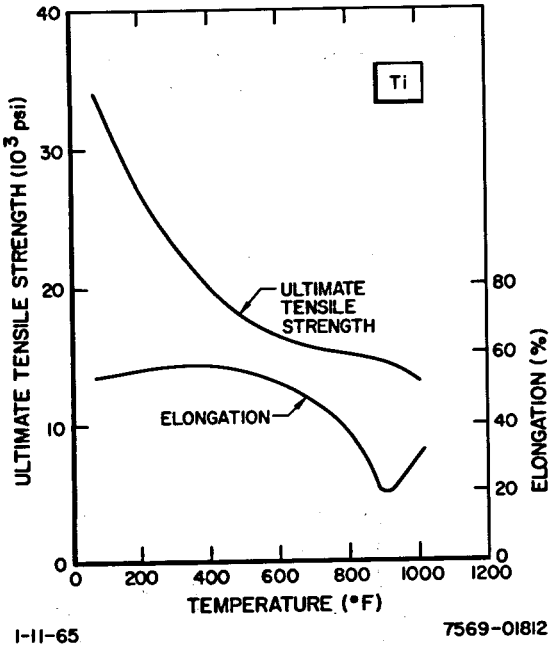

Figure 4.3.9. Elevated-Temperature Tensile Properties of Annealed High-Purity (99.9%) Titanium (Reference 4.11)

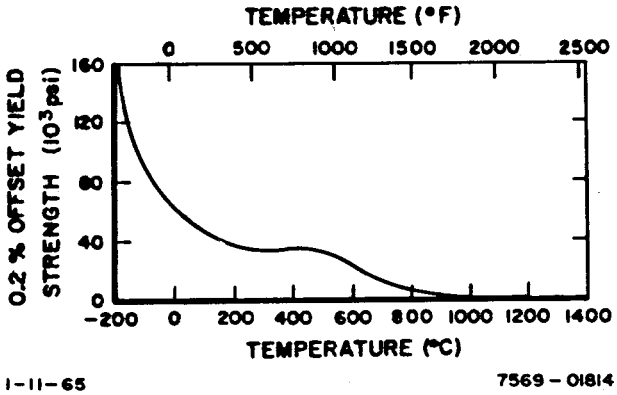

Figure 4.3.10. Ultimate Tensile Strength vs Temperature of Recrystallized Vanadium (Reference 4.6)

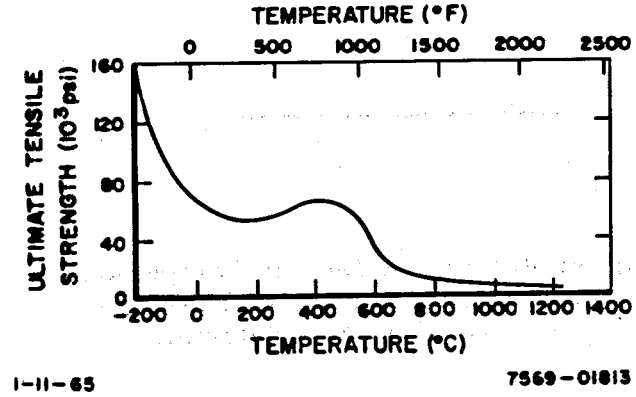

Figure 4.3.11. Yield Strength vs Temperature of Recrystallized Vanadium (Reference 4.6)

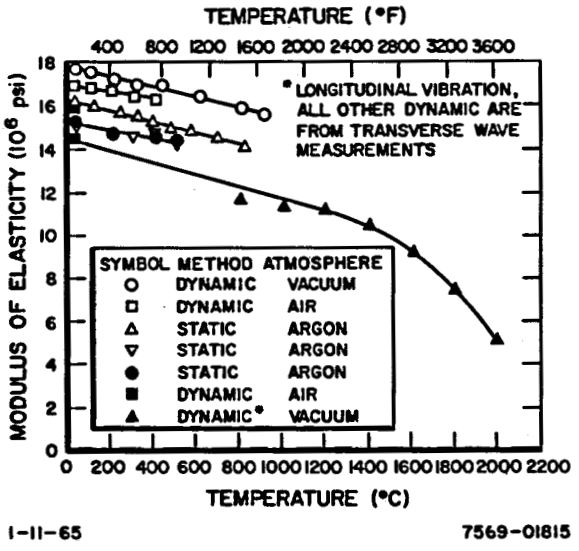

Figure 4.3.12. Modulus of Elasticity of Columbium vs Test Temperature

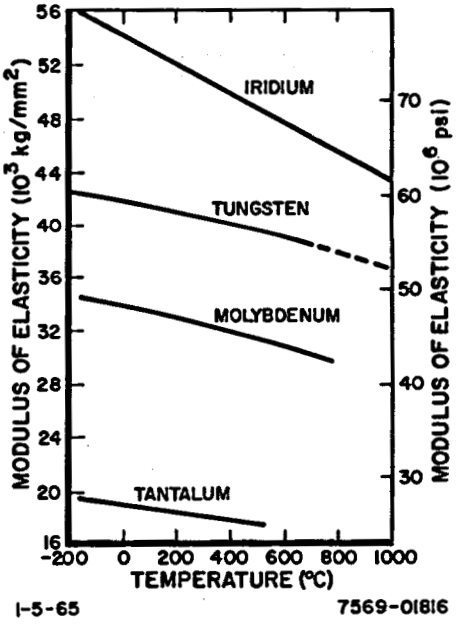

Figure 4.3.13. Temperature Dependence of the Elastic Modulus of Ir, Mo, Ta, and W (Reference 4.14)

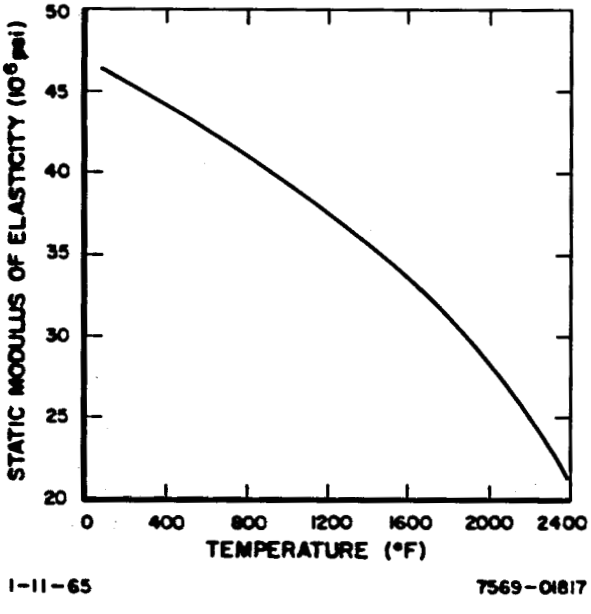

Figure 4.3.14. Effect of Temperature on the Static Modulus of Elasticity of Arc-Cast Molybdenum

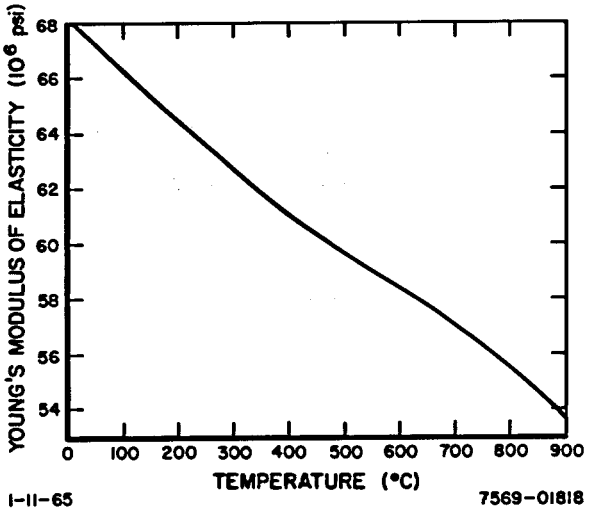

Figure 4.3.15. Variation of the Modulus of Elasticity of Re with Temperature (Reference 4.19)

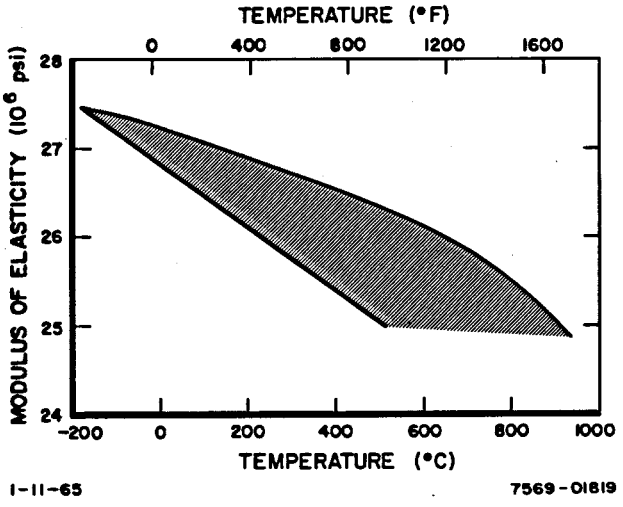

Figure 4.3.16. Effect of Temperature on the Modulus of Elasticity of Tantalum (Reference 4.12)

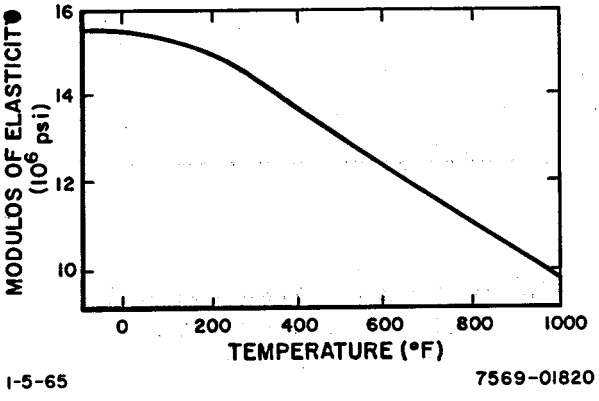

Figure 4.3.17. Modulus of Elasticity at Various Temperatures of Ti (Reference 4.5)

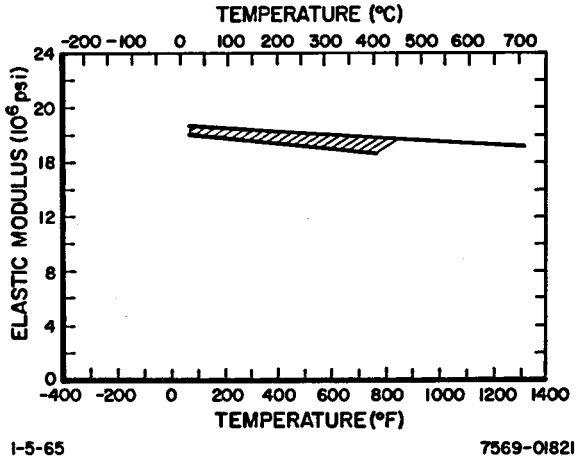

Figure 4.3.18. Dynamic Modulus of Elasticity of Vanadium vs Temperature (Reference 4.6)

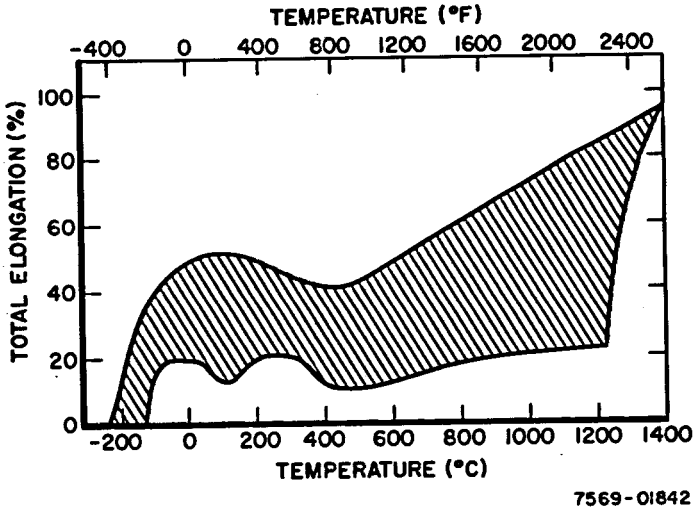

Figure 4.3.19. Elongation of Cb vs Temperature (Reference 4.6)

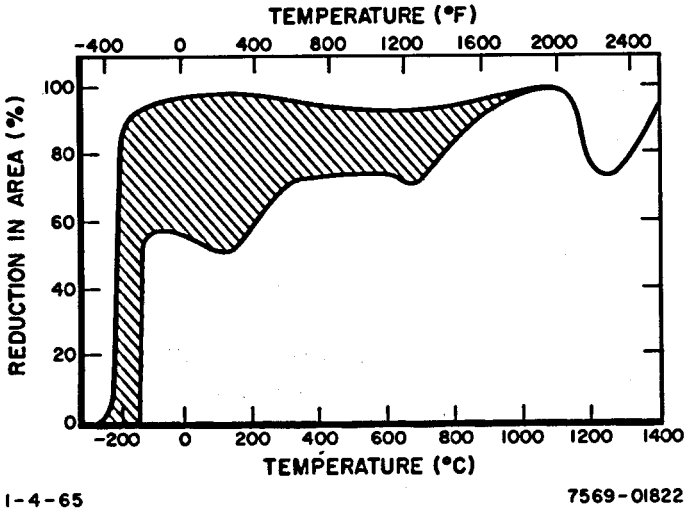

Figure 4.3.20. Area Reduction of Cb vs Temperature (Reference 4.6)

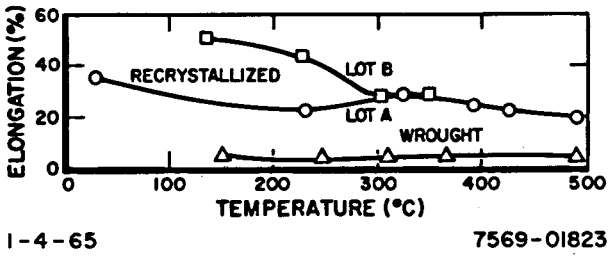

Figure 4.3.21. Tensile Elongation Property vs Temperature of High-Purity Tantalum Sheet (Reference 4.12)

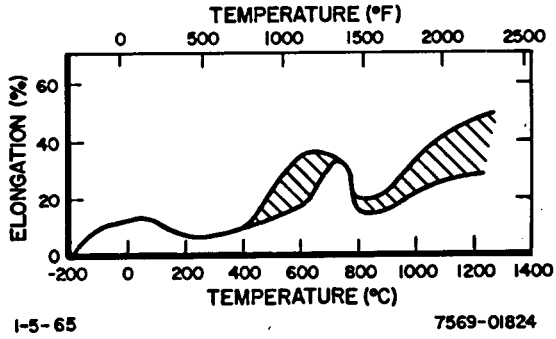

Figure 4.3.22. Tensile Elongation vs Temperature of Recrystallized Vanadium (Reference 4.6)

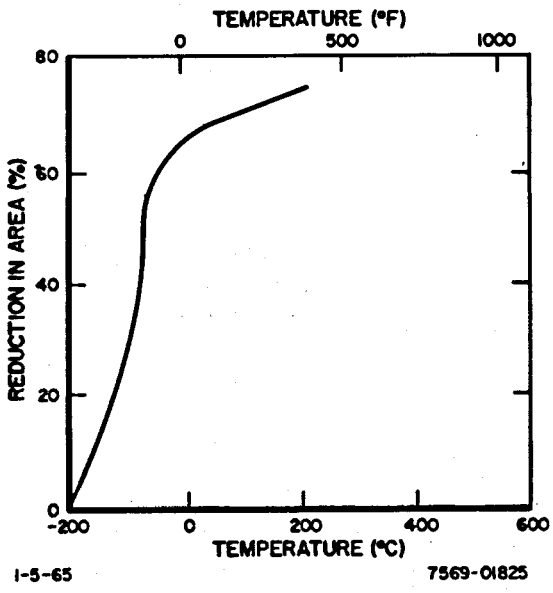

Figure 4.3.23. Tensile Area Reduction vs Temperature of Recrystallized Vanadium (Reference 4.6)

4.3.1.2 Hardness

Figure 4.3.24 presents hardness properties data on Cb as a function of temperature.

No data exist to illustrate the effect of temperature on the hardness of Ir, Re, Ta, Ti, and V.

The effect of temperature on the hardness of unalloyed arc-cast Mo is illustrated in Figure 4.3.25. Additional data on the effect of temperature on the hardness of Mo sheet are presented in Figure 4.3.26. Also hardness data on W are presented in this figure.

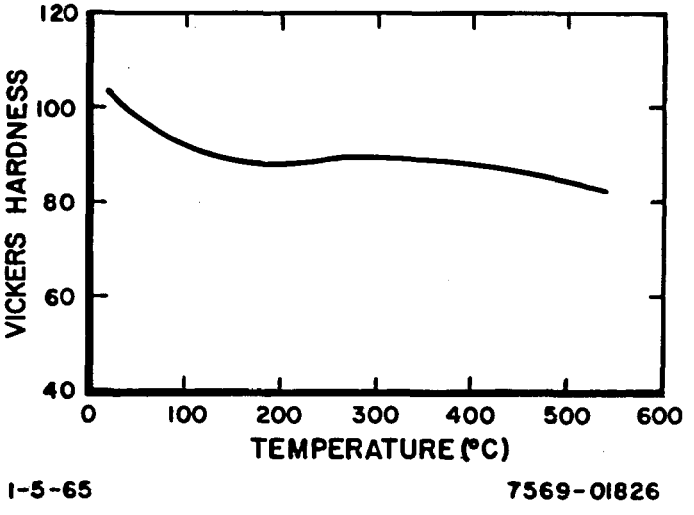

Figure 4.3.24. Hardness of Columbium vs Temperature (Reference 4.17)

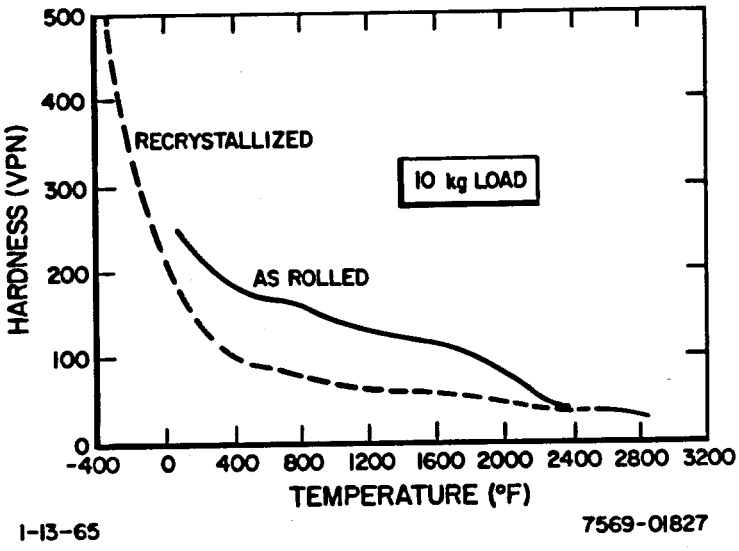

Figure 4.3.25. Effect of Temperature on the Hardness of Unalloyed Arc-Cast Molybdenum (Reference 4.13)

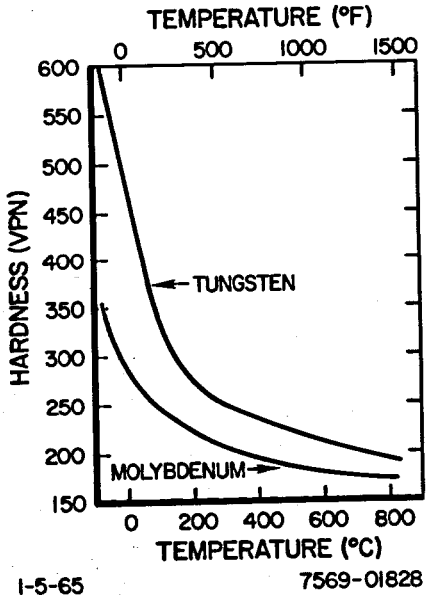

Figure 4.3.26. Hardness vs Temperature of Tungsten and Molybdenum Sheet (Reference 4.14)

4.3.2 Long Time

4.3.2.1 Stress Rupture

Figure 4.3.27 presents stress rupture data of electron beam melted Cb sheet as well as Ta sheet on a Larson-Miller plot.

No data are available to illustrate the effect of temperature and time on the stress rupture properties of Ir, Re, Ti, V, and W.

Figure 4.3.28 presents stress rupture curves for unalloyed arc-cast Mo. This figure also illustrates the difference in stress rupture properties of stress relieved and recrystallized Mo. The stress relieved material was held at 1800°F for 1 hr while the recrystallized material was held at 2150°F for 1 hr.

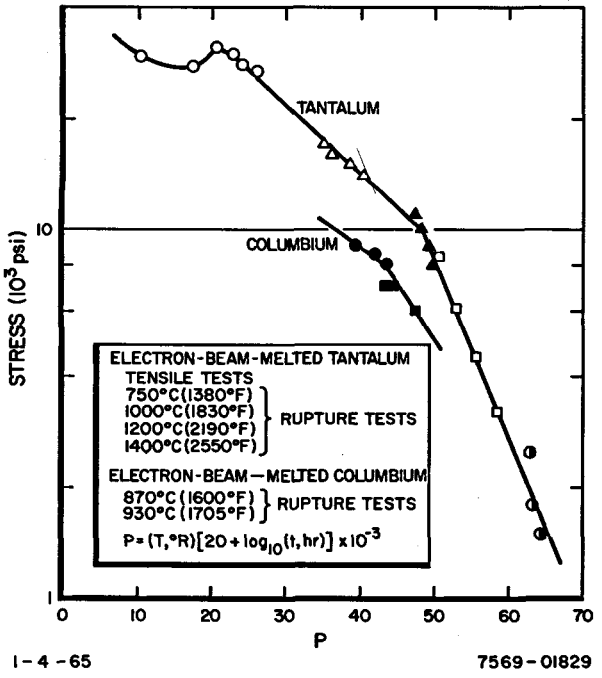

Figure 4.3.27. Larson-Miller Plot Comparing Rupture Properties of Electron-Beam-Melted Tantalum and Columbium Sheet (Reference 4.12)

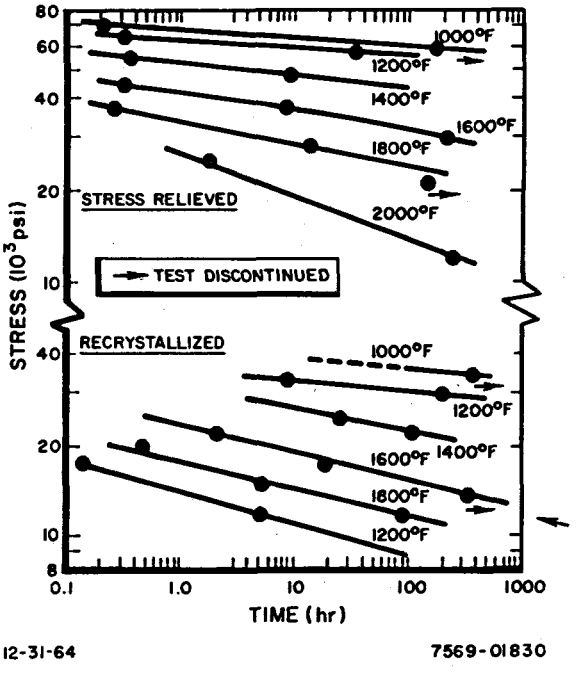

Figure 4.3.28. Stress-Rupture Curves for Unalloyed Arc-Cast Molybdenum, as Stress Relieved (1800°F — 1 hr) or Recrystallized (2150°F — 1 hr) (Reference 4.13)

4.3.2.2 Creep

Figure 4.3.29 presents creep stress data as a function of rupture time for Cb at high temperatures. Lower temperature data for Cb is presented in Figure 4.3.30.

No data were found to illustrate the effect of rupture time on the creep stress of Ir, Re, Ti, and V. Creep properties at 1800°F as a function of time are presented in Figure 4.3.31 for unalloyed arc-cast Mo. In addition, the difference between creep properties of stress relieved and recrystallized material is illustrated in this figure. The stress relieved material was held for 1 hr at 1800°F while the recrystallized material was held for 1 hr at 2150°F.

Figures 4.3.32 to 4.3.35 present creep strength properties as a function of temperature of recrystallized high purity Ta sheet on various percentages of creep.

Minimum creep rate properties as a function of stress and temperature of recrystallized W are presented in Figure 4.3.36.

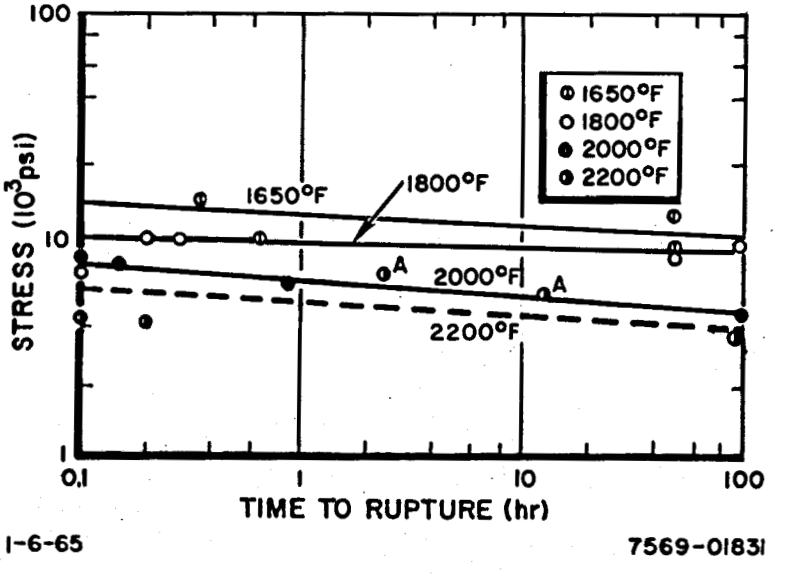

Figure 4.3.29. Creep Stress vs Rupture Time for Columbium at High Temperatures (Reference 4.6)

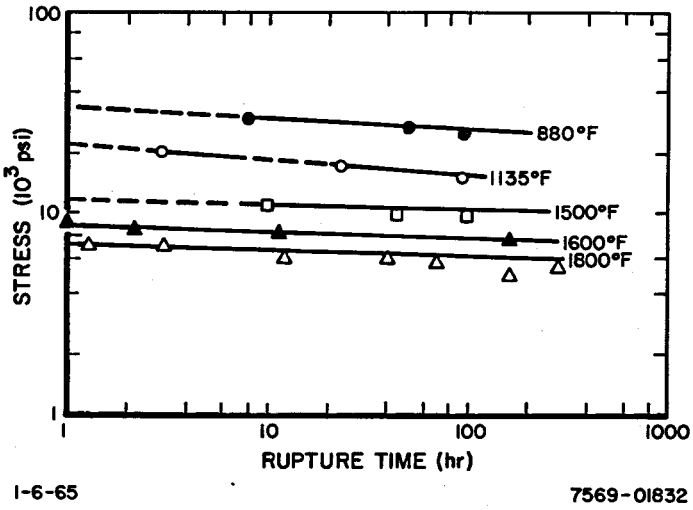

Figure 4.3.30. Creep Stress vs Rupture Time for Columbium at Lower Temperatures (Reference 4.6)

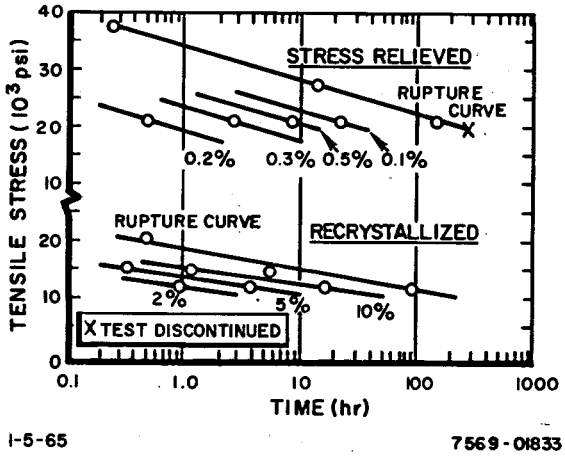

Figure 4.3.31. Creep at 1800°F for Unalloyed Arc-Cast Molybdenum, as Stress Relieved (1800°F – 1 hr) or Recrystallized (2150°F – 1 hr) (Reference 4.13)

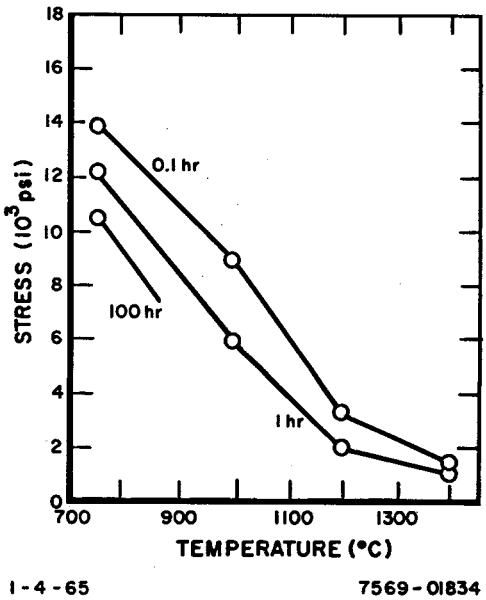

Figure 4.3.32. 0.5% Creep Strength vs Temperature of Recrystallized High-Purity Ta Sheet (Reference 4.12)

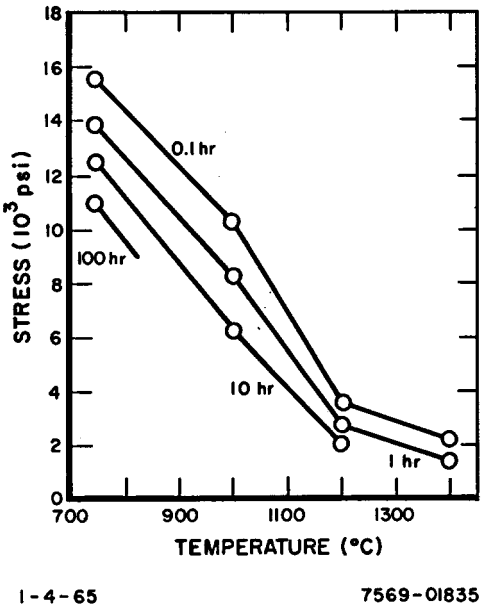

Figure 4.3.33. 1.0% Creep Strength vs Temperature of Recrystallized High-Purity Ta Sheet (Reference 4.12)

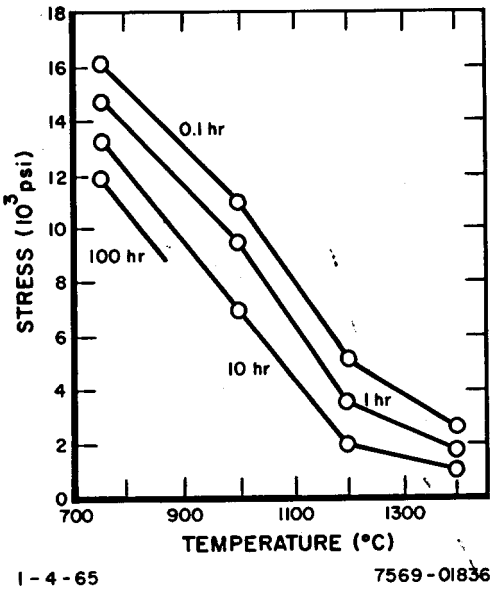

Figure 4.3.34. 2% Creep Strength vs Temperature of Recrystallized High-Purity Ta Sheet (Reference 4.12)

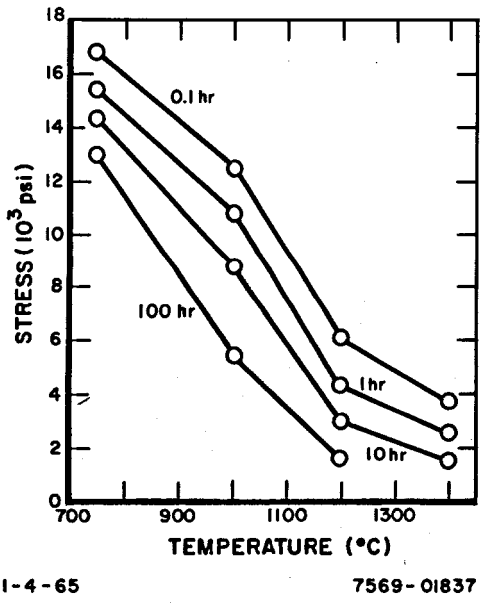

Figure 4.3.35. 5% Creep Strength vs Temperature of Recrystallized High-Purity Ta Sheet (Reference 4.12)

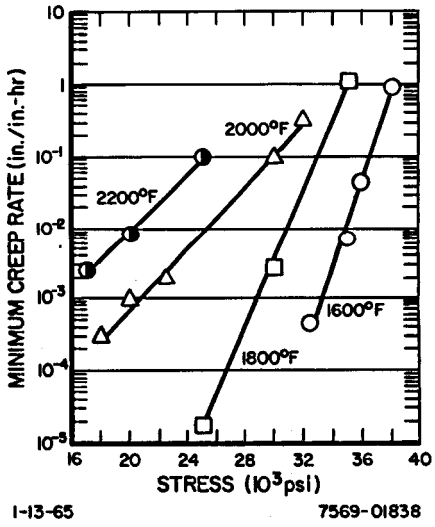

Figure 4.3.36. Creep Rate vs Stress and Temperature for Recrystallized Tungsten (Reference 4.14)

4.3.2.3 Fatigue Strength

No fatigue strength properties as a function of temperature are available for Cb, Ir, Re, V, and W materials. Figure 4.3.37 illustrates the effect of temperature on the fatigue limit and fatigue ratio of unalloyed arc-cast Mo. The material was recrystallized for 20 min at 2800°F to a grain size of ASTM 6/7 (transverse) and 3/6 (longitudinal). The specimens with a minimum diameter of 0.150 in. were tested in rotating bending using a cyclic frequency of 3450 cpm. Results were evaluated by the staircase statistical method using a run-out of 10 million cycles, except at 1100°F where fatigues were still being obtained at 25 million cycles. The tests that were conducted above 875°F were done in an argon atmosphere. Figure 4.3.38 presents fatigue strength properties at different temperatures of annealed tantalum sheet while Tables 4.3.4 and 4.3.5 present these properties of Ti-55 bar at different temperatures and Ti-70 sheet and bar material at room temperature, respectively.

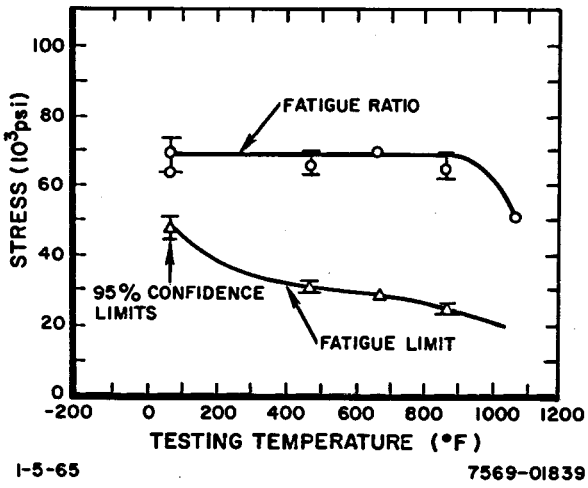

Figure 4.3.37. Effect of Temperature on the Fatigue Limit, Fatigue Ratio of Unalloyed Arc-Cast Molybdenum

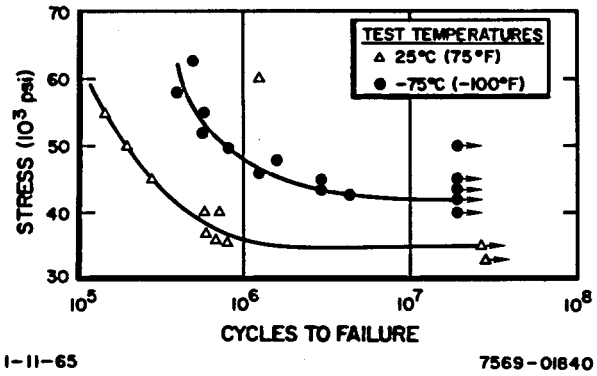

Figure 4.3.38. Fatigue Characteristics of Annealed Tantalum Sheet (Reference 4.12)

TABLE 4.3.4

FATIGUE PROPERTIES OF Ti-55 BAR
(Ref. 4.5)

Alloy	Ti-55					
Form	Bar					
Condition	Annealed					
Temperature (°F)	Method	Stress Ratio		Stress Concentration	Fatigue Strength — ksi at Cycles	
		A	R		(10^6)	(10^7)
-312	Rev bend	∞	-1	Smooth K = 1	-	100
				Notched K = 2.7	-	46
RT				Smooth K = 1	42	41
				Notched K = 2.7	-	35
600				Smooth K = 1	22	21

TABLE 4.3.5

FATIGUE PROPERTIES OF Ti-70 SHEET AND BAR AT ROOM TEMPERATURE (Ref. 4.5)

Alloy	Ti-70						
Condition	Annealed						
Form	Method	Stress Ratio		Stress Concentration	Fatigue Strength — ksi at Cycles		
		A	R		(10^5)	(10^6)	(10^7)
Bar	Notched beam	∞	-1	Smooth K = 1	75	68	62
				Notched K = 2.7	42	38	36
Sheet	Direct stress	0.25	0.6	Smooth K = 1	-	-	78

4.4 Irradiation Properties

4.4.1 Nuclear Cross Sections

Table 4.4.1 lists the microscopic and macroscopic absorption and scattering and 8 refractory materials for thermal energy neutrons.

TABLE 4.4.1

THERMAL ABSORPTION AND SCATTERING CROSS SECTIONS
(Reference 4.20)

Element	Absorption		Scattering	
	σ_a(barns)	Σ_a(cm^{-1})	σ_s(barns)	Σ_s(cm^{-1})
Cb	1.16	0.0632	5	0.272
Ir	440	30.9	—	0
Mo	270	0.173	7	0.448
Re	86	8.16	14	1.33
Ta	21	1.16	5	0.276
Ti	5.8	0.328	4	0.226
V	5.0	0.352	5	0.352
W	19.2	1.19	5	0.310

4.4.2 Radiation Effects

The effects of nuclear irradiation upon the tensile properties of Cb have been investigated to a limited extent. Cb containing about 0.16% oxygen was exposed to a neutron dose of 2.3×10^{20} neutron/cm^2 of energies less than 0.6 ev and 1×10^{20} neutron/cm^2 of energies greater than 0.6 ev. Irradiation is seen to increase the strength and decrease the ductility of Cb in much the same manner as cold work. This effect has been attributed to the formation of lattice vacancies created by neutron irradiation. At low temperature exposure (60°F) thermal activation was not sufficient to allow interstitials to accumulate at these sites of imperfections and yield point disappears at this result. However, by annealing at about 400°F, thermal energy was sufficient to condense impurity diffusivity and this resulted in additional increases in strength and the return of yield point behavior.[4.21]

No data exists to illustrate the effect of irradiation on the properties of Ir, Re, and V.

Figure 4.4.1 illustrates the effect of neutron irradiation upon the tensile hardness and notch bar transition temperature properties of Mo. In general, irradiation increases the yield strength of Mo and raises the ductile-brittle transition temperature. In many cases the irradiation hardening is moderate and does not reflect the significant embrittlement that may have occurred. Theoretically, these changes would not take place if irradiation was done at high enough temperatures; tests at 750°F and an estimated 3×10^{20} thermal nvt (3×10^{19} for 1 nv) indicated that still higher temperatures would be needed to avoid embrittlement.

Effect of irradiation in the properties of Ta is moderate. Commercially pure Ta when subjected to an estimated integrated flux have 1.10^{19} slow and 5×10^{19} fast neutrons, showed an increase of about 20% in hardness and strength with a decrease in ductility of about 20%. This irradiation also caused a slight decrease in density and die measures and a slight increase in the electrical resistivity.[4.1]

Very little data are available to illustrate the effect of irradiation on the properties of Ti. When commercially pure Ti-75A was exposed to a total flux of 2.2 to 6.6×10^{20} nvt thermal neutrons, it increased in yield strength from

59,500 to 105,000 psi. The ultimate strength increased from 81,200 initially to 105,000 psi after irradiation and the elongation decreased from 26 to 13.4%. The results indicated that the effects had approached saturation. An increase of 6.7 to 7.7% in electrical resistivity was noted in Ti-75A after a similar exposure of 2.2 to 6.6 x 10^{20} nvt thermal neutrons. After an exposure of 4 x 10^{20} nvt/cm^2 Ti showed a lattice parameter increase of 0.14% by annealing at 700°C resulting in a return to nearly the original parameter.[4.1]

Tungsten exposed to 1 x 10^{19} nvt slow and 5 x 10^{19} nvt fast neutrons showed no significant change in the hardness. The electrical resistivity increased nearly 40% and the density decreased 0.1 to 0.15%. After a similar exposure a decrease of approximately 22% was observed in the tensile strength of tungsten wire. However, the samples were brittle and difficult to align the tensile grips and a decrease may not be entirely related to irradiation.[4.1]

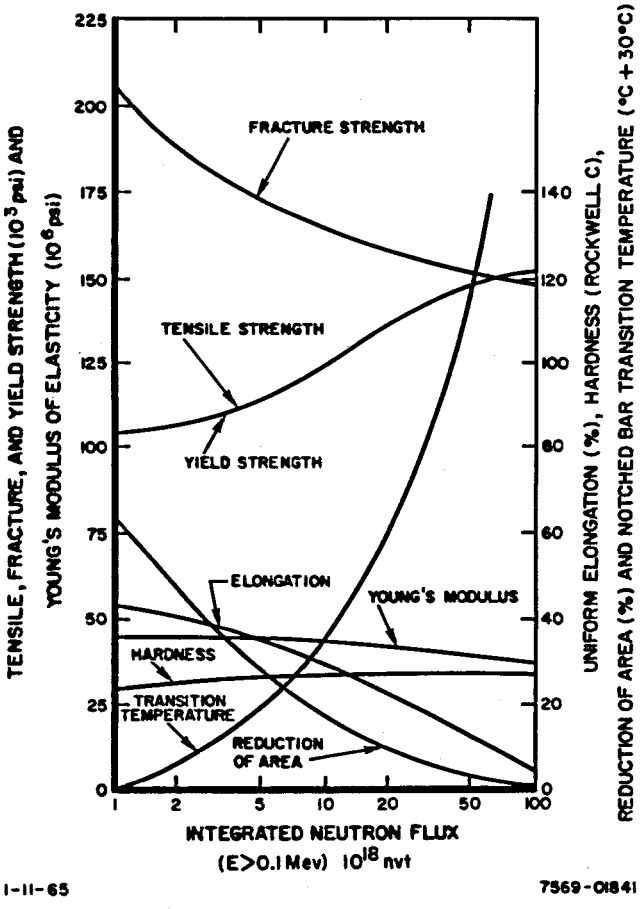

Figure 4.4.1. Effect of Irradiation on Properties of Molybdenum (Reference 4.13)

REFERENCES

4.1 C. R. Tipton, Jr., Reactor Handbook, Vol. I - Materials, Interscience Publishers, Inc. (1960)

4.2 E. L. Francis, "Vanadium Data Manual," IGR-R/R-306 (1959)

4.3 R. E. Taylor and R. A. Finch, "The Specific Heat and Resistivities of Mo, Ta, and Re from Low to Very High Temperatures," NAA-SR-6034 (1961)

4.4 T. Lyman, et al., Metals Handbook, Vol. I - Properties and Selection of Metals, American Society For Metals, 8th Edition (1961)

4.5 V. Weiss, Editor, "Aerospace Structural Metals Handbook, Vol. II - Non-Ferrous Alloys," Syracuse University Press (March 1963)

4.6 T. E. Tietz and J. W. Wilson, "Mechanical, Oxidation, and Thermal Property Data for Seven Refractory Metals and Their Alloys," AD 266824 (September 1961)

4.7 K. K. Kelly, "Contributions to the Data on Theoretical Metallurgy XIII," Bureau of Mines Bulletin 584.

4.8 R. W. Webb, "Hydrogen Permeation Through Metals," NAA-SR-TDR-9844 (April 1964)

4.9 S. Dushman, Scientific Foundations of Vacuum Technique, Wiley Publishing Company, New York (1962)

4.10 W. Rostocker, The Metallurgy of Vanadium, Wiley Publishing Company, New York

4.11 F. R. Schwartzberg, F. C. Holden, H. R. Ogden, and R. I. Jaffee, "The Properties of Titanium Alloys at Elevated Temperatures," TML-82-September 1957

4.12 F. F. Schmidt, "Tantalum and Tantalum Alloys," DMIC 133 (July 1960)

4.13 "Molybdenum Metal," Climax Molybdenum Company, A Division of American Metal Climax, Inc. (1960)

4.14 V. D. Barth, "Physical and Mechanical Properties of Tungsten and Tungsten Base Alloys," DMIC-127

4.15 E. L. Francis, "Niobium Data Manual," IGR-R/R-304 (1959)

4.16 "Metals Handbook, Vol. I," American Society for Metals, Cleveland, Ohio (1962)

4.17 H. G. Vaughan and R. G. Rose, "The Tensile Properties of Niobium," IGR-TN/C-583 (1958)

4.18 C. T. Sims, et al., "Survey of the Literature on Rhenium," WADC-TR-56-319 (January 1956)

4.19 C. T. Sims, et al., "Investigations of Rhenium," WADC-TR-54-371 (June 1954)

4.20 R. N. MacDonald and H. H. Baucom, Jr., "Nuclear Data for Reactor Studies," Nucleonics, Vol. 20. No. 8, p 158 (August 1962)

4.21 E. S. Bartlett and J. A. Houck, "Physical and Mechanical Properties of Columbium and Columbium-Base Alloys," DMIC-125 (February 1960)

5.0 USEFUL INFORMATION

5.1 Units Conversion

1 atmosphere	= 14.7 $lb_f/in.^2$
1 cal (mean)	= 0.00397 Btu (mean)
1 cal/gm-°C	= 1.0 Btu/lb_m-°F
1 cal/sec-cm-°C	= 241.8 Btu/hr-ft-°F
1 $cal/sec-cm^2$	= 13,272 $Btu/hr-ft^2$
1 $cal/sec-cm^2$-°C	= 7373 $Btu/hr-ft^2$-°F
1 cm	= 0.03281 ft
1 cm	= 0.3937 in.
1 cm/sec	= 118.116 ft/hr
1 cm^2	= 0.001076 ft^2
1 cm^2	= 0.155 $in.^2$
1 cm^3	= 3.531 x 10^{-5} ft^3
1 cm^3	= 0.06103 $in.^3$
1 gm	= 0.002205 lb_m
1 gm/cm^3	= 62.43 lb_m/ft^3
1 gm/cm^2	= 0.01422 psi
1 kg	= 2.205 lb_m
1 kg/cm^2	= 0.9678 atm
1 kg/cm^2	= 2.048 lb_m/ft^2
1 kg/cm^2	= 14.22 $lb_m/in.^2$
1 kw	= 3415 Btu/hr
1 l	= 0.0353 ft^3
1 m	= 39.37 in.
1 m/sec	= 3.281 ft/sec
1 mm of Hg	= 0.001316 atm
1 Torr	= 1.0 mm of Hg
1 Torr	= 0.001316 atm
1 watt/cm-°C	= 57.79 Btu/hr-ft-°F
1 watt/sec	= 0.000948 Btu
1 $watt/cm^2$	= 3171 $Btu/hr-ft^2$
1 $watt/cm^2$-°C	= 1761 $Btu/hr-ft^2$-°F

TABLE 5.2
TEMPERATURE CONVERSIONS*

459.4° to 0°			1° to 60°			61° to 290°			300° to 890°			900° to 3000°		
C	C / F	F	C	C / F	F	C	C / F	F	C	C / F	F	C	C / F	F
-273	-459.4		-17.2	1	33.8	16.1	61	141.8	149	300	572	482	900	1652
-268	-450		-16.7	2	35.6	16.7	62	143.6	154	310	590	488	910	1670
-262	-440		-16.1	3	37.4	17.2	63	145.4	160	320	608	493	920	1688
-257	-430		-15.6	4	39.2	17.8	64	147.2	166	330	626	499	930	1706
-251	-420		-15.0	5	41.0	18.3	65	149.0	171	340	644	504	940	1724
-246	-410		-14.4	6	42.8	18.9	66	150.8	177	350	662	510	950	1742
-240	-400		-13.9	7	44.6	19.4	67	152.6	182	360	680	516	960	1760
-234	-390		-13.3	8	46.4	20.0	68	154.4	188	370	698	521	970	1778
-229	-380		-12.8	9	48.2	20.6	69	156.2	193	380	716	527	980	1796
-223	-370		-12.2	10	50.0	21.1	70	158.0	199	390	734	532	990	1814
-218	-360		-11.7	11	51.8	21.7	71	159.8	204	400	752	538	1000	1832
-212	-350		-11.1	12	53.6	22.2	72	161.6	210	410	770	549	1020	1868
-207	-340		-10.6	13	55.4	22.8	73	163.4	216	420	788	560	1040	1904
-201	-330		-10.0	14	57.2	23.3	74	165.2	221	430	806	571	1060	1940
-196	-320		-9.4	15	59.0	23.9	75	167.0	227	440	824	582	1080	1976
-190	-310		-8.9	16	60.8	24.4	76	168.8	232	450	842	593	1100	2012
-184	-300		-8.3	17	62.6	25.0	77	170.6	238	460	860	604	1120	2048
-179	-290		-7.8	18	64.4	25.6	78	172.4	243	470	878	616	1140	2084
-173	-280		-7.2	19	66.2	26.1	79	174.2	249	480	896	627	1160	2120
-169	-273	-459.4	-6.7	20	68.0	26.7	80	176.0	254	490	914	638	1180	2156
-168	-270	-454	-6.1	21	69.8	27.2	81	177.8	260	500	932	649	1200	2192
-162	-260	-436	-5.6	22	71.6	27.8	82	179.6	266	510	950	660	1220	2228
-157	-250	-418	-5.0	23	73.4	28.3	83	181.4	271	520	968	671	1240	2264
-151	-240	-400	-4.4	24	75.2	28.9	84	183.2	277	530	986	682	1260	2300
-146	-230	-382	-3.9	25	77.0	29.4	85	185.0	282	540	1004	693	1280	2336
-140	-220	-364	-3.3	26	78.8	30.0	86	186.8	288	550	1022	704	1300	2372
-134	-210	-346	-2.8	27	80.6	30.6	87	188.6	293	560	1040	732	1350	2462
-129	-200	-328	-2.2	28	82.4	31.1	88	190.4	299	570	1058	760	1400	2552
-123	-190	-310	-1.7	29	84.2	31.7	89	192.2	304	580	1076	788	1450	2642
-118	-180	-292	-1.1	30	86.0	32.2	90	194.0	310	590	1094	816	1500	2732
-112	-170	-274	-0.6	31	87.8	32.8	91	195.8	316	600	1112	843	1550	2822
-107	-160	-256	0.0	32	89.6	33.3	92	197.6	321	610	1130	871	1600	2912
-101	-150	-238	0.6	33	91.4	33.9	93	199.4	327	620	1148	899	1650	3002
-96	-140	-220	1.1	34	93.2	34.4	94	201.2	332	630	1166	927	1700	3092
-90	-130	-202	1.7	35	95.0	35.0	95	203.0	338	640	1184	954	1750	3182
-84	-120	-184	2.2	36	96.8	35.6	96	204.8	343	650	1202	982	1800	3272
-79	-110	-166	2.8	37	98.6	36.1	97	206.6	349	660	1220	1010	1850	3362
-73	-100	-148	3.3	38	100.4	36.7	98	208.4	354	670	1238	1038	1900	3452
-68	-90	-130	3.9	39	102.2	37.2	99	210.2	360	680	1256	1066	1950	3542
-62	-80	-112	4.4	40	104.0	37.8	100	212.0	366	690	1274	1093	2000	3632
-57	-70	-94	5.0	41	105.8	43	110	230	371	700	1292	1121	2050	3722
-51	-60	-76	5.6	42	107.6	49	120	248	377	710	1310	1149	2100	3812
-46	-50	-58	6.1	43	109.4	54	130	266	382	720	1328	1177	2150	3902
-40	-40	-49	6.7	44	111.2	60	140	284	388	730	1346	1204	2200	3992
-34	-30	-22	7.2	45	113.0	66	150	302	393	740	1364	1232	2250	4082
-29	-20	-4	7.8	46	114.8	71	160	320	399	750	1382	1260	2300	4172
-23	-10	14	8.3	47	116.6	77	170	338	404	760	1400	1288	2350	4262
-17.8	0	32	8.9	48	118.4	82	180	356	410	770	1418	1316	2400	4352
			9.4	49	120.2	88	190	374	416	780	1436	1343	2450	4442
			10.0	50	122.0	93	200	392	421	790	1454	1371	2500	4532
			10.6	51	123.8	99	210	410	427	800	1472	1399	2550	4622
			11.1	52	125.6	100	212	413.6	432	810	1490	1427	2600	4712
			11.7	53	127.4	104	220	428	438	820	1508	1454	2650	4802
			12.2	54	129.2	110	230	446	443	830	1526	1482	2700	4892
			12.8	55	131.0	116	240	464	449	840	1544	1510	2750	4982
			13.3	56	132.8	121	250	482	454	850	1562	1538	2800	5072
			13.9	57	134.6	127	260	500	460	860	1580	1566	2850	5162
			14.4	58	136.4	132	270	518	466	870	1598	1593	2900	5252
			15.0	59	138.2	138	280	536	471	880	1616	1621	2950	5342
			15.6	60	140.0	143	290	554	477	890	1634	1649	3000	5432

*Locate temperature in middle column. If in degrees Centigrade, read Fahrenheit equivalent in right hand column; if in degrees Fahrenheit, read Centigrade equivalent in left hand column.

5.2 Useful Formulas

To convert vol % to wt % of an individual component in a mixture of x and y:

$$(\text{wt \% of x}) = (\text{vol \% of x})\left(\frac{\rho_x}{\rho_m}\right)$$

$$= \frac{(\text{vol \% of x})(100\ \rho_x)}{(\text{vol \% of x})(\rho_x - \rho_y) + \rho_y} \quad .$$

To convert vol % to wt % of an individual component in a mixture of x and y:

$$(\text{vol \% of x}) = (\text{wt \% of x})\left(\frac{\rho_m}{\rho_x}\right)$$

$$= \frac{(\text{wt \% of x})(100\ \rho_y)}{(100\ \rho_x) - (\text{wt \% of x})(\rho_x - \rho_y)} \quad ,$$

where ρ_x and ρ_y is the density of the individual components prior to mixing and ρ_m is the density of the mixture.